AN EXPERIMENTAL AND ANALYTICAL STUDY OF WEB FLUTTER

By

YOUNG BAE CHANG

Bachelor of Science in Engineering
Hankuk Aviation College
Seoul, Korea
1979

Master of Science
Korea Advanced Institute of Science & Technology
Seoul, Korea
1981

Submitted to the Faculty of the Graduate College
of the Oklahoma State University
in partial fulfillment of the requirements
for the Degree of
DOCTOR OF PHILOSOPHY
December, 1990

AN EXPERIMENTAL AND ANALYTICAL STUDY OF

WEB FLUTTER

Thesis Approved:

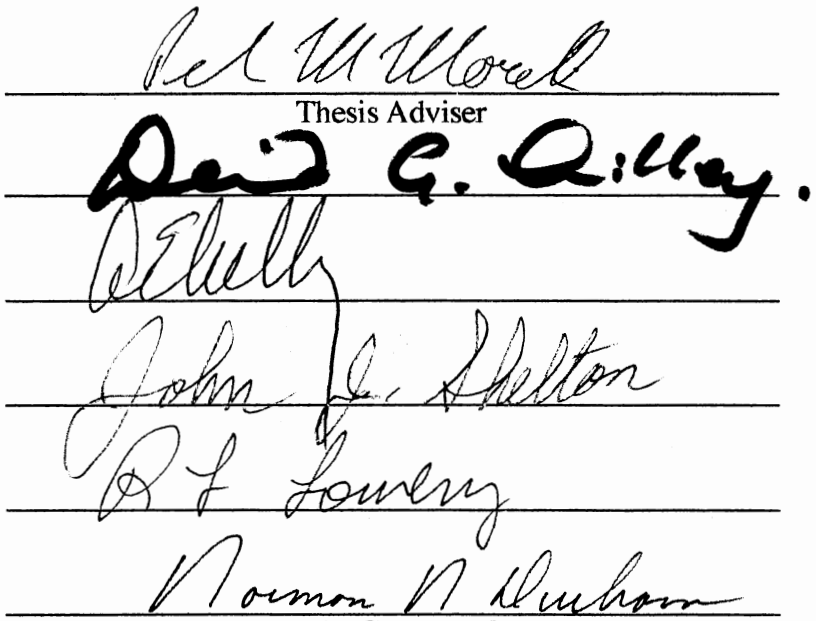

Thesis Adviser

Dean of the Graduate College

ACKNOWLEDGEMENT

I would like to express my deepest gratitude to my advisor, Dr. P.M. Moretti, for his excellence in guiding and encouraging his student; I am indebted to him for his inspiration and knowledge. I would also like to thank Dr. R.L. Lowery, Dr. J.J. Shelton, Dr. D.G. Lilley, and Dr. A.E. Kelly for their helpful comments and discussions; they were willing to help me and shared their precious time with me.

I extend my appreciation to my parents, brothers, and sisters who helped me and prayed for me. I thank my wife who endured difficult times and prayed for me; she is a blessing from God. This work is dedicated to them.

This work was supported by the Web Handling Research Center (WHRC) at Oklahoma State University.

1394987

TABLE OF CONTENTS

LIST OF TABLES

LIST OF FIGURES

NOMENCLATURE

A	Amplitude of oscillation
A_R	Aspect ratio (d/L)
B	Width of enclosure
B_a	Coefficient of total damping due to air loading
b_a	Coefficient of damping per unit area due to air loading
C_a	Added-mass coefficient
C_d	Drag coefficient
c	Phase speed of wave on membrane in vacua ($\sqrt{T/m}$)
c_o	Sound speed in undisturbed air
c_w	Phase speed of wave on membrane or plate in air flow
D	Bending stiffness of plate
D_r	Nondimensional bending stiffness ($D\kappa^2/T$)
d	Width of web (Dimension in cross-machine direction), or Span of a body in air flow (Dimension in cross-flow direction)
E	Young's modulus
F	Force on unit area
f	Vibration frequency
g	Gravitational acceleration
H	Height of enclosure
i	$\sqrt{-1}$
K	Spring constant
k	Wave number of pressure wave in air

L	Length of web (Dimension in machine direction)
M_a	Total added mass
m	Mass per unit length of string, or mass per unit area of web
m_a	Added mass per unit area (Equal to m_1)
m_1	Added mass associated with transverse acceleration
m_2	Added mass associated with Coriolis acceleration
m_3	Added mass associated with centripetal acceleration
n	Order of mode
q	Dynamic pressure ($\rho U^2/2$)
R_r	Radiation resistance
r_i	Mass ratio (m_i/m)
S	Area
s	Slenderness ratio (L/d or S/d^2)
T	Tension of string, or tension of web per unit width
t	Time
U	Flow speed
U_{div}	Critical flow speed for static instability (divergence)
U_{flt}	Critical flow speed for dynamic instability (flutter)
v	Traveling speed of string or web
x	Coordinate in direction of web motion (Machine direction)
X_r	Radiation reactance
y	Coordinate across web motion (Cross-machine direction)
z	Coordinate normal to the web surface
Z_r	Radiation impedance
δ	Boundary layer thickness, or Logarithmic decrement of oscillation
δ^*	Displacement thickness

η	Deflection in z direction
κ	Wave number on web
λ	Wave length
θ	Momentum thickness
ρ	Air density
ω	Angular frequency
ψ	Free vibration shape, or Stream function

CHAPTER I

INTRODUCTION

1.1 Definition of the Problem

Thin and flexible materials such as papers, polymer films, and magnetic media are called webs. Those materials are usually manufactured in continuous forms. High productivity of webs requires high-speed operation; but the operating speed is limited by many factors. One of the most serious obstacles to high speed operation is web flutter (vibrations) which causes quality problems or breaks in the web [A1, 2]. The flutter problems can be serious in paper machines producing light-weight papers with an operating speed higher than 2000 fpm; especially in or near dryer sections where the paper is still weak and exposed to high-speed air flows.

Figure 1 shows a simplified view of paper running in a dryer section. The paper web running at speed v is subjected to highly turbulent air flows in both x and y directions. The air flow in the x direction (machine direction) is due to the traveling speed of the web; while the air flow in the y direction, which has the highest speed near the free edges, is caused mainly by the ventilation system. Web flutter has two basic components which can appear separately or together:

(1) The one limiting case is string-mode flutter as shown in Figure 2(a); there is little y-dependent variation of web deflection and the wide web behaves like a string traveling between two rollers.

(2) The other extreme is edge flutter as shown in Figure 2(b); ripples travel in the y direction with the largest amplitude appearing at the free edges.

In order to cope with the flutter problems we need to identify the causes and mechanisms of the flutter phenomena. But there are arguments concerning the main causes of web flutter and the mechanisms are not clearly understood. It is necessary, therefore, to carry out fundamental studies on the various possible mechanisms of web flutter and to find flutter prediction criteria.

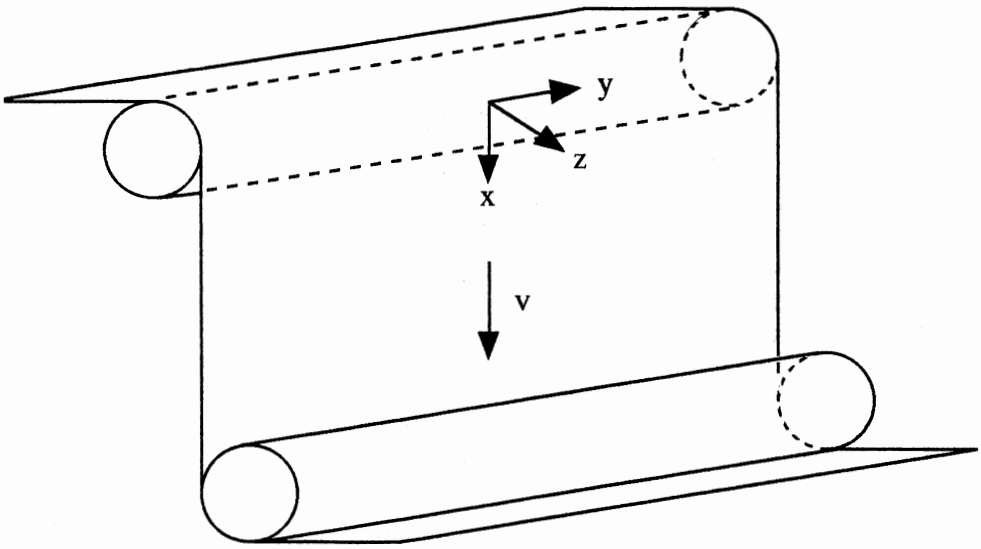

Figure 1 A Schematic of a Running Web and Its Coordinate System

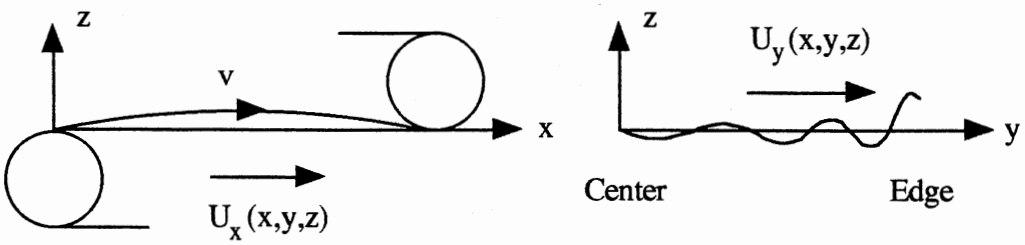

(a) String-Mode Flutter (b) Edge Flutter

Figure 2 Flutter Modes of a Paper Sheet in Dryer Section

1.2 Areas in Needs of Research

String-Mode Instability

The review of previous studies, given in Chapter II, shows that the following are areas that need research associated with string-mode instability:

(1) Aerodynamic forces acting on the web. The air loading is affected by the flow speed, slenderness of the web, and the presence of rollers, enclosure, and adjacent web span.

(2) The velocity profile for x-directional (machine-directional) air flow $U_x(x,y,z)$. The main driving force that induces U_x is the running motion of the web, but the speed profile is affected by many factors.

(3) The effect of turbulence of the air flow.

(4) The distribution of x-directional tension $T_x(x,y)$; the paper slackens near the free edges.

(5) Nonlinear behavior of the web due to large amplitude.

(6) Damping of the oscillating web.

(7) The effect of viscoelasticity of the web material.

(8) Parametric vibration due to tension fluctuation.

(9) The effect of nonuniform mass distribution. Does it really cause flutter?

(10) The effect of air entrainment between the web and rollers. Air entrainment changes the boundary conditions of the web and can be a cause of web excitation.

Edge Flutter

Though the edge flutter is also very important and serious, no in-depth study of edge flutter has been found in the literature search. Some areas that need research include:

(1) Aerodynamic forces on the web. Especially, interaction between the web and air flow near the free edge is the most difficult aspect of edge flutter.

(2) The velocity profile for y-directional (cross-machine-directional) air flow $U_y(x,y,z)$. U_y is caused mainly by the ventilation system and also by the interaction among paper sheet, felts, and rollers.

(3) The distribution of T_x and $T_y(x,y)$. T_y is caused by T_x, air drag, and also by the vibration of the web.

1.3 Objectives and Scope

The present study is focused on the effects of air-web interaction. The following are the major objectives of this study:

(1) To develop an analytical model of string-mode instability of a web. The effects of web speed and x-directional air flow are considered.

(2) To verify the analytical model through experiments. Experiments are limited to the case of a non-traveling web in an air flow. The tests, though limited, are sufficient for fundamental study of air-web interaction.

(3) To find important variables that affect edge flutter and find their effects through experiments. Like the string-mode tests, edge flutter tests are limited to the case of a non-traveling web.

(4) To provide design guides (stability criteria) for preventing or solving flutter problems.

1.4 Methods of Approach

In order to analyze string-mode instability of a moving web the well known analytical model of a "traveling threadline" is used. The traveling threadline model is generalized by including aerodynamic terms. The generalized threadline model is solved for arbitrary values of aerodynamic terms. The aerodynamic force terms of the "swimming slender fish" model are used for slender (narrow and long) webs in an infinite air space. The finite-difference method is used to evaluate the air loading on a web in an enclosure.

Wind tunnel tests are carried out for slender paper webs for verification of the aerodynamic effects on the string-mode instability. Leading and trailing edges are restrained from out-of-plane motion, while the other sides are free. Tension is applied in the x direction (flow direction).

A dimensional analysis is performed to find nondimensional parameters for edge flutter tests. Wind tunnel tests are performed. The trailing edge of the test web is free to move while the other three sides are fixed. Tension is applied in the y direction (cross-flow direction) by using weights. Stability criteria are provided through experiments and dimensional analysis.

CHAPTER II

LITERATURE REVIEW

2.1 Field Studies of Web Flutter

Most of the field studies of web flutter are concerned about the flutter problems in the dryers of paper-making machines. But there have been many arguments concerning the causes of web flutter. Vennos & DeCrosta [A2, 5] and many others [A4, 6, 9, 16, 20, 22, 24, 26, 28-31] attribute the web flutter to the air flows around the web. Studies of the air flow in dryer pocket are found in [A1-8, 10-16]. Some of the suspected causes of web flutter in paper machines are:

(1) Excessive machine speed

(2) Air pumping caused by highly permeable dryer fabrics

(3) Y-directional (cross-machine-directional) air flow U_y in dryer pockets

(4) Differences in the y-directional air flow U_y on both sides of the web

(5) Turbulent flow caused by head bolts

(6) Unbalanced ventilation systems

(7) Variation of basis weight

(8) Headbox edge effects

(9) Uneven sheet shrinkage

(10) Tension variation

(11) Adhering of the sheet to the cylinder or to the felt

(12) Felt seam disturbance

Among them, (1)-(6) are related with air flow around the web and (7)-(9) are causes of nonuniform tension distribution. They do not occur independently; most of them interact with each other and some of them are causes of others.

Proposed or tried methods for preventing web flutter in the dryers of paper machines include:

(1) Using less permeable felts

(2) Single felting (uno-run, serpentine felting)

(3) Making the sheet run between two felts

(4) Using blow boxes

(5) Rearranging felt rollers

(6) Mounting baffles

(7) Shrouding the cylinder head bolts

(8) Mounting support rolls which hold the web in the open draw

(9) Using lick-up mechanism

(10) Mounting wrinkle irons

(11) Making the edges slightly heavier than the sheet average

The causes and preventing methods of web flutter discussed by different authors are summarized in Table I, where [A29] and [A30] are for the problems in printing presses and all the others are related to paper machines.

TABLE I

CAUSES AND CURES OF WEB FLUTTER

Vennos & Decrosta (1967, 1968) [A2, 5]

Cause: Excessive machine speed (>2000 fpm) & highly permeable dryer fabrics which cause cross-machine directional air flow in the dryer pocket

---

Race, et al. (1968) [A4]

Cause: Excessive machine speed & high fabric permeability which cause air pumping by dryer fabrics

Cure: Choosing proper felts (proper permeability)

Kottick (1969) [A6]

Cause: Excessive air carried by permeable clothing (felt)

Cure: Air deflector to prevent air build up on clothing
Fabrics with lower permeability
Different felt roll configurations

Cedercreutz (1971) [A9]

Cause: Excessive machine speed (>2100 fpm) & highly permeable dryer fabrics which cause cross-machine directional airstreams in the dryer pocket
Difference in the cross-machine directional flow speeds on both sides of the sheet
Clipper seam of felt

Cure: Wrinkle irons or support rolls which hold the sheet in the open draw
Making the edges slightly heavier than the sheet average
Using felts with reduced permeability on the edges
Making the sheet run between two felts

TABLE I (Continued)

Mujumdar (1974) [A16]

Cause: Passage of the felt seam
Vibration of the dryer rolls
Eccentricity of the rolls
Nonuniform web tension in the cross-machine direction
Unequal flow (and pressure) on both sides of the sheet
Cross-machine directional air flow induced due to pocket geometry

Cure: Using new dryer such as the Papridryer
Mounting suction system

Smook (1976) [A20]

Cause: Headbox edge effects
Dryer pocket air flows
Dryer clothing seam disturbance
Nonuniform basis weight
Nonuniform moisture level

Edgar (1977) [A21]

Cure: Single felting (uno-run) with lower permeability

Sahay (1977) [A22]

Cause: Excessive machine speed & highly permeable felts & wide web which cause pocket air flow

Cure: Single fabric (uno-run) with low permeability

Palazzolo (1978) [A24]

Cure: Serpentine felt arrangement (single felting, uno-run) with low permeability

TABLE I (Continued)

Bringman and Jamil (1978) [A26]

Cause: Air pumping
Adhering of the sheet to the cylinder or to the felt
Variation of basis weight (nonuniform tension)
Variation of moisture (nonuniform tension)
Uneven press loading (nonuniform tension)
Headbox edge effect (nonuniform tension)
Uneven sheet shrinkage (nonuniform tension)
Highly permeable open felts (turbulent flow in dryer pockets)
Felt seam
Cylinder head bolts (turbulent flow)
Pocket ventilation equipment (turbulent flow)
Unbalanced ventilation system (turbulent flow)

Cure: Using less permeable felts
Shrouding the cylinder head bolts
Making the sheet run in between two felts
Single felting

Sahay and Edgar (1980) [A28]

Cause: Air entrainment

Cure: Baffles
Lick-up mechanism

Meinander and Lindqvist (1982) [A29]

Cause: Tension fluctuation (parametric vibration) due to asymmetries in the printing press

Cure: Increasing web tension

Eriksson [A30]

Cause: Tension fluctuation (parametric vibration) caused by deformed or eccentric rolls

TABLE I (Continued)

Hill (1988) [A31]	
Cause:	Excessive air pumping Over-pressurization of the hood Improper control of the dryer steam pressure in uno-run group Poor drainage of the dryer in uno-run group
Cure:	Air deflector Blow box Using thin felt Using lick-down transfer in between two different sections Using a felt with less permeability

2.2 Dynamics of a Traveling Threadline

Linear Vibrations

Skutsch [B1] studied the lateral vibrations of a string which travels under constant tension at constant speed through two fixed points. By considering a superposition of two waves running in opposite directions Skutsch calculated the fundamental resonance frequency and derived a formula for determining the free vibration configuration of the string. Stamets [B2] studied the dynamic loading of high-speed power chains. It was noted that there exists centrifugal force, $m\ v^2$, on both tight and loose lengths of chain. He derived a formula for optimum chain speed. Sack [B3] modified Skutsch's model in order to include the effects of fluctuating boundary conditions and the effect of damping. It was assumed that the damping is proportional to $\partial\eta/\partial t$. Mahalingam [B4] studied the vibration of power transmission chains. He pointed out that a damping force should be proportional to $(\partial\eta/\partial t + v\ \partial\eta/\partial x)$. That conclusion is based on the experimental observations which showed that the resonance amplitude decreases with increase of speed. But there is

uncertainty concerning the form of damping force, and no study is found in the literature survey on the value of damping coefficient. Archibald and Emslie [B5] derived the equation of motion of a moving string using the Hamilton's principle. He discussed similar effects as Sack [B3]. Miranker [B6] generalized the problem to include the effect of variational velocity. It was shown that the energy of that portion of the string between the pulleys is not conserved, but there is a periodic transfer of energy into and out of the system. Swope and Ames [B7] applied the method of characteristics to explore the vibrations of the threadline under boundary excitation.

Nonlinear Vibrations

Zaiser [B8] did pioneering work on nonlinear vibration of a traveling string. His equations include the effects of variable displacement, axial velocity, tension and mass. Both geometric and material nonlinearities are considered. Mote [B9] analyzed nonlinear vibration of a string traveling with constant speed. It was noted that the relationship between smallness of displacement and linearity for the stationary string cannot be extrapolated to the axially moving string. As the traveling speed increases, the effect of tension variation during oscillation becomes increasingly significant and the linear theory fails at sufficiently high speed. Bapat and Srininvasan [B10] obtained the same results by using the method of harmonic balance. Ames, Lee, and Zaiser [B11] studied nonlinear vibration of a traveling threadline under planar periodic boundary excitation. They performed experiments using a threadline which had a diameter of 0.125 in. and a mass density of 1.7×10^{-4} Lb/in . The greatest difficulty was in the measurement of high speed tension. A three-dimensional ballooning was observed at low tension. Lee [B13] investigated the nonlinear problem using the method of characteristics and discussed the effects of transverse impact on a string and traveling force. Studies of nonlinear vibration of a traveling string are found also in Shih [B17], which deals with three-dimensional problem, and in Kim and Tabarrok [B18] which is for two-dimensional case. Wickert and

Mote [B20] investigated the mechanical energy of an axially moving material and obtained three important conclusions: (1) the total mechanical energy of the string is not constant, (2) although the system is not conservative the application of the Hamilton's principle is valid, and (3) for subcritical transport speeds, the amplitudes of the eigenfunction are constant.

Parametric Vibrations

Mahalingam [B4], in his study of the lateral vibration of chain drives, showed that the governing equation of the chain running under fluctuating tension can be changed to the Mathieu form. But no further analysis was done. Naguleswaran and Williams [B12] indicated that it is difficult to obtain a solution which satisfies both the Mathieu type equation and boundary conditions. Galerkin's method was used to solve the problem. They determined the conditions for stable operation of a belt and verified their theoretical results through an experiment. Rhodes [B16] also studied a similar problem analytically and experimentally.

Effect of Elastic Foundation

Linear [B21] and nonlinear [B19] behaviors of a threadline traveling on an elastic foundation between two eyelets were studied. Both studies show that even though the natural frequencies are affected by the elastic foundation, the critical traveling speed for instability is not affected at all.

2.3 Dynamics of a Running Web

Mujumdar and Douglas [C1] discussed two simple analytical models of web flutter: "traveling threadline model" and "flexible membrane model." The effect of surrounding air was not considered in the traveling threadline model. It was noted that the web speed v can be near the wave speed c in high-speed paper machines and the web flutter problem is much different from those encountered in other industries where $v << c$. Based on the fact

that wrinkles occur commonly near the edges at a slight angle to the edge they noted that wrinkle might occur in the region of maximum variation in the wave speed, i.e., web tension. They implied a possibility of vortex excitation at the edge of paper due to the cross-machine-directional air flow. Their discussion of the flexural membrane model is based on Binnie [E9] and Kornecki [E10]. The model predicts flutter of webs in a wind. It was confirmed that the adjacent wall, which is parallel to the web, has negligible effect if the distance is longer than one half of the wave length. The flexural membrane model does not include the effect of open draw length and this fact was pointed as the most serious drawback of the model. Soininen [C2, 3] asserted that the tension caused by centrifugal force $T = mv^2$, coupled with the variation in basis weight , can induce web flutter. But it is uncertain if the variation of basis weight can really cause flutter problem. Pramila [C4 , 5] studied the threadline model of a running web including aerodynamic effect. His analytical model is

$$m\left(\frac{\partial}{\partial t} + v\frac{\partial}{\partial x}\right)^2 \eta - T\frac{\partial^2 \eta}{\partial x^2} = F \qquad (2.3.1)$$

where m is mass per unit area of the web, v is web speed, T is web tension for unit width, and F is the lift force per unit area having the form

$$F = - m_a\left(\frac{\partial}{\partial t} + v\frac{\partial}{\partial x}\right)^2 \eta \qquad (2.3.2)$$

where m_a is the aerodynamic mass of rectangular plate having the same length and width as the web. For the aerodynamic mass m_a, Pramila used the numerical results of Meyerhoff [G10] and the simplified analytical results of Greenspon [G7]. Meyerhoff's

study is for unbaffled plates while Greenspon's model is for baffled plates. The natural frequency of Pramila's model is

$$f_n = \frac{nc'}{2L}\left[1 - \left(\frac{v}{c'}\right)^2\right] \tag{2.3.3}$$

where

$$c' = \sqrt{\frac{T}{m + m_a}} \tag{2.3.4}$$

Later Pramila [C6] considered the possibility that the fluid particles may slip at the sheet surface. The lift force becomes

$$F = - m_a \frac{\partial^2 \eta}{\partial t^2} \tag{2.3.5}$$

By this new formulation the resonant frequency becomes

$$f_n = \frac{nc}{2L}\left[1 - \left(\frac{v}{c}\right)^2\right] \frac{1}{\sqrt{1 - (m_a/m)\left[1 - (v/c)^2\right]}} \tag{2.3.6}$$

where $c = \sqrt{T/m}$. Practically, calculating the aerodynamic mass of the running web is not so simple. Two sides of the web are supported by rollers and the other two edges are free; the web may run in an enclosure; and the adjacent span may have strong aerodynamic interaction especially when the web runs along serpentine paths. Niemi & Pramila [C7] used the finite-element method to analyze transverse vibration of an axially moving membrane. The membrane was considered as a two-dimensional element. The fluid was

assumed to be inviscid and the effect of air flow was not considered. The added mass of the membrane was calculated for various slenderness ratio including the effect of the surrounding structural boundaries.

2.4 Plate Flutter

Most of the studies of panel flutter are dealing with supersonic problems, while the problem under consideration is a subsonic one. Those two, supersonic and subsonic, cases have essentially different aspects. The most prominent differences are: (1) the Kutta condition which is essential in subsonic flow is not required in supersonic case [D1], and (2) at high supersonic Mach numbers the principal aerodynamic pressure is proportional to the plate slope while at subsonic flows it is proportional to plate curvature [D23]. Extensive reviews on subsonic and supersonic plate instabilities are found in [D5, 6, 8, 18, 19]. This section is focused on the studies of subsonic flutter. Also, a few studies of supersonic flutter which can be related to the web flutter are briefly reviewed.

Types of Instability

A plate experiences different kinds of instability depending both on its boundary conditions and on the Mach number. This point has been a long debate, and there is still disagreement among investigators.

Subsonic Flutter

Jordan [D2] discussed the physics underlying panel flutter. He pointed out that we cannot use the classical normal-mode approach for the analysis of panel flutter. He argues that: (1) according to the normal-mode analysis a thin panel exposed to a subsonic air flow is always stable and it becomes unstable as the sonic speed is passed, but (2) in actuality a thin panel can flutter in subsonic flow and not in supersonic flow, (3) the point is that a thin panel does not exhibit standing wave but flutters forming traveling wave. He showed that

the wave reflected at the trailing edge damps out in a short distance and the existence of the trailing edge is not very important. In order to prove that, he used the expression of displacement of a thin panel as

$$\eta(x,t) = A \exp\left[\frac{2\pi x\delta}{\lambda} + i\omega(t - \frac{x}{c_w})\right] \tag{2.4.1}$$

where δ is the logarithmic decrement per wave length and c_w is the wave speed. Another assumption is that the local aerodynamic force is proportional to the local downwash

$$\frac{\partial \eta}{\partial t} + U\frac{\partial \eta}{\partial x} \tag{2.4.2}$$

which corresponds to the linear quasi-steady supersonic theory. Another important conclusion of Jordan's study is that the critical air speed is the same as the wave speed in still air. Greenspon, Goldman, and Jordan [D3] investigated subsonic and supersonic flutter of thin panels. They discussed the disagreements among theories concerning the possibility of subsonic flutter. Ishii [D9] and Weaver and Unny [D16] have examined the instability of a two-dimensional panel in a subsonic air flow by first obtaining expressions for the generalized pressures associated with uniform, two-dimensional, inviscid flow past a panel of finite chord in a rigid surface. Gislason [D17] conducted an experimental investigation of the post-divergence, as well as the onset of divergence, behavior of a flat, rectangular panel at low airspeeds.

Nonlinear Flutter

Dowell [D13, 14] studied nonlinear flutter of two-dimensional curved plates. He found that the effect of streamwise curvature is detrimental both in lowering the air speed and in increasing the flutter amplitude after flutter begins. It is concluded that nonlinear

effects may be important when the Mach number, multiplied by the ratio of amplitude to plate length, is greater than 0.1. Kuo and Morino [D21] developed a systematic way of applying both perturbation methods and harmonic balance methods to nonlinear panel flutter problems.

Effect of Damping

The effect of damping on panel flutter is briefly discussed by Voss and Dowell [D7]. The analysis by Kornecki [D12] shows that very small external damping acts as a destabilizing factor in both subsonic and supersonic flows.

Effect of Turbulence

Vaicaitis, Jan, and Shinozuka [D20] investigated the vibration of a simply supported plate due to turbulent boundary-layer flows by using a Monte Carlo technique. The boundary-layer pressure field was assumed as a homogeneous, multi-dimensional Gaussian random process with zero mean. Both subsonic and supersonic flow problems were studied. That study was expanded to consider more realistic models of boundary-layer turbulence and to analyze the case of clamped support conditions [D22].

2.5 Membrane Flutter

Stearman [E2] studied subsonic membrane flutter. He performed wind tunnel tests using membrane models made of Mylar polyester film. The membrane has a length of 28 inches, spans of 5 and 6 inches, and thicknesses of 1, 3, and 7.5 mils. The leading and trailing edges of the membrane were restrained from vertical motion while the other two edges were free. Tension was applied through the trailing edge; it ranged from 0 to 1.7 lb/in. Two types of flutter were observed: small amplitude flutter first occurred at lower critical flow speed which had a shallow wave-like motion traveling in the streamwise direction and then violent flutter occurred at higher critical speed. In between those two

critical speeds, there existed a narrow equilibrium zone or boundary. The first (lower) stability boundary was independent upon membrane mass and is given as

$$\frac{qd}{T} = 1.01 \tag{2.5.1}$$

where q is critical dynamic pressure, d is membrane width, and T is tension per unit width. The second (higher) stability boundary is dependent on the membrane mass but correlation was not obtained. Stearman tried analytical study but failed to explain his experimental findings. Ellen [E4] studied approximate solution of supersonic flutter of finite membrane. Sundararajan [E6] studied the equilibrium shapes and the stability of a two-dimensional membrane supported at its ends and placed above a rigid inclined wall. It was found that (1) in a parallel nozzle the membrane experiences static divergence only, and (2) a membrane placed in a divergent nozzle experiences static instability or flutter depending on the angle of inclination of the membrane and rigid wall. Supersonic membrane flutter was studied by Spriggs et al. [E8] by using singular-perturbation methods. Binnie [E9] analyzed the stability of infinite membrane in a subsonic air flow using the same method as that used by Squire [E1]. Binnie's stability boundary is

$$\frac{U_c}{c} = \sqrt{1 + \frac{\kappa m}{2\rho}} \tag{2.5.2}$$

where U_c is critical flow speed, $c = \sqrt{T/m}$, m is areal density of membrane, κ is wave number, and ρ is air density.

2.6 Flag Flutter

A flag is a flexible material fixed at its leading edge with the other three edges free to move. The physics of flag flutter is very similar to that of edge flutter of web.

Fairthorne [F1] measured the drag of rectangular and triangular flags in a wind tunnel. The areal densities of the tested materials ranged from $5.2\text{x}10^{-5}$ to $2.2\text{x}10^{-4}$ Lb/in^2. It was found that for both rectangular and triangular flags the drag coefficient can be expressed as

$$C_d = 0.39 \frac{m}{\rho d} s^{-1.25} + 0.012 \qquad (2.6.1)$$

where s is the slenderness ratio defined by

$$s = \frac{S}{d^2} \qquad (2.6.2)$$

and d is span (width), S is the surface area of one side, and the drag coefficient is defined by

$$D = \tfrac{1}{2} \rho U^2 C_d S \qquad (2.6.3)$$

Thoma [F2] analyzed average (temporal) tension in an oscillating rope. His result shows that

$$\overline{T} + \frac{1}{2} m \overline{v^2} = \text{constant} \qquad (2.6.4)$$

where m is mass per unit length, v is the velocity of transversal motion, and the upper bar indicates time average. From the above formula, we can conclude that, if we neglect the air drag, tension at a stationary point of a flag is equal to $m\overline{v^2}/2$ of its free end. Hoerner [F4] pointed out that the drag of a fluttering flag is considerably higher than that of a stationary flat plate in a wind. He explained that the difference is the pressure drag due to flow separation, which is caused by flutter, which is caused in turn by flow separation. In his

analytical study of flag flutter Thoma [F3] noted that the Helmholtz instability does not explain the flag flutter, and he described how a flag extracts energy from the air flow. He considered an infinitely long membrane oscillating in the form

$$\eta = c_1 \cos (x - t) \sin (0.05\, x - 0.025\, t) \tag{2.6.5}$$

Sparenberg [F5] studied wave motion of a half infinite membrane placed in an incompressible fluid flow. It was concluded that the flutter frequency can be obtained by demanding the Kutta condition to be satisfied. Uno [F6] performed flutter tests on flags of various materials in a vertical wind tunnel. In order to set up a semi-empirical formula, he assumed that the flag has the mode shape

$$\eta = c_1\, x \sin (c_2\, x + c_3\, t) \tag{2.6.6}$$

where c_i are constants. Datta and Gottenberg [F7] experimentally studied the stability of a long, thin elastic strip hanging vertically in a downward flowing airstream like the test models of Uno [F6]. They used the slender body approximation. Air friction and gravity effects were considered in the analysis. The equation of motion was solved by Galerkin's method.

CHAPTER III

THEORIES

3.1 Dynamics of a Traveling Threadline

Some fundamentals of traveling threadline problems are discussed. The discussion is limited to linear behavior.

Formulation

- Natural frequency of a stationary (non-traveling) threadline is

$$f_n = \frac{nc}{2L} = \frac{n}{2L}\sqrt{\frac{T}{m}} \tag{3.1.1}$$

where n is the order of mode, L is length of the threadline, T is tension, and m is mass per unit length. The corresponding mode shape is

$$\psi_n(x) = \sin\frac{n\pi x}{L} \tag{3.1.2}$$

When a threadline is running in its axial direction the lateral oscillatory behavior of the threadline is changed. In deriving the equation of motion of a traveling threadline it is assumed that

(1) its amplitude is very small,

(2) there is no damping,

(3) the effect of surrounding air is negligible,

(4) mass of the threadline is uniformly distributed,

(5) tension is constant,

(6) gravity effect is negligible, and

(7) traveling speed is constant.

Under the above assumptions, the instantaneous velocity of a small section of a traveling threadline is

$$v_x = v, \quad v_z = \frac{\partial \eta}{\partial t} + v \frac{\partial \eta}{\partial x} \tag{3.1.3}$$

where v is the traveling speed of the threadline. The kinetic energy in a segment dx of the threadline is

$$dT = \frac{1}{2} m (v_x^2 + v_z^2) dx$$

$$= \frac{1}{2} m \left[v^2 + \left(\frac{\partial \eta}{\partial t} + v \frac{\partial \eta}{\partial x} \right)^2 \right] dx \tag{3.1.4}$$

The potential energy in the same element is

$$dU = T(ds - dx)$$

$$= \frac{1}{2} T \left(\frac{\partial \eta}{\partial x} \right)^2 dx \tag{3.1.5}$$

According to the Hamilton's principle

$$\delta \int_{t_1}^{t_2} (T - U)\, dt = 0$$

that is

$$\delta \int_{t_1}^{t_2} \int_{x_1}^{x_2} \left[\frac{1}{2} m \left\{ v^2 + \left(\frac{\partial \eta}{\partial t} + v \frac{\partial \eta}{\partial x} \right)^2 \right\} - \frac{1}{2} T \left(\frac{\partial \eta}{\partial x} \right)^2 \right] dx dt = 0 \tag{3.1.6}$$

By performing variation, Eq. (3.1.6) becomes

$$\int_{t_1}^{t_2} \int_{x_1}^{x_2} [\, m(\dot{\eta} + v\eta')(\delta\dot{\eta} + v\delta\eta') - T\dot{\eta}\delta\eta' \,] dx dt = 0 \tag{3.1.7}$$

But

$$\delta\dot{\eta} = \frac{\partial}{\partial t}(\delta\eta) \quad \text{and} \quad \delta\eta' = \frac{\partial}{\partial x}(\delta\eta) \tag{3.1.8}$$

By the above relations, Eq. (3.1.7) can be rewritten

$$\int_{t_1}^{t_2} \int_{x_1}^{x_2} \Big[m \Big\{ \dot{\eta} \frac{\partial}{\partial t}(\delta\eta) + v\dot{\eta} \frac{\partial}{\partial x}(\delta\eta) + v\eta' \frac{\partial}{\partial t}(\delta\eta) + v^2\eta' \frac{\partial}{\partial x}(\delta\eta) \Big\}$$

$$- T\eta' \frac{\partial}{\partial x}(\delta\eta) \Big] dx dt = 0 \tag{3.1.9}$$

Integrating by parts yields

$$\int_{t_1}^{t_2}\int_{x_1}^{x_2}\left[\, m(\ddot{\eta} + 2v\,\dot{\eta}' + v^2\eta'') - T\,\eta''\right]\delta\eta\, dxdt \;= 0 \tag{3.1.10}$$

Since $\delta\eta$ is arbitrary, the integrands in the above equation must be zero. Thus,

$$m(\ddot{\eta} + 2v\,\dot{\eta}' + v^2\,\eta'') - T\,\eta'' = 0$$

or

$$\ddot{\eta} + 2v\,\dot{\eta}' + (v^2 - c^2)\,\eta'' = 0 \tag{3.1.11}$$

where $c^2 = T/m$.

Free Vibration of a Traveling Threadline

Assume a solution of the form

$$\eta(x,t) = A\,e^{i(\omega t - \kappa x)} \tag{3.1.12}$$

where ω is the angular speed which represents phase change per unit time, and κ is the wave number which indicates phase change per unit distance. Substituting Eq. (3.1.12) into Eq. (3.1.11) yields the characteristic equation

$$(c^2 - v^2)\,\kappa^2 + 2\,\omega\,v\,\kappa - \omega^2 = 0 \tag{3.1.13}$$

By solving the above equation for the wave number κ

$$\kappa = \frac{\omega}{c + v}, \quad \frac{-\omega}{c - v} \tag{3.1.14}$$

Therefore the lateral deflection of the threadline becomes

$$\eta(x,t) = A_1 e^{i\omega(t-\frac{x}{c+v})} + A_2 e^{i\omega(t+\frac{x}{c-v})} \tag{3.1.15}$$

The above expression indicates that $\eta(x,t)$ is a composition of two waves. The first one is a wave traveling in the positive x direction with a phase speed of (c + v), while the other one is a wave moving in the opposite direction with a phase speed of (c-v). The angular frequency ω in Eq. (3.1.15) can be solved by considering the boundary conditions,

$$\eta(0,t) = 0 \quad \text{and} \quad \eta(L,t) = 0 \tag{3.1.16}$$

By substituting Eq. (3.1.15) into Eq. (3.1.16) we obtain the natural frequency and free vibration shape

$$\omega_n = \frac{n\pi c}{L}\left[1 - (\frac{v}{c})^2\right] \tag{3.1.17}$$

or

$$f_n = \frac{n c}{2L}\left[1 - (\frac{v}{c})^2\right] \tag{3.1.18}$$

and

$$\psi_n(x,t) = \cos(\omega_n t + \frac{n\pi x}{L}\frac{v}{c}) \sin(\frac{n\pi x}{L}) \tag{3.1.19}$$

The frequency equation, as shown in Figure 3, implies that the natural frequency of a traveling threadline decreases as the traveling speed increases, and finally becomes zero at

$$v = c \tag{3.1.20}$$

This is the critical speed of the traveling threadline.

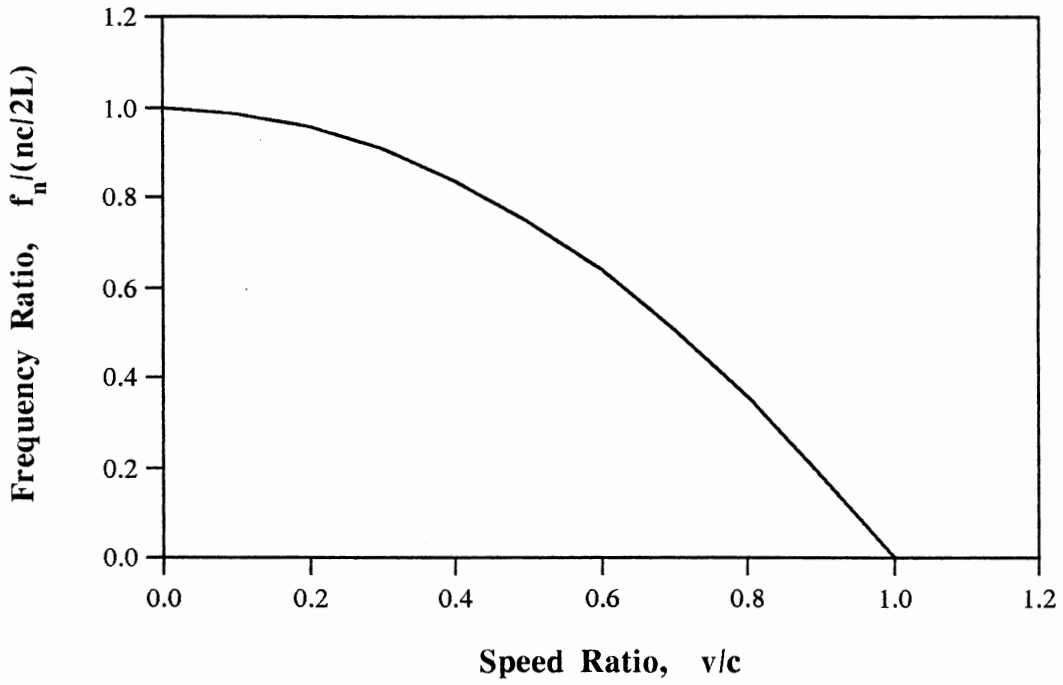

Figure 3 Natural Frequencies of a Traveling Threadline as a Function of Traveling Speed

The vibration shape of the traveling threadline is shown in Figure 4 (v/c = 0.1) and in Figure 5 (v/c = 0.9). It should be noted that each point along the length has different phase, and normal modes do not exist in a traveling threadline.

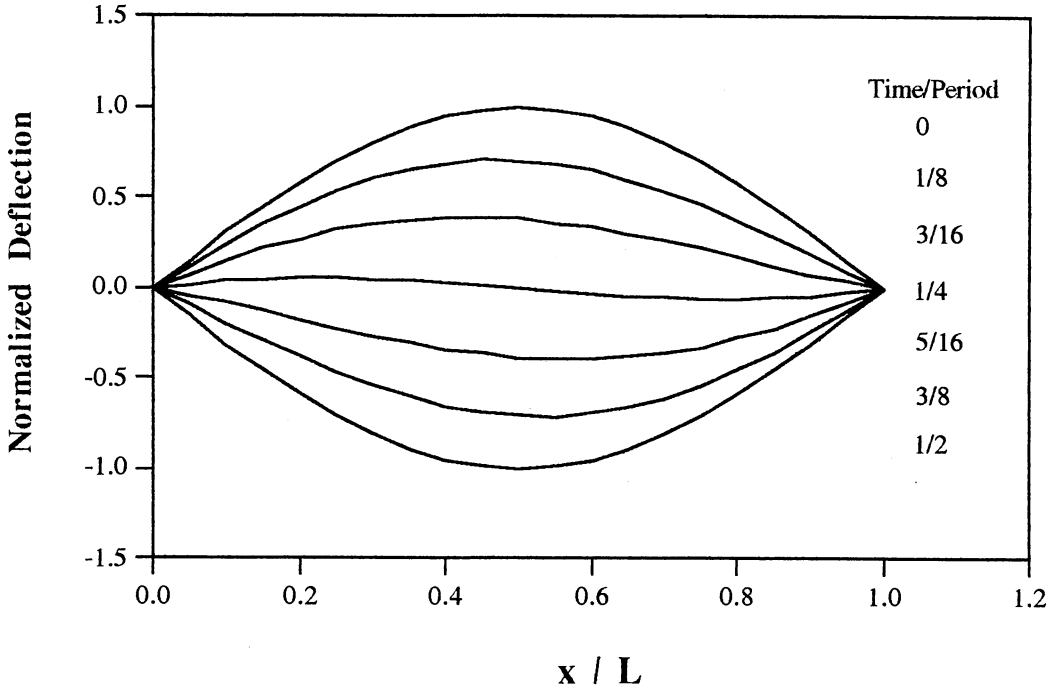

(a) First Half Cycle

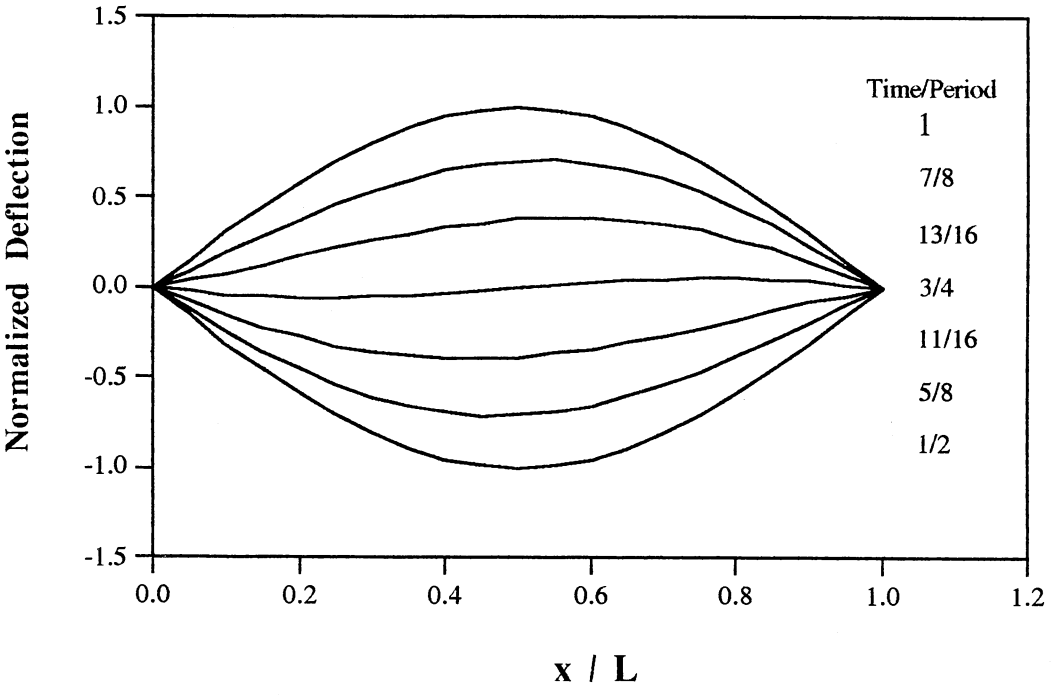

(b) Last Half Cycle

Figure 4 Free Vibration of a Traveling Threadline (v/c = 0.1)

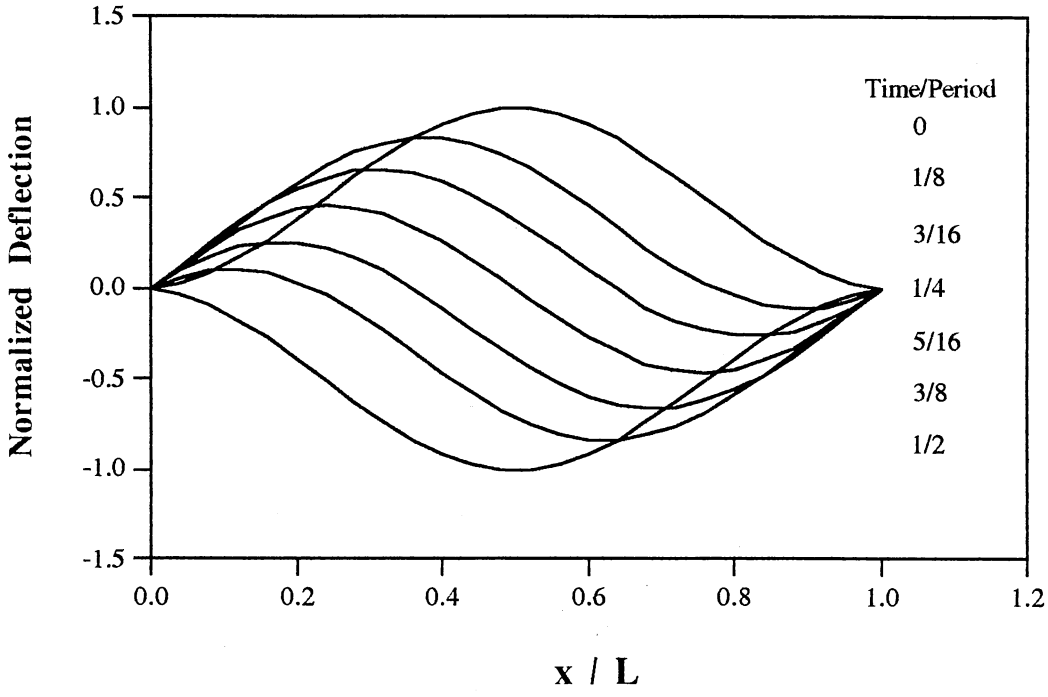

(a) First Half Cycle

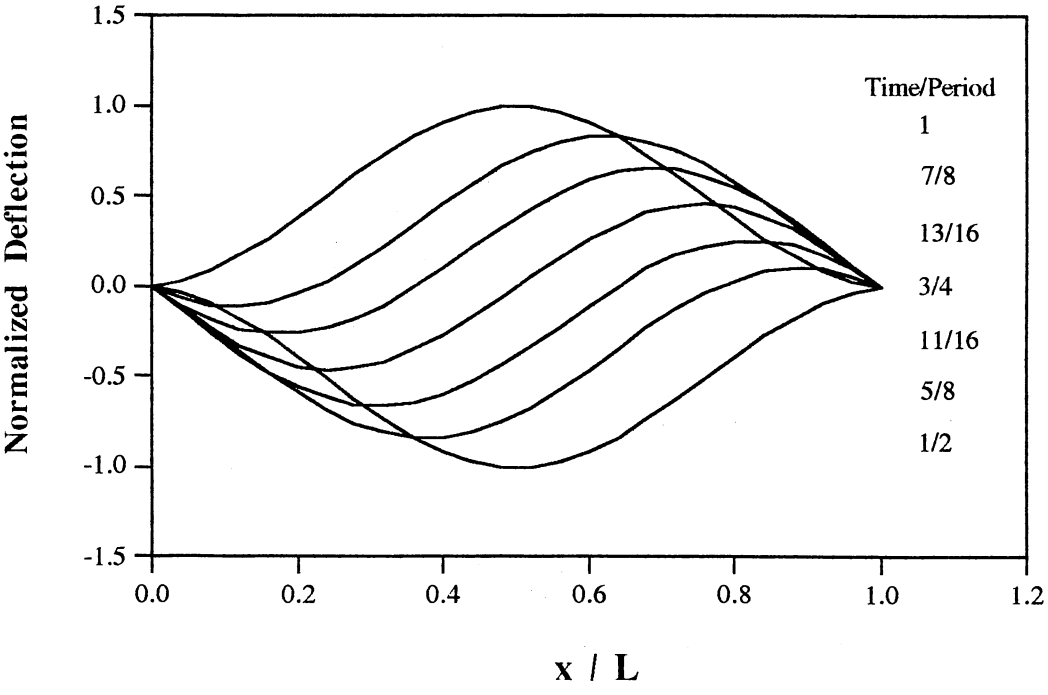

(b) Last Half Cycle

Figure 5 Free Vibration of a Traveling Threadline (v/c = 0.9)

Forced Vibration due to Transverse Excitation

Assume that one of the two boundaries oscillates so that the boundary conditions become

$$\eta(0,t) = C_1 e^{i\omega_1 t} \quad \text{and} \quad \eta(L,t) = 0 \tag{3.1.21}$$

From the above boundary conditions and Eq. (3.1.15)

$$\eta = \frac{C_1\left(\exp\left(\frac{i\omega_1 L}{c-v}\right)\exp\left[i\omega_1\left(t - \frac{x}{c+v}\right)\right] - \exp\left(\frac{-i\omega_1 L}{c+v}\right)\exp\left[i\omega_1\left(t + \frac{x}{c-v}\right)\right]\right)}{\exp\left(\frac{i\omega_1 L}{c-v}\right) - \exp\left(\frac{-i\omega_1 L}{c+v}\right)} \tag{3.1.22}$$

If the other end of the threadline oscillates, then

$$\eta(0,t) = 0 \quad \text{and} \quad \eta(L,t) = C_2 e^{i\omega_2 t} \tag{3.1.23}$$

Applying the above boundary conditions yields

$$\eta = \frac{C_2\left[\exp\left\{i\omega_2\left(t - \frac{x}{c+v}\right)\right\} - \exp\left\{i\omega_2\left(t + \frac{x}{c-v}\right)\right\}\right]}{\exp\left(\frac{-i\omega_2 L}{c+v}\right) - \exp\left(\frac{i\omega_2 L}{c-v}\right)} \tag{3.1.24}$$

Response of the traveling threadline is the sum of Eq. (3.1.22) and Eq. (3.1.24).

3.2 Aerodynamic Forces on an Oscillating Web

In analyzing web flutter the most important and difficult part is the interaction between the web and the surrounding air. The surrounding air can appreciably affect the dynamic characteristics of the web and if the air is flowing the interaction becomes much more complicated. Aerodynamic forces for various situations are discussed in this section. Discussions in this section, along with the study of a traveling string, will provide the basis of analytical modeling of string-mode web flutter.

Radiation Impedance and Air Loading

The concept of radiation impedance is very useful in studying the interaction between the web and stationary air. Radiation impedance is defined as [G12]

$$Z_r = \frac{F}{u} \tag{3.2.1}$$

where F is the force exerted by the air on one side of the web and u is the out-of-plane velocity of the web. Z_r is divided by its real and imaginary parts

$$Z_r = R_r + iX_r \tag{3.2.2}$$

where R_r is the radiation resistance and X_r is the radiation reactance. If we assume that the motion of the surface is harmonic

$$\eta = A e^{i\omega t} \tag{3.2.3}$$

then the total aerodynamic force acting on both sides of the vibrating web is

$$F = 2\dot{\eta}(R_r + iX_r)$$

$$= 2(- \omega X_r + i\omega R_r)\eta \qquad (3.2.4)$$

But

$$F = M_a\ddot{\eta} + B_a\dot{\eta}$$

$$= (- \omega^2 M_a + i\omega B_a)\eta \qquad (3.2.5)$$

where M_a and B_a are the equivalent mass and damping coefficients respectively. Therefore,

$$M_a = \frac{2X_r}{\omega} \qquad (3.2.6)$$

$$B_a = 2R_r \qquad (3.2.7)$$

Radiation Impedance of an Unbaffled Web

The interaction between an unbaffled web (a web having free edges only) and stationary air is considered. Radiation impedance, for small κr (low frequency limit), of an unbaffled circular piston is [G6]

$$Z_r = \rho c_o S\left[\frac{1}{4}(\kappa r)^2 + i\frac{1}{2}\kappa r\right] \qquad (3.2.8)$$

where ρc_o is the characteristic impedance of the undisturbed air, S is the area of the circular piston, κ is the wave number, and r is the radius of the piston. If we consider the equivalent radius of a rectangular piston which has width d and length L

$$r = \sqrt{Ld/\pi} \tag{3.2.9}$$

then the radiation impedance of a rectangular piston becomes

$$Z_r = \rho c_o S\left(\frac{1}{4}\kappa^2\frac{Ld}{\pi} + i\frac{1}{2}\kappa\sqrt{\frac{Ld}{\pi}}\right) \tag{3.2.10}$$

Corresponding added mass and damping coefficients per unit area of the piston are

$$m_a = \frac{2X_r}{\omega S} = \frac{\rho c_o \kappa\sqrt{Ld}}{\omega\sqrt{\pi}} \tag{3.2.11}$$

$$b_a = \frac{2R_r}{S} = \frac{\rho c_o \kappa^2 Ld}{2\pi} \tag{3.2.12}$$

But

$$c_o \kappa = \omega$$

Thus

$$m_a = \frac{1}{\sqrt{\pi}}\rho\sqrt{Ld} \tag{3.2.13}$$

$$b_a = \frac{\rho\omega^2 Ld}{2\pi c_o} \tag{3.2.14}$$

It should be noted that the damping term is a function of frequency and its low frequency limit value is zero. If we define the added-mass coefficient C_a by

$$m_a = C_a \frac{\pi}{4} \rho d \tag{3.2.15}$$

then, with the slenderness ratio defined by s = L/d,

$$C_a = \frac{4}{\pi^{1.5}} \sqrt{s}$$

$$= 0.718 \sqrt{s} \tag{3.2.16}$$

The above expression is valid only when the slenderness ratio is neither very small nor very large. For a slender ($d << L$) web [G2]

$$C_a = 1.0 \tag{3.2.17}$$

A closed form solution of radiation impedance of a rectangular web having arbitrary slenderness ratio is very difficult to obtain if not impossible. Numerical data of radiation reactance (or added mass) are available for a few values of slenderness ratio [G10]. Because of the analytical difficulties, fluid loading for a rectangular web is usually obtained by experimental methods. Available experimental and numerical data along with empirical formulae are compared with Eq. (3.2.16) in Figure 6. Empirical formulae are listed below:

Pabst [G1] $$C_a = 1 - \frac{1}{2s} \tag{3.2.18}$$

Yu [G3] $$C_a = \frac{1}{\sqrt{1 + 1/s^2}} \tag{3.2.19}$$

Blagov. [G8] $$C_a = \frac{1}{\sqrt{1 + 1/s^2}}\left(1 - 0.425\,\frac{s}{1 + s^2}\right) \tag{3.2.20}$$

Povisky [G8] $$C_a = \frac{1}{1 + 0.8/s} \tag{3.2.21}$$

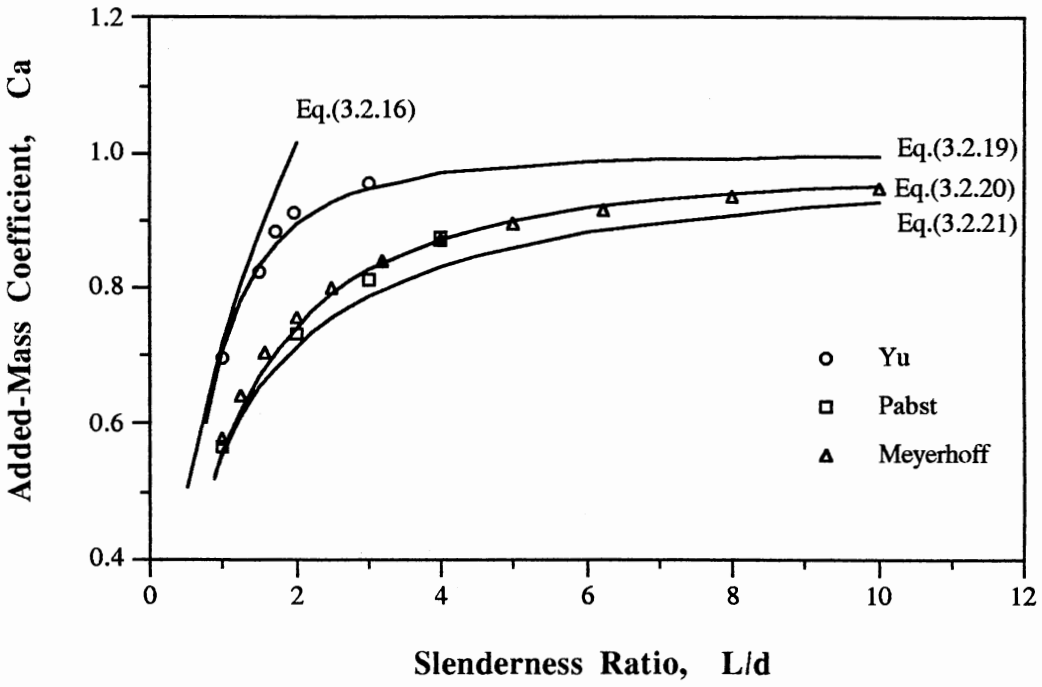

Figure 6 Added-Mass Coefficient of an Unbaffled Rectangular Web

It is found that the approximation, Eq. (3.2.16), overestimates. Pabst's experimental results and Meyerhoff's computational results agree very well. Both Eq. (3.2.18) and Eq. (3.2.20) are based on the same experimental data obtained by Pabst, but the latter fits better. Blagoveshchensky's formula, Eq. (3.2.20), is recommended. There is one thing

that needs to be noted. Keulegan and Carpenter [G4] found that the added-mass coefficient of a plate in an oscillating fluid is a function of the Keulegan-Carpenter number defined as

$$KC = \frac{A\,\tau}{d} \tag{3.2.22}$$

where A is the amplitude of flow oscillation, τ is the period of oscillation, and d is the width of plate. The change of added mass with the Keulegan-Carpenter number is believed to be related to the change of vortices. Therefore, the differences in the experimental data might be caused by the differences in the vibration frequency, amplitude, and sizes of the tested plates.

Radiation Impedance of a Baffled Web

A baffle is an acoustic barrier which is in-plane with the web. The radiation impedance of a baffled circular piston is [G9]

$$Z_r = \pi r^2 \rho c_o(\theta_o + i\chi_o) \tag{3.2.23}$$

where

$$\theta_o = 1 - \frac{1}{2\kappa r} J_1(2\kappa r) \tag{3.2.24}$$

$$\chi_o = \frac{4}{\pi}\int_0^{\pi/2} \sin(2\kappa r \cos\alpha)\sin^2\alpha\, d\alpha \tag{3.2.25}$$

which, for low frequency limit ($\kappa r << 1$), converges to

$$\theta_o = \frac{1}{2}(\kappa r)^2$$

$$\chi_o = \frac{8}{3}\frac{\kappa r}{\pi}$$

If again we use the equivalent area, then

$$\theta_o = \frac{1}{2}\kappa^2(Ld/\pi) \tag{3.2.26}$$

$$\chi_o = \frac{8\kappa}{3\pi}\sqrt{Ld/\pi} \tag{3.2.27}$$

The added mass becomes

$$m_a = \frac{2X_r}{\omega \pi r^2}$$

$$= \frac{16}{3\pi^{1.5}}\rho\sqrt{Ld} \tag{3.2.28}$$

from which the added-mass coefficient is obtained as

$$C_a = \frac{64}{3\pi^{2.5}}\sqrt{s}$$

$$= 1.22\sqrt{s} \tag{3.2.29}$$

Radiation impedance of a rectangular piston is [G9]

$$Z_r = \frac{\rho c_o Ld}{L^2 - d^2}\left[L^2\theta(\kappa L) - d^2\theta(\kappa d) + i\,L^2\chi(\kappa L) - i\,d^2\chi(\kappa d)\right] \tag{3.2.30}$$

where

$$\theta(z) = \frac{2}{z^2}\int_0^z \theta_o(y)\, y\, dy = 1 - 4\frac{1 - J_o(z)}{z^2} \tag{3.2.31}$$

$$\chi(z) = \frac{2}{z^2}\int_0^z \chi_o(y)\, y\, dy = \frac{8}{\pi z}\left[1 - \frac{1}{z}\int_0^{\pi/2} \sin(z\cos u)\, du\right] \tag{3.2.32}$$

Limit values, for $z << 1$, are

$$\theta = z^2/16$$

$$\chi = 8z/9\pi$$

Therefore,

$$Z_r = \rho c_o Ld\left[\frac{1}{16}\kappa^2(L^2 + d^2) + i\frac{8}{9\pi}\kappa\frac{L^2 + Ld + d^2}{L + d}\right] \tag{3.2.33}$$

The added mass is

$$m_a = \frac{2X_r}{\omega Ld}$$

$$= \frac{16}{9\pi}\rho d\left(1 + \frac{s^2}{1 + s}\right) \tag{3.2.34}$$

from which the added-mass coefficient is obtained as

$$C_a = \frac{64}{9\pi^2}\left(1 + \frac{s^2}{1+s}\right)$$

$$= 0.721\left(1 + \frac{s^2}{1+s}\right) \qquad (3.2.35)$$

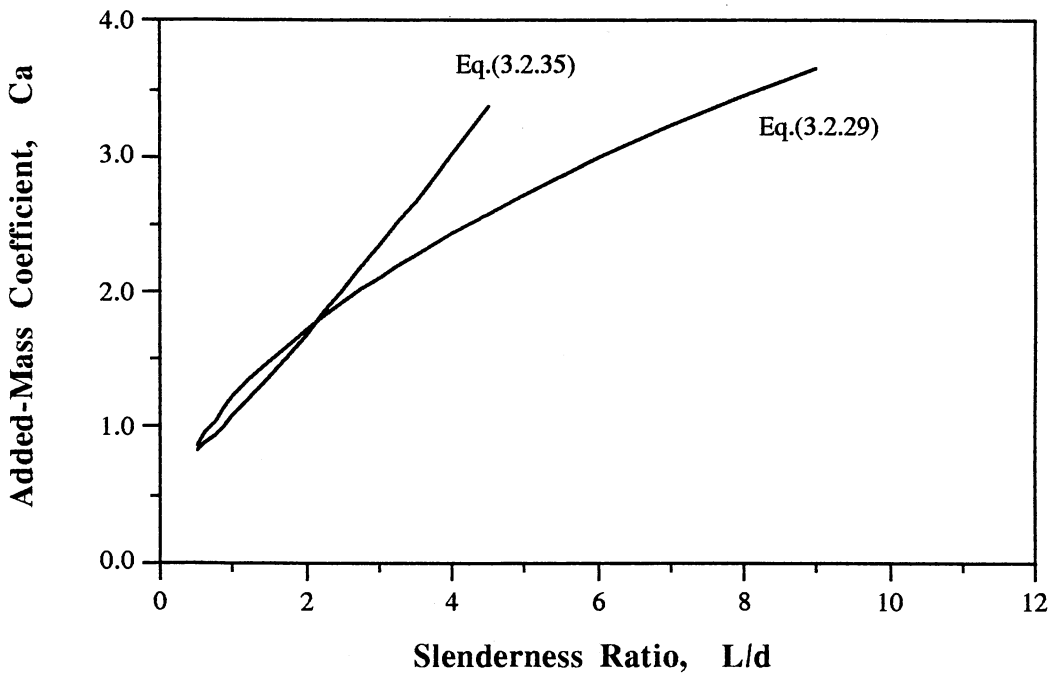

Figure 7 Added-Mass Coeffient of a Baffled Rectangular Web

As shown in Figure 7, the two equations (3.2.29) and (3.2.35) agree well if the slenderness ratio is in the range of

$$0.5 < s < 2.5 \qquad (3.2.36)$$

If the slenderness ratio is very small or very large then both equations are invalid. A more refined formula which is valid in a wider range of slenderness ratio needs to be obtained.

Radiation Impedance for Ripples Having Short Wavelength

Consider a traveling wave on a web as shown in Figure 8, where $\lambda \ll d$ and $\lambda \ll L$. Web displacement is assumed as

$$\eta = A e^{i(\omega t - \kappa x)} \tag{3.2.37}$$

then the pressure wave in the upper half space ($z > 0$) of the air can be written as

$$p(x,z,t) = \tilde{p} e^{i(\omega t - \kappa x - k_z z)} \tag{3.2.38}$$

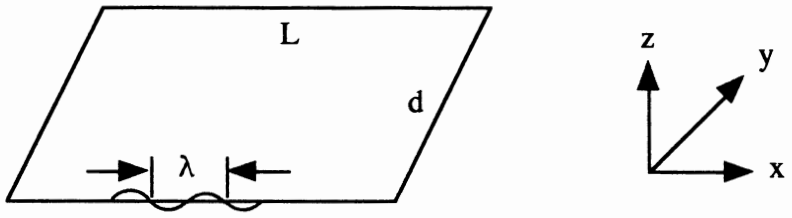

Figure 8 Coordinate System of a Web with Small Ripples

The pressure gradient on the web surface is, from Eq. (3.2.38),

$$\frac{\partial p(x,0,t)}{\partial z} = - i k_z p(x,0,t) \tag{3.2.39}$$

The momentum equation for the air on the web surface is

$$\frac{\partial p}{\partial z} + \rho \frac{\partial^2 \eta}{\partial t^2} = 0 \qquad (3.2.40)$$

For harmonic motion, Eq. (3.2.40) becomes

$$\frac{\partial p}{\partial z} = - i \omega \rho \frac{\partial \eta}{\partial t} \qquad (3.2.41)$$

Substituting Eq. (3.2.41) into Eq. (3.2.39) yields

$$\omega \rho \frac{\partial \eta}{\partial t} = k_z p(x,0,t)$$

Therefore the radiation impedance becomes

$$Z_r = \frac{p(x,0,t)\, S}{\partial \eta / \partial t}$$

$$= \frac{\omega \rho S}{k_z} \qquad (3.2.42)$$

where S is a reference area. Wave equation for the air is

$$\nabla^2 p - \frac{1}{c_o^2} \frac{\partial^2 p}{\partial t^2} = 0 \qquad (3.2.43)$$

Assuming harmonic oscillation

$$\nabla^2 p = - \left(\frac{\omega}{c_o}\right)^2 p$$

$$= - k^2 p \qquad (3.2.44)$$

where c_o and k are sound speed and wave number in the air. Substituting Eq. (3.2.38) into Eq. (3.2.44) yields the relationship among wave numbers

$$\kappa^2 + k_z^2 = k^2 \tag{3.2.45}$$

From which

$$k_z = \pm \sqrt{k^2 - \kappa^2} \tag{3.2.46}$$

Radiation impedance is

$$Z_r = \frac{\omega \rho S}{\pm \sqrt{k^2 - \kappa^2}}$$

If $\kappa < k$ (wave speed on the web c_w is higher than the sound speed in the air c_o), then the impedance is purely resistive and the wave energy is dissipated into the far field of the air. If $\kappa > k$ ($c_w < c_o$), then the impedance is purely reactive and

$$Z_r = \frac{\omega \rho S}{-i\sqrt{\kappa^2 - k^2}}$$

where only negative sign is retained for the pressure wave, expressed by Eq. (3.2.38) and Eq. (3.2.46), to be finite at $z = \infty$. Therefore, the added mass becomes

$$m_a = \frac{2X_r}{\omega S}$$

$$= \frac{2\rho}{\kappa\sqrt{1-(k/\kappa)^2}}$$

From which

$$m_a = \frac{\rho\lambda}{\pi}\frac{1}{\sqrt{1-(c_w/c_o)^2}} \tag{3.2.47}$$

Usually $c_w >> c_o$, so that the above equation becomes

$$m_a = \frac{\rho\lambda}{\pi} \tag{3.2.48}$$

or

$$C_a = \frac{4(\lambda/d)}{\pi^2} \tag{3.2.49}$$

Air Loading of a Slender Web in an Enclosure

Added mass of a slender web surrounded by an enclosure is considered. The air is assumed stationary. The added mass can be calculated by assuming potential flow, obtaining the stream-function by the finite-difference method, summing up the kinetic energy in the flow field, and referring it to the web velocity. A set of sample computations was carried out for the simple geometry shown in Figure 9.

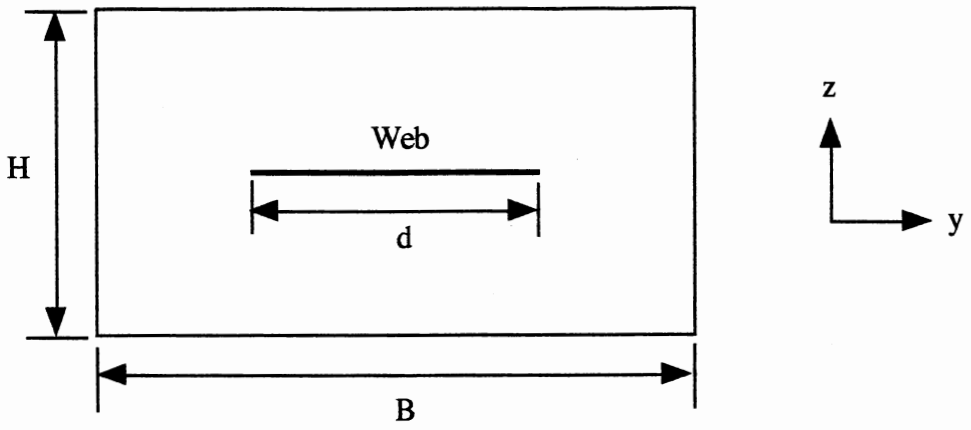

Figure 9 Geometry of Web and Enclosure

For each set of values of H and B, only a quarter of the enclosed air needs to be computed because of symmetry. That quarter was divided into thousands of square cells. The governing equation of two-dimensional motion in an incompressible, inviscid fluid is that the Laplacian of either the velocity potential or the stream-function is equal to zero; this can be changed to a simple finite-difference equation which states that the value of the stream-function at any point is equal to the average of the values at the adjacent points.

$$\psi(i,j) = \frac{1}{4}[\psi(i-1,j) + \psi(i+1,j) + \psi(i,j-1) + \psi(i,j+1)] \qquad (3.2.50)$$

For computational optimization, the following formula was used [G13]

$$\psi(i,j) = (1-\omega)\psi'(i,j) + \frac{1}{4}[\psi(i-1,j) + \psi(i+1,j) + \psi(i,j-1) + \psi(i,j+1)] \qquad (3.2.51)$$

where $\psi'(i,j)$ indicates the previous value, and ω is defined as

$$\omega = \frac{8 - 4\sqrt{4 - \alpha^2}}{\alpha^2} \qquad (3.2.52)$$

$$\alpha = \cos(\pi/m) + \cos(\pi/n)$$

and m and n are the total numbers of increments into which the horizontal and vertical sides of the rectangular region are divided. Boundary conditions used were unit velocity at the web ($U_z = -\partial\psi/\partial y = 1$), parallel flow at the wall (ψ = constant), and zero horizontal velocity in the (horizontal) plane of the web ($U_y = \partial\psi/\partial z = 0$).

From the resulting stream-function, the velocity components in each cell were then calculated relative to the unit vertical velocity of the web, and the total kinetic energy in the flow field summed up. Since the nominal velocity of the web was taken as unity, the added mass was obtained by setting this kinetic energy equal to 1/2 m_1. The results are shown in Figure 10. As expected, C_a approaches 1.0 when the height and width of the enclosure are much larger than the web width. For smaller enclosures, both width and height affect C_a significantly.

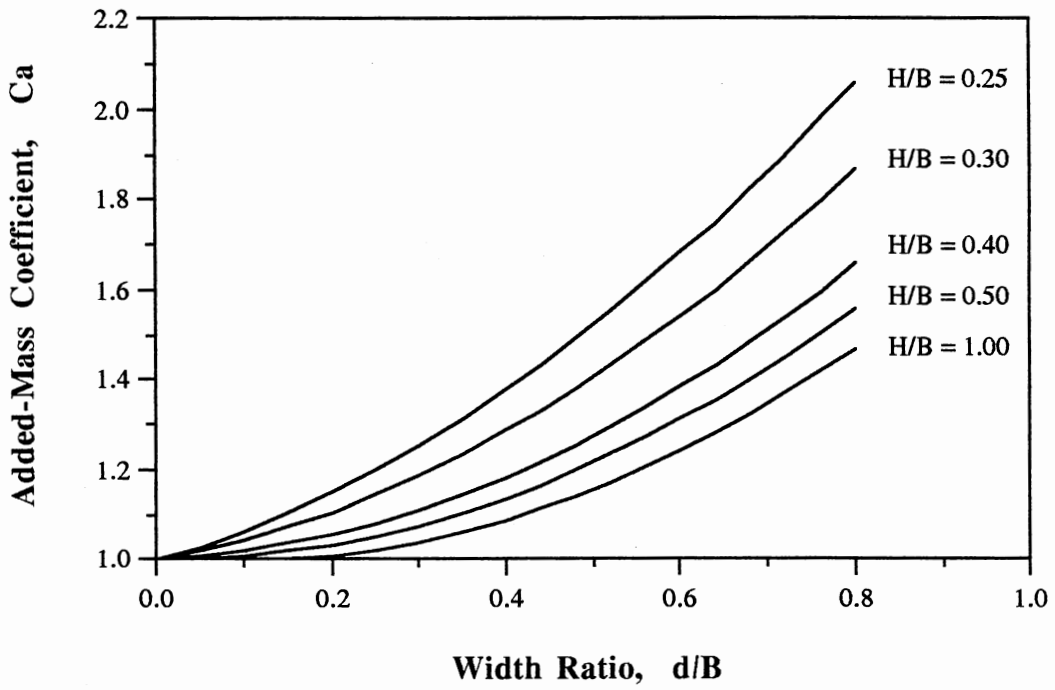

Figure 10 Added-Mass Coefficient of a Web in an Enclosure

Air Loading of a Web in an Air Flow

The air loading of a web subjected to a steady, in-plane (parallel to the web) air flow is considered. For supersonic flow cases, depending on the Mach number range of interest we can use different expressions of aerodynamic pressure [D5]: (1) linearized supersonic theory (M > 1), (2) quasi-steady theory ($M > \sqrt{2}$), and (3) linear piston theory (M >> 1). The piston theory is widely used as a very powerful and convenient tool for hypersonic problems. For subsonic cases, the air loading of a rectangular web cannot be expressed in such a simple form as for the supersonic case. Fortunately, if the web is slender (narrow and long, d << L), we can use the so called "swimming slender fish" model of Lighthill [G5]. This section discusses how the "swimming slender fish" model can be expanded for general applications.

Swimming Slender Fish Model. The lift per unit area of a slender body swimming in the negative x direction is [G5]

$$F = -\frac{\pi}{4}\rho d\left(\frac{\partial}{\partial t} + U\frac{\partial}{\partial x}\right)^2 \eta$$

$$= -\frac{\pi}{4}\rho d\left(\frac{\partial^2 \eta}{\partial t^2} + 2U\frac{\partial \eta}{\partial x} + U^2\frac{\partial^2 \eta}{\partial x^2}\right) \qquad (3.2.53)$$

It is seen that Eq. (3.2.53) has the same form as the dynamic terms of a traveling threadline. If we include the above aerodynamic terms then the equivalent mass of a traveling web becomes

$$m + \frac{\pi}{4}\rho d$$

It is known [D4] that the slender body theory for a wing is valid if the aspect ratio is not greater than one

$$A_R \leq 1$$

that is

$$s = L/d \geq 1$$

If the above result is applicable to web flutter then we can use the "swimming slender fish" model for a wide range of flutter problems. But, for practical applications, we need to consider those cases where (1) the web is not slender, i.e., d > L, and (2) the flow field is not uniform because of complex geometries and ventilation systems.
For the case where the swimming fish model is not valid the aerodynamic force can be generalized as

$$F = -\left(m_1 \frac{\partial^2 \eta}{\partial t^2} + 2m_2 U \frac{\partial^2 \eta}{\partial t \partial x} + m_3 U^2 \frac{\partial^2 \eta}{\partial x^2}\right) \tag{3.2.54}$$

where m_1, m_2, and m_3 are the aerodynamic masses associated with transverse, Coriolis, and centripetal accelerations respectively, and U is a reference velocity. The above form of aerodynamic loading seems proper for a wide range of air-web interaction problems. Therefore, our purpose is to determine the (equivalent) aerodynamic masses for each case we are interested in.

Air Loading due to Transverse Acceleration The mass m_1 (or m_a) is associated with transverse acceleration. Some limiting cases for evaluating m_1 are:

(1) If the span L is much longer than the web width d (the "slender body" case), the midspan section undergoes almost uniform deflection and the air moves largely around the edges of the web, then the added mass per unit area of the web due to the potential-flow field becomes

$$m_1 = \frac{\pi}{4}\rho d \tag{3.2.55}$$

(2) If the web shows higher-mode transverse ripples, with a wave length much shorter than the width of the web d, the added mass is

$$m_1 = \frac{\rho\lambda}{\pi} \tag{3.2.56}$$

(3) For comparison, the added mass of an unbaffled rectangular sheet (i.e., having free edges all around) moving as a unit is

$$m_1 = \frac{\pi}{4}\rho d \frac{1}{\sqrt{1 + 1/s^2}}\left(1 - \frac{0.425\,s}{1 + s^2}\right) \tag{3.2.57}$$

where s is the slenderness ratio L/d, and L > d.

(4) On the other hand, the added mass of a baffled rectangular sheet (i.e., surrounded by a fixed plate in the same plane) moving as a unit is

$$m_1 = 0.96\,\rho d\sqrt{s} \tag{3.2.58}$$

This equation is valid only when the slenderness ratio is near one.

These limiting cases give us an indication of the magnitude of m_1. If neither Eq. (3.2.55) nor Eq. (3.2.56) can be applied, the added mass of a web should be between the values given by Eq. (3.2.57) and Eq. (3.2.58), since the ends are baffled while the edges are free. Equations (3.2.57) and (3.2.58) are compared in Figure 11.

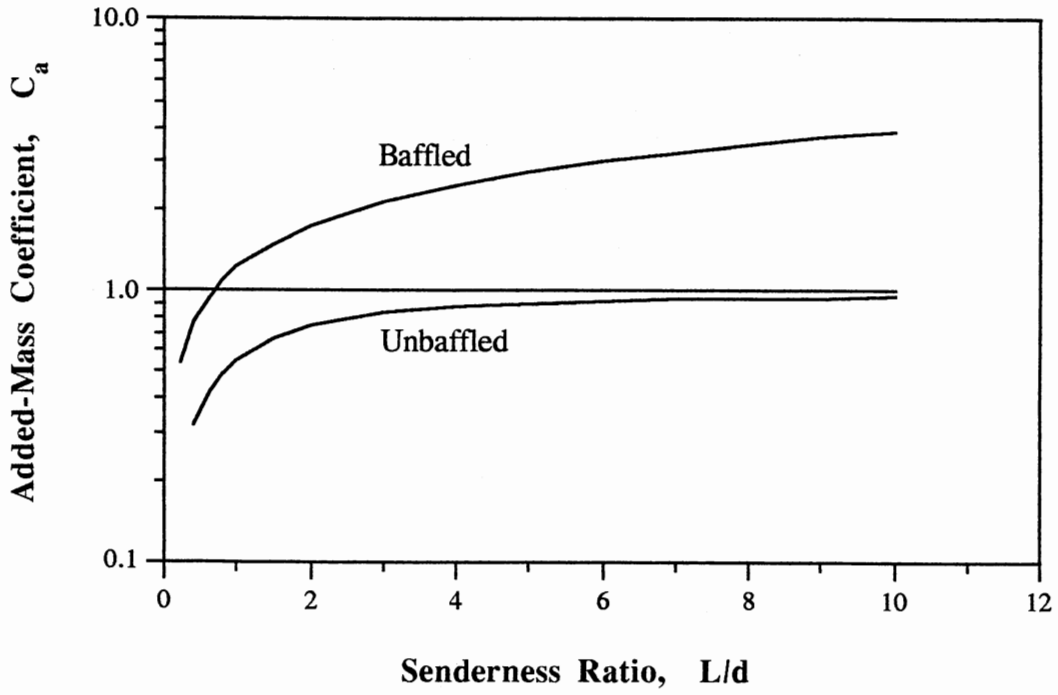

Figure 11 Added-Mass Coefficient of a Rectangular Web

When a web is slender and surrounded by a rectangular enclosure, then m_1 is obtained from Figure 10.

Air Loading due to Coriolis Acceleration. The mass m_2 is associated with the Coriolis force. The effect of the surrounding air depends not only on the amount of air moving, but also on whether it moves with or against the web; if it moves with the web,

the air adds to the mass, if opposite the web motion, it reduces the effective mass. Two limiting cases are:

(1) If the web is slender (L >> d) and also all the air moves with the web, then

$$m_2 = \frac{\pi}{4}\rho d \tag{3.2.59}$$

(2) If the surrounding air is stationary except for a thin boundary layer, the effective mass can be calculated from the integral of the velocity through both upper and lower boundary layer thicknesses

$$m_2 = \rho\left(\delta_U^* + \delta_L^*\right) \tag{3.2.60}$$

where δ^* is the displacement thickness defined as

$$\delta^* = \pm\left|\frac{1}{v}\int_0^{\delta} U(h)\,dh\right| \tag{3.2.61}$$

where the positive sign corresponds to the air flow flowing in the same direction as the running web; while the negative sign is for opposing flow.

Air Loading due to Centripetal Acceleration. The mass m_3 is associated with the centrifugal force due to curvature of the moving web. The effect of the surrounding air depends on the amount of air moving with the web. Two limiting cases are:

(1) If the web is slender (L >> d) and all the air around the web moves with it

$$m_3 = \frac{\pi}{4}\rho d \tag{3.2.62}$$

(2) If the flow field of surrounding air is stationary, and the boundary layer of air moving with the web is relatively thin, the added mass can be calculated from the integral of the square of the velocity of the air U(h) through both boundary layer thicknesses:

$$m_3 = \rho (\theta_U + \theta_L) \tag{3.2.63}$$

where θ is the momentum thickness defined as

$$\theta = \frac{1}{v^2}\int_0^{\delta} U^2(h)\, dh \tag{3.2.64}$$

Note that the equations for boundary layer growth on a flat plate are not applicable to a moving web, since the leading-edge condition is completely different; new calculations and measurements are required.

3.3 String-Mode Instability

Instability of a Running Web

String-mode instability of a web running from one roller to another is considered. The coordinate system is shown in Figure 2(a) on page 2. The governing equation of motion of the web is

$$m\left(\frac{\partial}{\partial t} + v\frac{\partial}{\partial x}\right)^2 \eta - T\frac{\partial^2 \eta}{\partial x^2} + D\frac{\partial^4 \eta}{\partial x^4} = F \tag{3.3.1}$$

which is the same governing equation of a traveling threadline except that the bending stiffness term and aerodynamic term F are added. The aerodynamic force term is, as discussed in Section 3.2,

$$F = -\left(m_1 \frac{\partial^2 \eta}{\partial t^2} + 2m_2 v \frac{\partial^2 \eta}{\partial t \partial x} + m_3 v^2 \frac{\partial^2 \eta}{\partial x^2}\right)$$

The corresponding equation of motion is

$$(m + m_1)\frac{\partial^2 \eta}{\partial t^2} + 2(m + m_2)v\frac{\partial^2 \eta}{\partial t \partial x} + \left[(m + m_3)v^2 - T\right]\frac{\partial^2 \eta}{\partial x^2} + D\frac{\partial^4 \eta}{\partial x^4} = 0 \qquad (3.3.2)$$

In the above equation, the $(m + m_1)$ term is the inertia associated with transverse acceleration, the $(m + m_2)$ term is the Coriolis force caused by linear and angular motions, and $(m + m_3)$ term is the centrifugal force caused by curvature of the web.

Static Instability. The last two terms in Eq. (3.3.2) are restoring forces; the web becomes statically unstable (diverges) when these terms vanish. Therefore the critical condition for static instability is

$$\left[(m + m_3)v^2 - T\right]\frac{\partial^2 \eta}{\partial x^2} + D\frac{\partial^4 \eta}{\partial x^4} = 0 \qquad (3.3.3)$$

Assume a solution as

$$\eta = A e^{i\kappa x} \qquad (3.3.4)$$

then Eq. (3.3.3) becomes

$$-(m + m_3)v^2 + T + D\kappa^2 = 0 \tag{3.3.5}$$

from which

$$v_{div} = \sqrt{\frac{T + D\kappa^2}{m + m_3}} \tag{3.3.6}$$

or in a nondimensional form

$$\left(\frac{v}{c}\right)_{div} = \sqrt{\frac{1 + D_r}{1 + r_3}} \tag{3.3.7}$$

where $c = \sqrt{T/m}$, $D_r = D\kappa^2/T$, and $r_3 = m_3/m$.

Dynamic Instability: Traveling-Wave Solution. Assume a trial solution to Eq. (3.3.2) as

$$\eta = A e^{i(\omega t - \kappa x)} \tag{3.3.8}$$

where the wave number κ is assumed real. By substituting Eq. (3.3.8) into the governing equation (3.3.2) we get the characteristic equation

$$(m + m_1)\omega^2 - 2(m + m_2)v\,\kappa\omega + \left[(m + m_3)v^2 - T\right]\kappa^2 - D\kappa^4 = 0 \tag{3.3.9}$$

or in a nondimensional form

$$(1 + r_1)\left(\frac{\omega}{\kappa c}\right)^2 - 2(1 + r_2)\left(\frac{v}{c}\right)\left(\frac{\omega}{\kappa c}\right) + (1 + r_3)\left(\frac{v}{c}\right)^2 - 1 - D_r = 0 \tag{3.3.10}$$

The two roots of the characteristic equation are

$$\frac{\omega}{\kappa c} = \frac{(1 + r_2)(\frac{v}{c}) \pm \sqrt{(1 + r_2)^2(\frac{v}{c})^2 - (1 + r_1)(1 + r_3)(\frac{v}{c})^2 + (1 + r_1)(1 + D_r)}}{1 + r_1} \tag{3.3.11}$$

If the two roots are real, then the system is dynamically neutral and the two roots represent nondimensional phase speeds. For the web to be (dynamically) unstable the roots should have imaginary parts. In that case the real part of the roots is

$$(\frac{\omega}{\kappa c})_R = \frac{(1 + r_2)}{1 + r_1}(\frac{v}{c}) \tag{3.3.12}$$

which implies that the phase speed is

$$c_w = \frac{\omega}{\kappa} = \frac{(1 + r_2)}{1 + r_1} v \tag{3.3.13}$$

The critical condition for dynamic instability is obtained by equating the discriminant in Eq. (3.3.11) to be zero

$$(\frac{v}{c})_{flt} = \sqrt{\frac{(1 + r_1)(1 + D_r)}{(1 + r_1)(1 + r_3) - (1 + r_2)^2}} \tag{3.3.14}$$

The above equation implies that if $r_1 = r_2 = r_3$ (for the case of a string or a slender web in an infinite air field moving with the web) the critical speed is infinite; the system can diverge but cannot flutter. If the web is running in a relatively small enclosure so that $1 << r_1$ and $r_2, r_3 << r_1$ then the critical speed for flutter approaches that of divergence. In between those two limiting cases the web has two critical speeds, and the critical speed for flutter is always higher than the critical speed for divergence. Practically it may not be possible to operate the machinery at a speed higher than the critical speed for divergence. But a web can oscillate due to other causes such as tension fluctuation, machinery vibration, and air buffeting.

Dynamic Instability: Modal Solution. Boundary conditions of the web impose more restrictions to the solution, leading to a modal solution. Boundary conditions of the web are

$$\eta(0,t) = 0, \quad \eta(L,t) = 0 \tag{3.3.15}$$

For convenience the characteristic equation (3.3.10) can be rewritten as

$$\left[(1 + r_3)\left(\frac{v}{c}\right)^2 - 1 - D_r\right]\left(\frac{\kappa c}{\omega}\right)^2 - 2(1 + r_2)\left(\frac{v}{c}\right)\left(\frac{\kappa c}{\omega}\right) + (1 + r_1) = 0 \tag{3.3.16}$$

Its two roots are

$$\frac{\kappa c}{\omega} = \frac{(1 + r_2)\left(\frac{v}{c}\right) \pm \sqrt{(1 + r_2)^2\left(\frac{v}{c}\right)^2 - (1 + r_1)\left[(1 + r_3)\left(\frac{v}{c}\right)^2 - 1 - D_r\right]}}{(1 + r_3)\left(\frac{v}{c}\right)^2 - 1 - D_r} \tag{3.3.17}$$

Therefore the solution becomes

$$\eta = \exp(i\omega t)\exp\left[\frac{i\omega(1+r_2)(\frac{v}{c})}{1+D_r-(1+r_3)(\frac{v}{c})^2}\frac{x}{c}\right]\cdot$$

$$\left[A_1\exp\left\{\frac{i\omega\sqrt{Disc}}{1+D_r-(1+r_3)(\frac{v}{c})^2}\frac{x}{c}\right\}+A_2\exp\left\{\frac{-i\omega\sqrt{Disc}}{1+D_r-(1+r_3)(\frac{v}{c})^2}\frac{x}{c}\right\}\right] \tag{3.3.18}$$

The first boundary condition of (3.3.15) yields

$$A_1 + A_2 = 0 \tag{3.3.19}$$

Therefore Eq. (3.3.18) can be simplified as

$$\eta = 2iA_1\exp(i\omega t)\exp\left[\frac{i\omega(1+r_2)(\frac{v}{c})}{1+D_r-(1+r_3)(\frac{v}{c})^2}\frac{x}{c}\right]\cdot$$

$$\sin\left[\frac{\omega\sqrt{Disc}}{1+D_r-(1+r_3)(\frac{v}{c})^2}\frac{x}{c}\right] \tag{3.3.20}$$

By substituting the above equation into the second boundary condition of (3.3.15)

$$\omega\frac{\sqrt{Disc}}{1+D_r-(1+r_3)(\frac{v}{c})^2}\frac{L}{c} = n\pi$$

From which the n^{th} natural frequency becomes

$$\omega_n = \frac{n\pi c}{L}\frac{1+D_r-(1+r_3)(\frac{v}{c})^2}{\sqrt{(1+r_2)^2(\frac{v}{c})^2-(1+r_1)\left[(1+r_3)(\frac{v}{c})^2-1-D_r\right]}} \tag{3.3.21}$$

The effects of aerodynamic terms are sketched in Figure 12 with $D_r = 0$, where $f_n = \omega_n/2\pi$. An increase of m_1 reduces f_n and causes the intercept at the ordinate to be depressed. The critical speed is affected only by the centrifugal inertia; an increase of m_3 reduces the critical speed, causing the intercept at the abscissa to move toward the origin. Coriolis inertia distorts the shape of the frequency curve; it acts in different ways depending on flow direction. Some examples are shown in Figure 13, again with $D_r = 0$. As shown Figure 13(b), the highest frequency curve is obtained when $r_2 = -1$. It should be noted that the curves for $r_2 = 0$ and $r_2 = 2$ overlap those for $r_2 = -2$ and $r_2 = -3$ respectively.

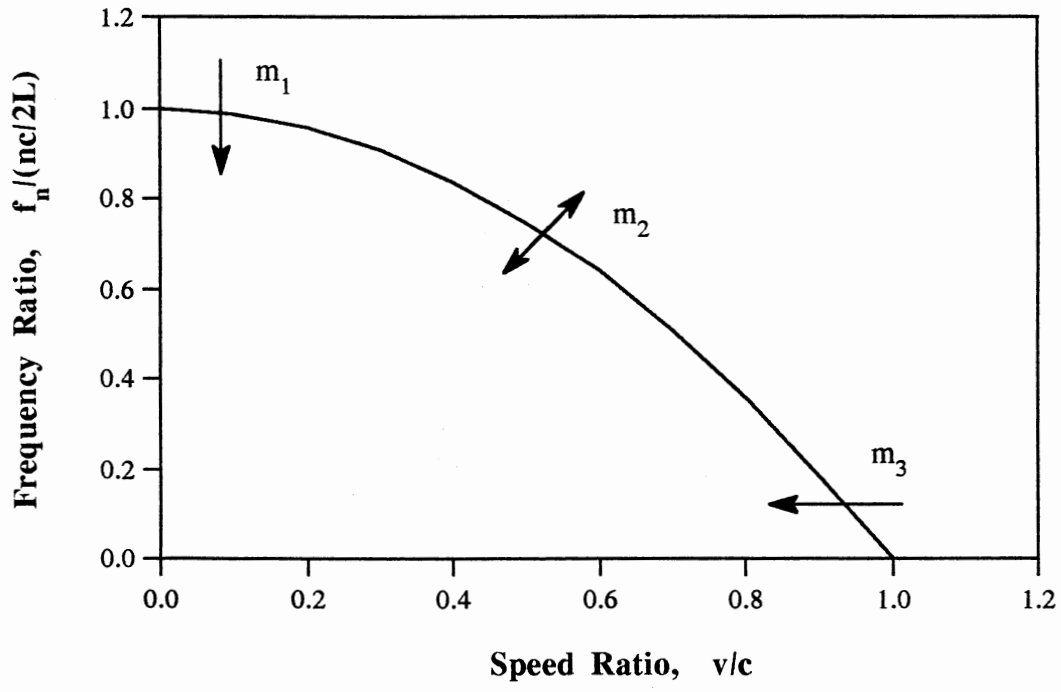

Figure 12 Effect of Aerodynamic Terms on the Dynamics of a Web

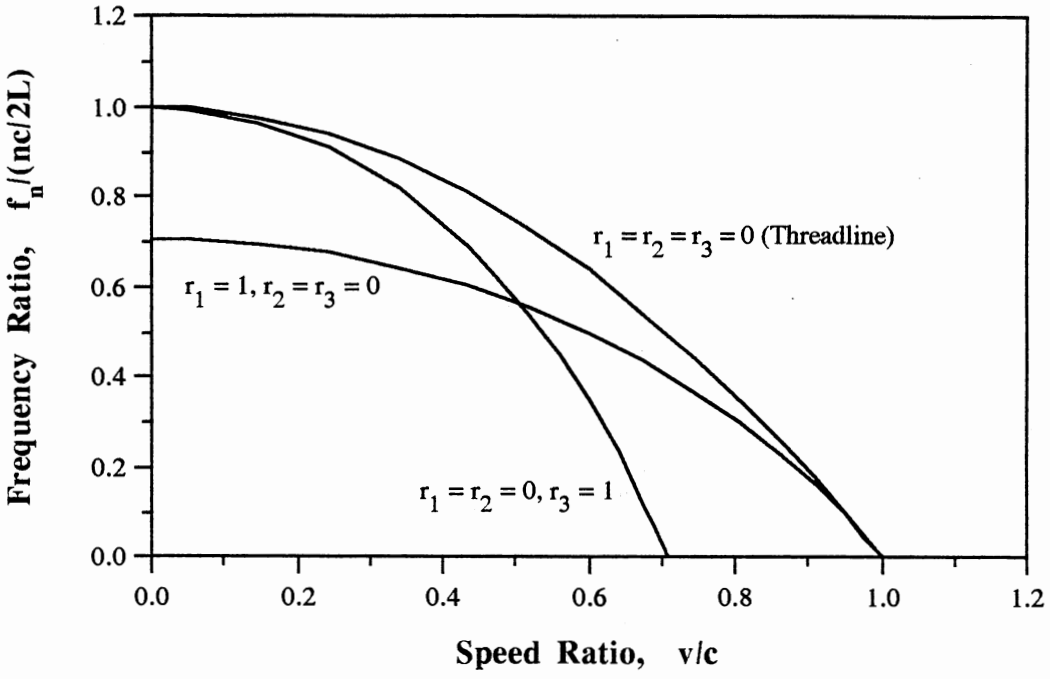

(a) Effect of m_1 and m_3

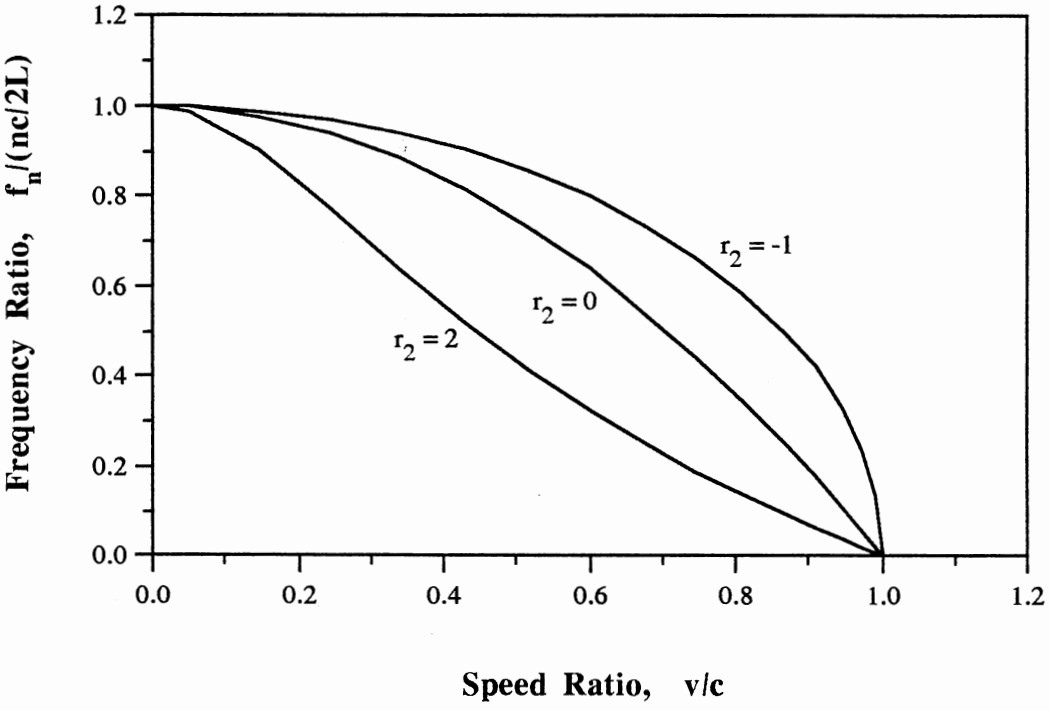

(b) Effect of m_2 ($m_1 = m_3 = 0$)

Figure 13 Effect of Aerodynamic Masses

The modal solution becomes

$$\psi_n(x,t) = \cos\left(\omega_n t + K\frac{v}{c}\frac{n\pi x}{L}\right)\sin\left(\frac{n\pi x}{L}\right) \tag{3.3.22}$$

where

$$K = \frac{(1 + r_2)}{\sqrt{(1 + r_2)^2\left(\frac{v}{c}\right)^2 - (1 + r_1)\left[(1 + r_3)\left(\frac{v}{c}\right)^2 - 1 - D_r\right]}}$$

The sine term is equivalent to the mode shape of a nontraveling string and the cosine term incorporates phase difference along the length of the web. $K = 1$ for a traveling threadline.

Instability of a Stationary Web in a Wind

The string-mode instability of a nontraveling web in an air flow is considered. The governing equation of motion of a stationary web in a wind is

$$(m + m_1)\frac{\partial^2\eta}{\partial t^2} + 2m_2 U\frac{\partial^2\eta}{\partial t\partial x} + (m_3 U^2 - T)\frac{\partial^2\eta}{\partial x^2} + D\frac{\partial^4\eta}{\partial x^4} = 0 \tag{3.3.23}$$

Static Instability. The critical air speed for static instability is obtained by letting the restoring force term be zero:

$$U_{div} = \sqrt{\frac{T + D\kappa^2}{m_3}} \tag{3.3.24}$$

For a slender web in an infinite uniform flow field

$$U_{div} = \sqrt{\frac{4(T + D\kappa^2)}{\pi\rho d}} \tag{3.3.25}$$

which is a function of web width but independent of web mass.

Dynamic Instability: Traveling-Wave Solution. In the same way as before, the characteristic equation is

$$(m + m_1)\omega^2 - 2m_2 U\kappa\omega + (m_3 U^2 - T)\kappa^2 - D_x\kappa^4 = 0 \qquad (3.3.26)$$

or in a nondimensionalized form

$$(1 + r_1)(\frac{\omega}{\kappa c})^2 - 2r_2(\frac{U}{c})(\frac{\omega}{\kappa c}) + r_3(\frac{U}{c})^2 - 1 - D_r = 0 \qquad (3.3.27)$$

The roots of the characteristic equation are

$$\frac{\omega}{\kappa c} = \frac{r_2(\frac{U}{c}) \pm \sqrt{(1 + r_1)(1 + D_r) - (r_3 + r_1 r_3 - r_2^2)(\frac{U}{c})^2}}{1 + r_1} \qquad (3.3.28)$$

The system becomes unstable when a root has a non-zero imaginary part. The phase speed of wave for a dynamically unstable system is

$$c_w = \frac{r_2}{1 + r_1} U \qquad (3.3.29)$$

The critical flow speed for flutter is obtained by letting the discriminant be zero

$$(\frac{U}{c})_{flt} = \sqrt{\frac{(1 + r_1)(1 + D_r)}{r_3 + r_1 r_3 - r_2^2}} \qquad (3.3.30)$$

For a slender web in an infinite uniform flow field

$$(\frac{U}{c})_{flt} = \sqrt{(1 + \frac{1}{r})(1 + D_r)} \tag{3.3.31}$$

or

$$U_{flt} = \sqrt{\frac{T}{m}}\sqrt{(1 + \frac{4m}{\pi\rho d})(1 + \frac{D\kappa^2}{T})} \tag{3.3.32}$$

Figure 14 shows the effect of mass ratio on the critical flow speed for D = 0. Practically, the mass ratio can have fairly high value, and the critical flow speed for flutter is close to the wave speed in vacua.

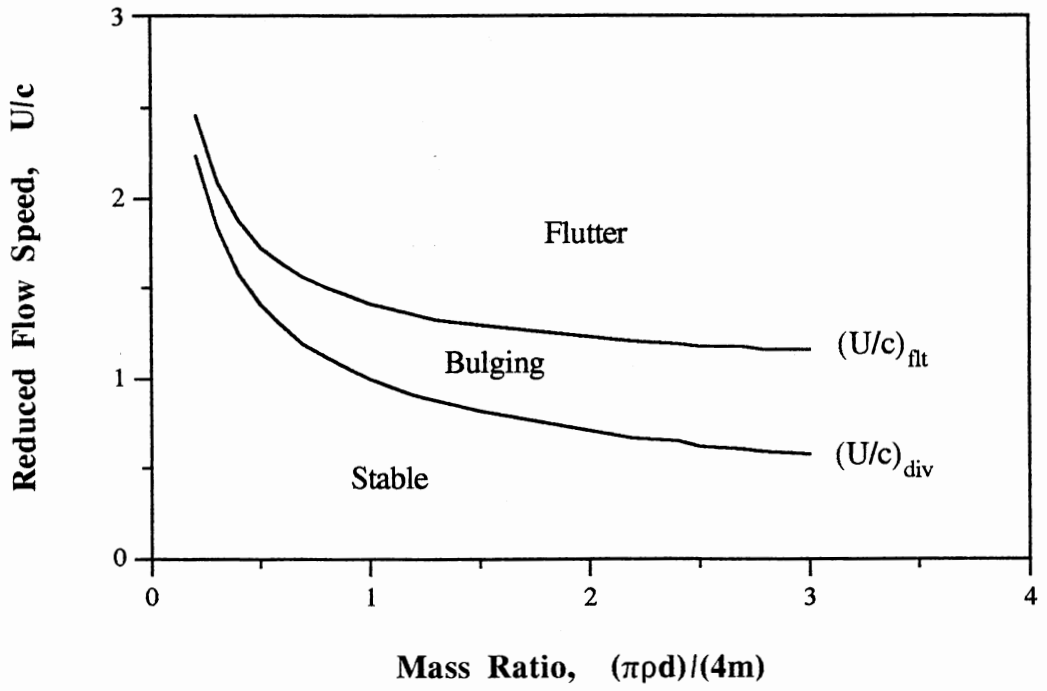

Figure 14 Stability Boundaries and Mass Ratio

Dynamic Instability: Modal Solution. The characteristic equation (3.3.28) can be rewritten as

$$\left[1 + D_r - r_3\left(\frac{U}{c}\right)^2\right]\left(\frac{\kappa c}{\omega}\right)^2 + 2r_2\left(\frac{U}{c}\right)\left(\frac{\kappa c}{\omega}\right) - (1 + r_1) = 0 \qquad (3.3.33)$$

The roots of the above equation are

$$\frac{\kappa c}{\omega} = \frac{-r_2\left(\frac{U}{c}\right) \pm \sqrt{(1 + r_1)(1 + D_r) - (r_3 + r_1 r_3 - r_2^2)\left(\frac{U}{c}\right)^2}}{1 + D_r - r_3\left(\frac{U}{c}\right)^2} \qquad (3.3.34)$$

Therefore the solution becomes

$$\eta = \exp\left[i\omega\left\{t + \frac{r_2\left(\frac{U}{c}\right)}{1 + D_r - r_3\left(\frac{U}{c}\right)^2}\left(\frac{x}{c}\right)\right\}\right] \cdot$$

$$\left[A_1 \exp\left\{\frac{i\omega\sqrt{\text{Disc}}\left(\frac{x}{c}\right)}{1 + D_r - r_3\left(\frac{U}{c}\right)^2}\right\} + A_2 \exp\left\{\frac{-i\omega\sqrt{\text{Disc}}\left(\frac{x}{c}\right)}{1 + D_r - r_3\left(\frac{U}{c}\right)^2}\right\}\right]$$

The natural frequency is obtained by applying the two boundary conditions (3.3.15).

$$\omega_n = \frac{n\pi c}{L} \frac{1 + D_r - r_3\left(\frac{U}{c}\right)^2}{\sqrt{(1 + r_1)(1 + D_r) - (r_3 + r_1 r_3 - r_2^2)\left(\frac{U}{c}\right)^2}} \qquad (3.3.35)$$

The corresponding mode shape is

$$\psi_n(x,t) = \cos\left(\omega_n t + K\frac{U}{c}\frac{n\pi x}{L}\right)\sin\left(\frac{n\pi x}{L}\right) \qquad (3.3.36)$$

where

$$K = \frac{r_2}{\sqrt{(1 + r_1)(1 + D_r) - (r_3 + r_1 r_3 - r_2^2)(\frac{U}{c})^2}}$$

CHAPTER IV

EXPERIMENTS

4.1 String-Mode Instability

Test Setup

Flow tests were performed in order to verify the effects of air flow discussed in Chapter III. Rectangular paper webs were tested in a subsonic wind tunnel. The characteristics of the tested paper webs are such that:

Basis weight	1.08×10^{-4} Lb/in^2
Young's modulus	9.9×10^5 psi
Thickness	4 mils
Dimensions	3"x 10" ($A_R = 0.30$)
	3"x 20" ($A_R = 0.15$)
	6"x 10" ($A_R = 0.60$)
	6"x 20" ($A_R = 0.30$)

Basis weight and thickness were measured by using precision measuring tools. Young's modulus was measured using an axial vibration technique; details are explained in the Appendix.

A schematic of the whole setup is shown in Figure 15. The test section is 24.5 inches wide and 16.25 inches high. The tested paper webs are narrow enough comparing to the tunnel dimensions so that the web can be considered to be in an infinite, uniform flow field. The leading and trailing edges are restrained from vertical motion; while the other two edges are free to move.

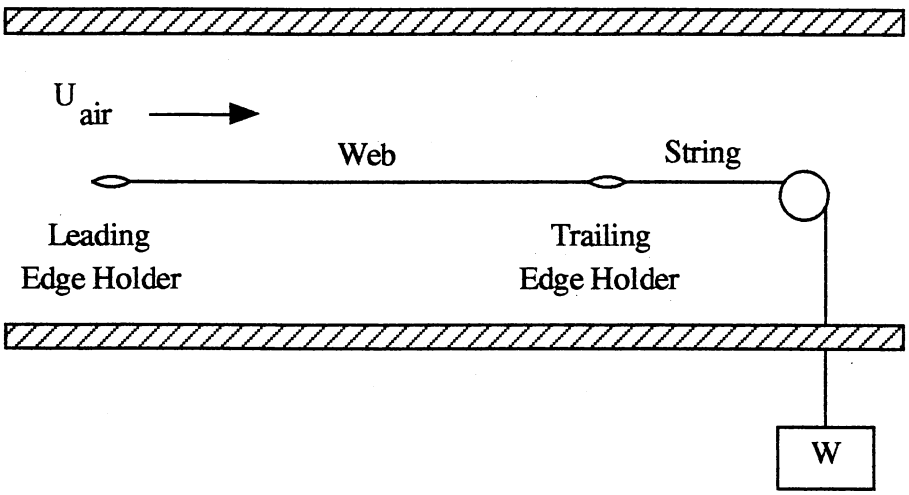

Figure 15 A Schematic of the Experimental Setup

In order to implement the desired boundary conditions of the web, a set of web holder, shown in Figure 16, was used. All the parts were made from thin aluminum plates and aligned carefully to minimize any undesirable aerodynamic effects such as asymmetric air flow and aero-excitation. The parts at which the web was attached have a streamlined shape. The only aerodynamic problem encountered was the drag on the moving part of trailing edge holder. This problem was solved by measuring the air drag and modifying the tension values. The leading edge is fixed, while the trailing edge can slide in the direction of the air flow. Tension is applied through the trailing edge, by using a thin string and a pulley mounted downstream of the test section, and a weight. Web tension could be changed by changing the weight. The test variables are (1) the width and length of the web, (2) tension, and (3) air speed.

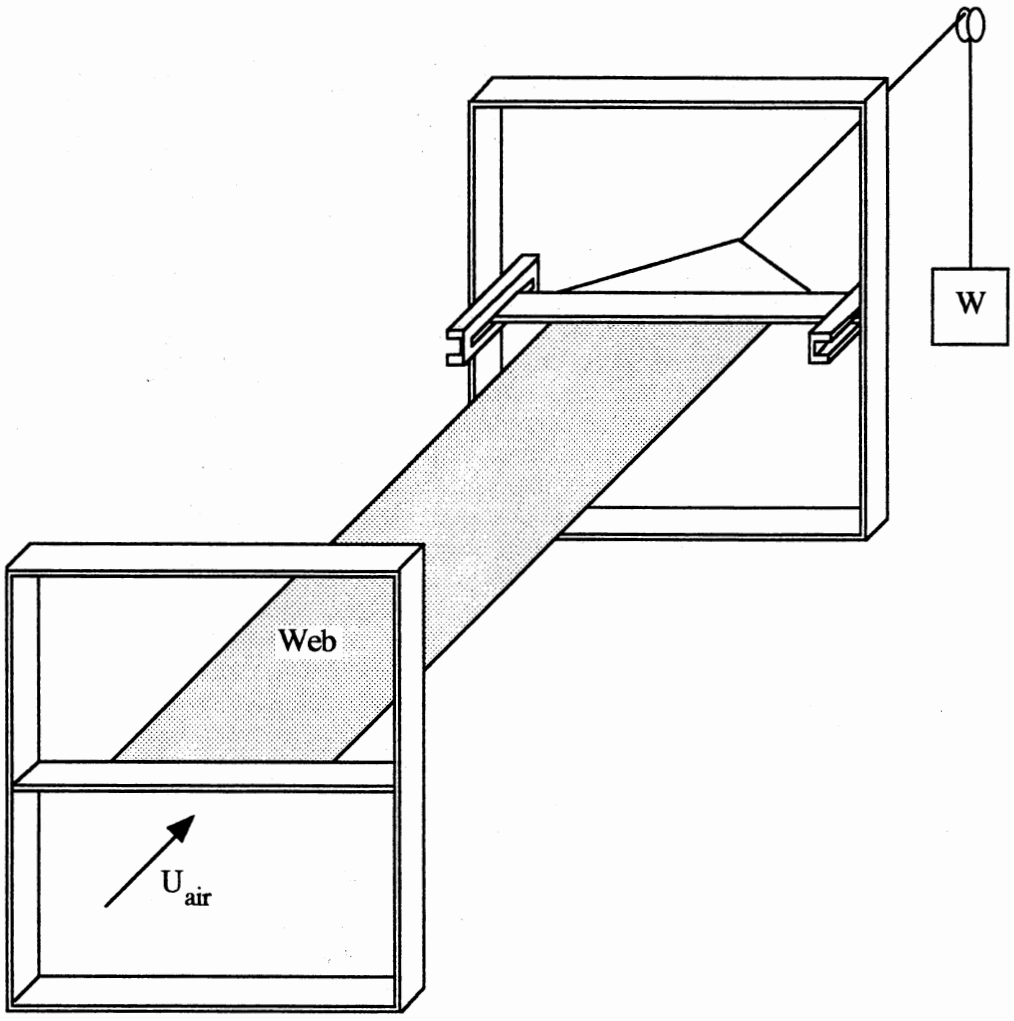

Figure 16 Setup for String-Mode Flutter Tests

Test Results

Both static divergence (steady deflection of the web) and dynamic instability (flutter of the web) were observed. Critical speed for dynamic instability is always higher than that of static instability, as expected from theory. As the wind speed is increased from zero the paper starts to diverge at a critical flow speed; it bulges out either upward or downward. If the flow speed is increased further then the displacement is also increased, and in some cases a higher mode (multiple-wave) divergence occurs as shown in Figure 17. Stearman's tests show no static instability [E2]. That contradiction raises an important question: Can a slender web clamped at its leading and trailing edges experience divergence or not? It is believed that the divergence observed in the present tests is not caused by non-zero angle of attack. The reason is that (1) the bulging occurs either upward or downward, (2) higher mode divergence would not occur in a skewed air flow, and (3) a hot-wires measurement (performed by another group) shows that flow direction does not change in a wide range of flow speed. Stearman [E2] controlled his test setup to compensate the change of flow direction observed in his wind tunnel.

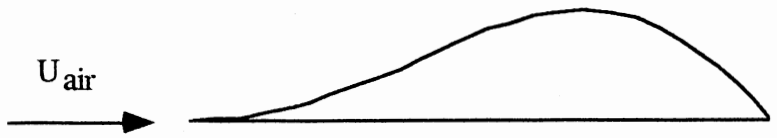

(a) Arch Shape Divergence

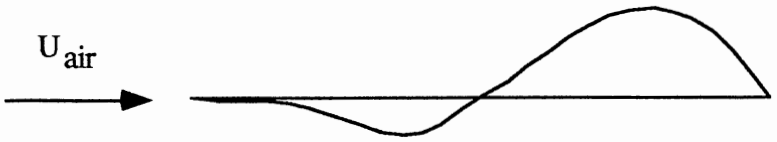

(b) Higher Mode Divergence

Figure 17 Shapes of Bulging

At flow speeds higher than the divergence speed a low-speed traveling wave occurs. The oscillation frequency and amplitude grow with the flow speed into a pronounced flutter, which becomes very violent at higher flow speeds. In some cases static divergence is suddenly changed to flutter by a little increase of the flow speed, in other cases there is a stable range between static and dynamic instability regions. Stearman observed two types of flutter: small-amplitude slow wave and large-amplitude fast wave [E2]. He could determine the critical flow speeds for those two types of flutter. In the present tests, the small-amplitude slow wave was not always observed.

Critical flow speeds for static instability and flutter were determined for each set of test conditions, i.e., for given web dimensions and tension. Figure 18 shows the stability boundaries of static divergence; each data point indicates a critical value of dynamic pressure q above which bulging occurs. The compared theoretical curve is

$$q = (\frac{2}{\pi})(\frac{T}{d}) \tag{4.1.1}$$

which is a variation of Eq. (3.3.25) with the effect of bending stiffness neglected. The experimental results are higher than the expected values, but they show the same tendency. The discrepancy manifests the inaccuracy of the centrifugal inertia term of the slender-body theory for the test model which has an arch-shaped deflection.

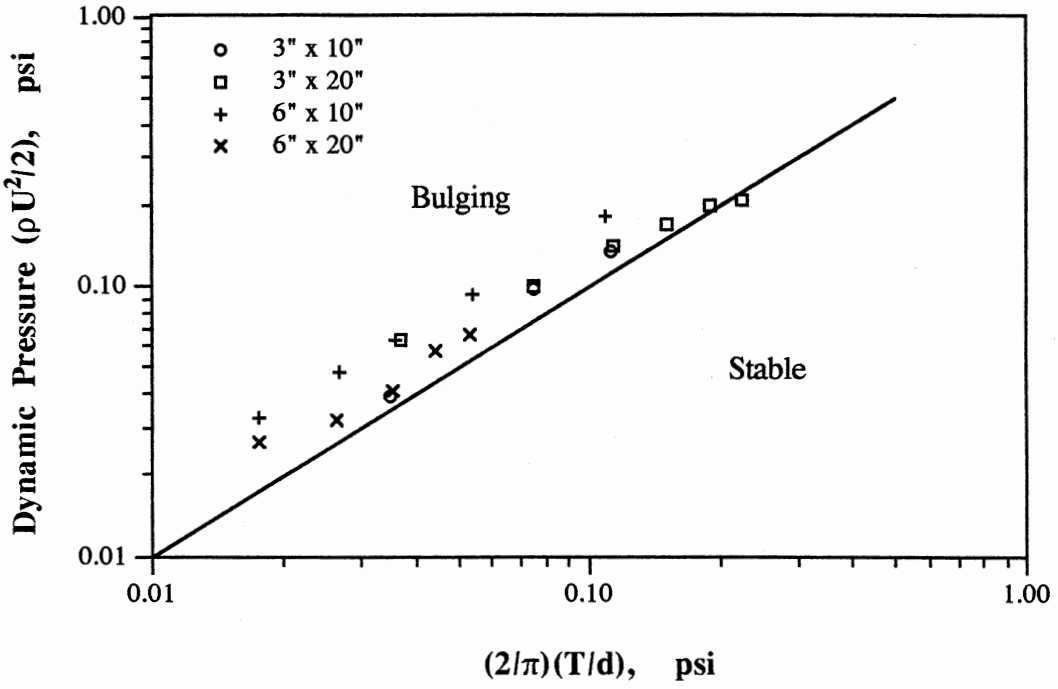

Figure 18 Static Stability Criteria of a Stationary Web in an Air Flow

The experimental results for flutter are compared with a theoretical curve in Figure 19, where the curve is

$$q = \left(\frac{2}{\pi} + \frac{\rho d}{2m}\right)\left(\frac{T}{d}\right) \tag{4.1.2}$$

which is from Eq. (3.3.32) neglecting the effect of bending stiffness. The experimental values fall below the prediction curve.

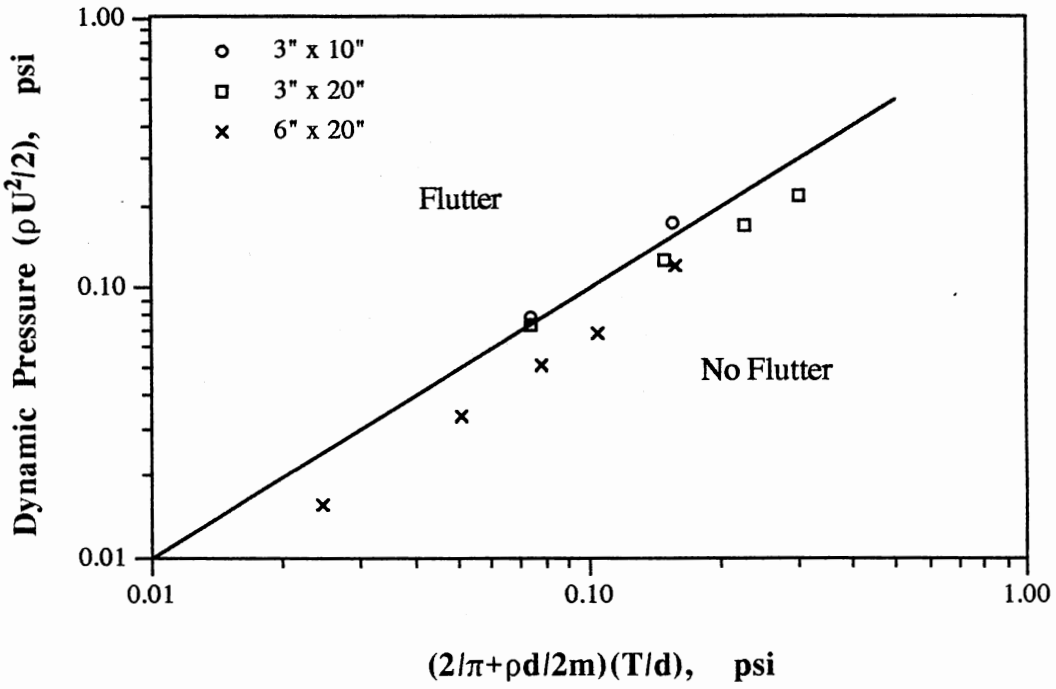

Figure 19 Dynamic Stability Criteria of a Stationary Web in an Air Flow

4.3 Edge Flutter

Test Setup

In paper machines, dryer felts cause complex, three-dimensional air flows. Also, the traveling speed of web and the interaction between the felt and paper web have appreciable effects on web dynamics. The experimental model is a non-traveling web in a uniform air flow. The test web simulates either edge of paper in a dryer section; the trailing edge of the test web is free while the other sides are fixed as shown in Figure 20. Tension is applied in the cross-flow direction to simulate machine-directional tension in paper machines.

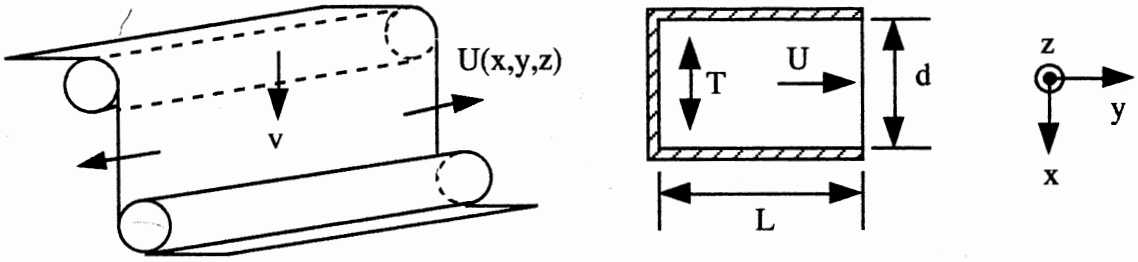

Figure 20 Experimental Modeling of Edge Flutter

In order to implement the test conditions, a web-holding jig, shown in Figure 21 and Figure 22, was mounted in the same wind tunnel described in Section 4.1. One side of the clamp is a slider, at which two weights are connected for tension control. The components in contact with the aluminum slider were made of brass for minimal friction. In order to obtain uniform tension distribution, the leading edge area of the web has holes and parallel cuts and the upstream clamp would be released and fastened again whenever tension is changed. Paper webs were used in the first series of experiments, but it was very difficult to obtain uniform tension distribution. Later, stretchable plastic materials were tested with ease of setting up. Straight lines were drawn on the web, one-inch apart in both x and y directions, for better observation of web motions. Material properties and test conditions are summarized in Table II.

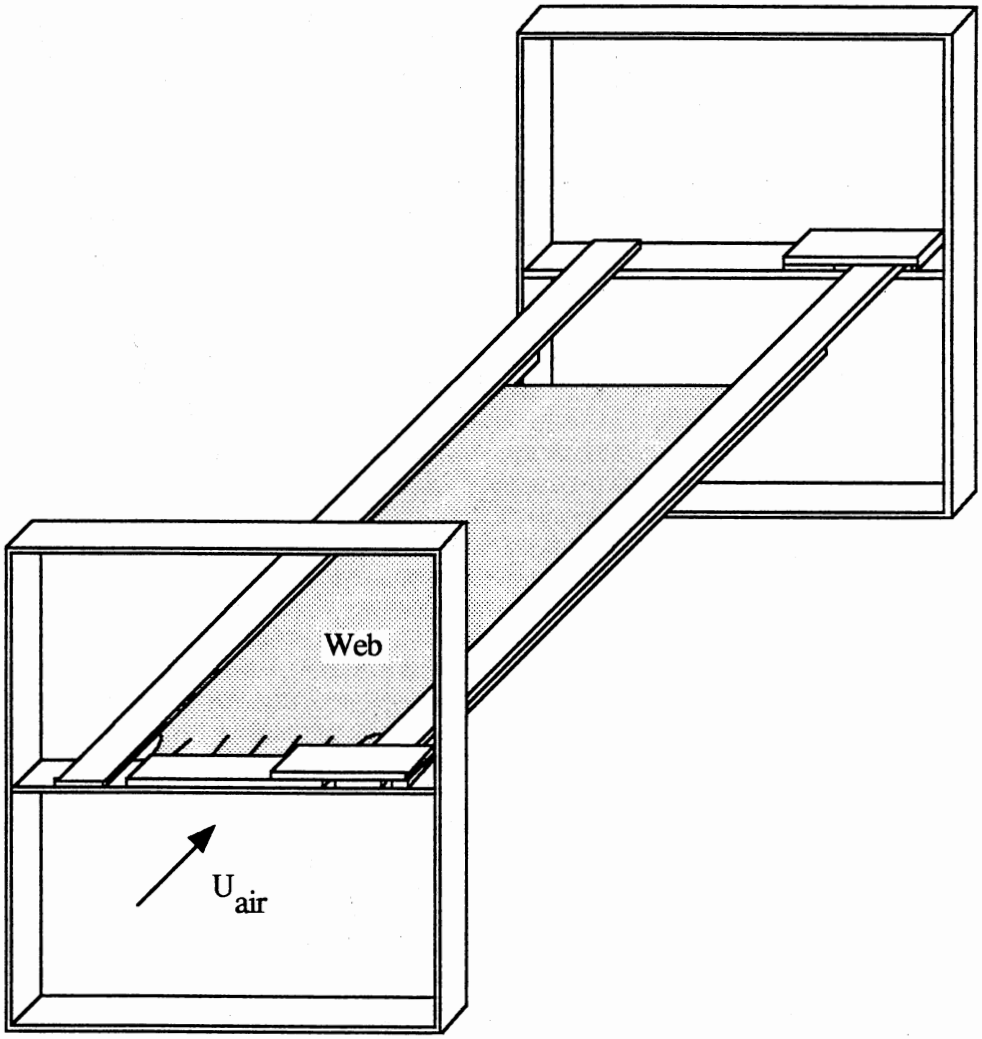

Figure 21 Setup for Edge Flutter Tests

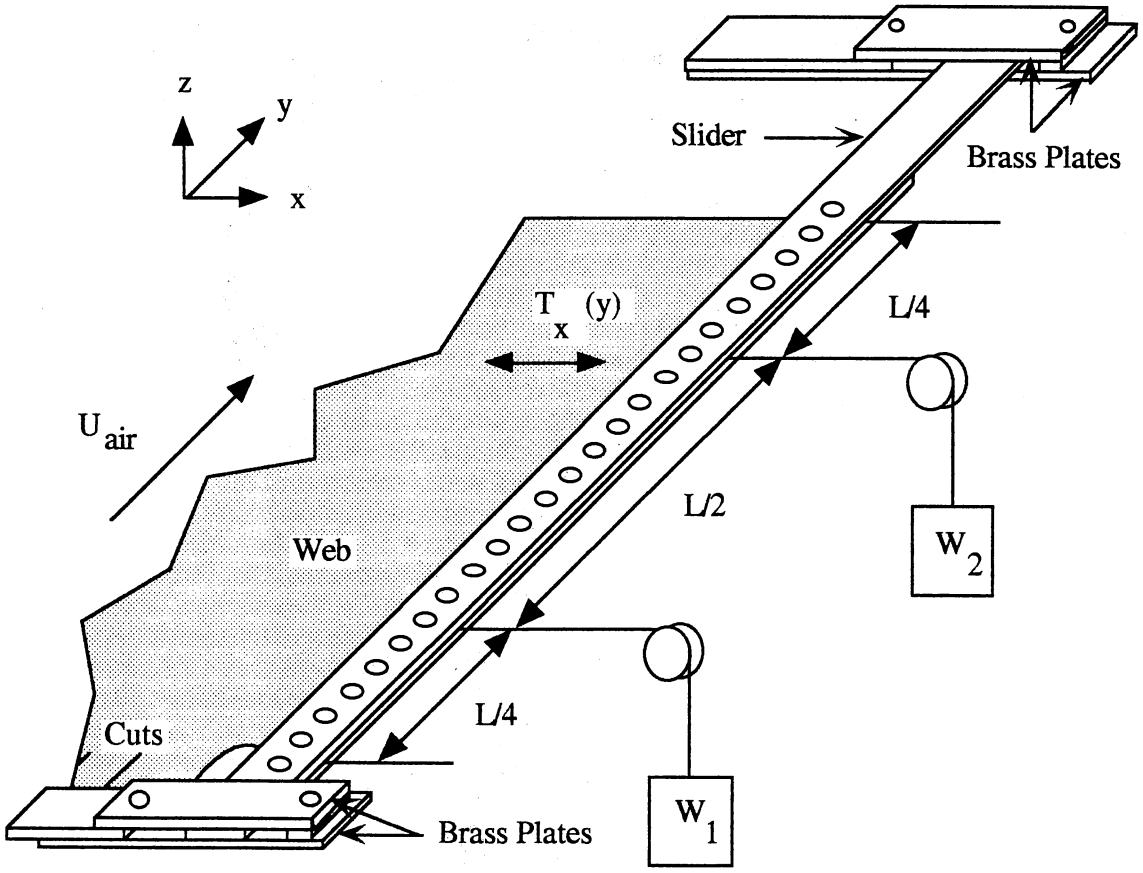

Figure 22 Setup for Edge Flutter Tests (Close up View)

TABLE II

MATERIAL PROPERTIES AND TEST CONDITIONS

	Paper	Plastic 1	Plastic 2	Plastic 3
m (Lb/in^2)	$8.2x10^{-5}$	$3.3x10^{-5}$	$1.7x10^{-4}$	$3.4x10^{-4}$
E (psi)	$9.9x10^{5}$	$7.2x10^{3}$ *	$7.2x10^{3}$ *	$7.2x10^{3}$ *
d (inches)	9	9	9	9
L (inches)	12, 15, 18	18	18	18
T (Lb/in)	0.05 - 0.4	0.2 - 0.4	0.1 - 0.4	0.05 - 0.4

* From static stress-strain measurements.

Instrumentation and Test Procedure

A set of stroboscope, sketched below, was used to figure out flutter pattern, vibration frequency, and amplitude. The operation range of the stroboscope is about 20 - 200 Hz. Though the measurement was not accurate it was good enough to determine the trends of web behavior and the critical air speeds for instability.

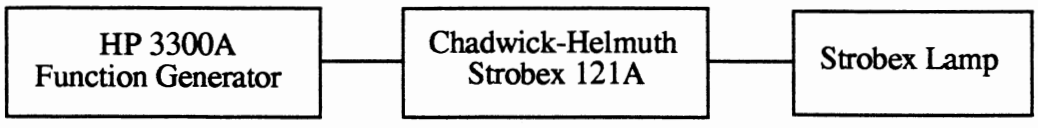

Test Results

General Response Characteristics. As the air speed is increased from zero, the free edge of the web starts to vibrate randomly with small amplitude. The amplitude grows with flow speed; and above a certain value of air speed (critical speed), the vibration becomes steady and violent as indicated in Figure 23. In most cases, the transition occurs so suddenly that the critical flow speed could be determined with little uncertainty in spite of the inaccuracy of the amplitude measurement.

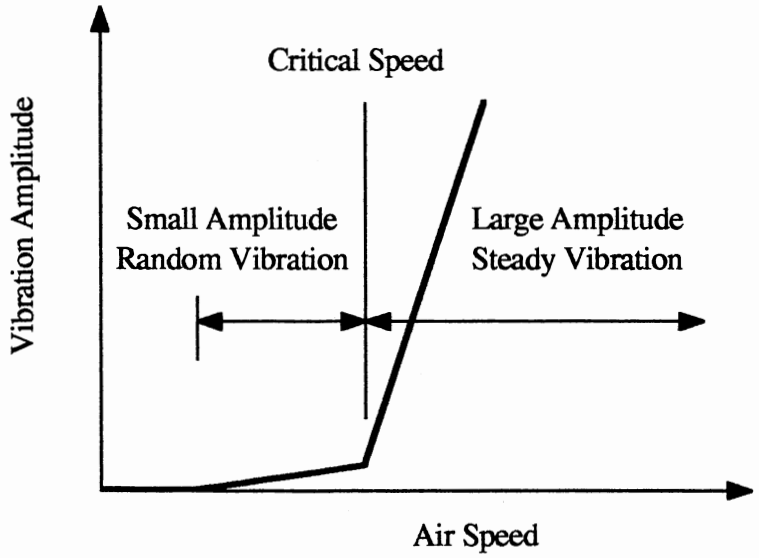

Figure 23 Typical Amplitude Response Characteristics of Edge Flutter

By using a stroboscope, flutter frequency could be measured accurately as far as the motion is steady and has single frequency component, which is the case of most runs. Once the web becomes unstable ($U > U_{crit}$), the flutter frequency usually increases with

flow speed. The frequency of vortex, shedded from the web-holding jig, is always much higher than the flutter frequency.

The free edge has the largest amplitude, and the amplitude changes exponentially along the flow direction, as shown in Figure 24. Appreciable deflection occurs only in the area near the free edge. Traveling-wave type flutter was observed. In some cases where a portion of the web had much lower tension than other areas, local flutter was observed in that area; again, the wave was traveling. With the light frequency (operation frequency of the stroboscope) little lower than the flutter frequency, the wave looked moving downstream; while with higher light frequency, the wave looked moving upstream. It simply means that the wave was always running downstream with the air flow.

The effect of reflected wave was not clearly observed. Usually, when a wave encounters a free (or fixed) boundary, the wave is reflected with the same amount of deflection (or stress) so that (1) the deflection (or stress) is doubled at the boundary, and (2) standing wave appears. The wave observed near the fluttering free edge is much different from that. It seems that (1) the kinetic energy of the free edge is not transferred from the upstream waves but induced by the local interaction between the free edge and the air, and (2) the reflected wave running against the air flow is damped so heavily that its effect could not be observed. It should be noted that the Galerkin's method is not applicable for this problem where normal modes do not exist.

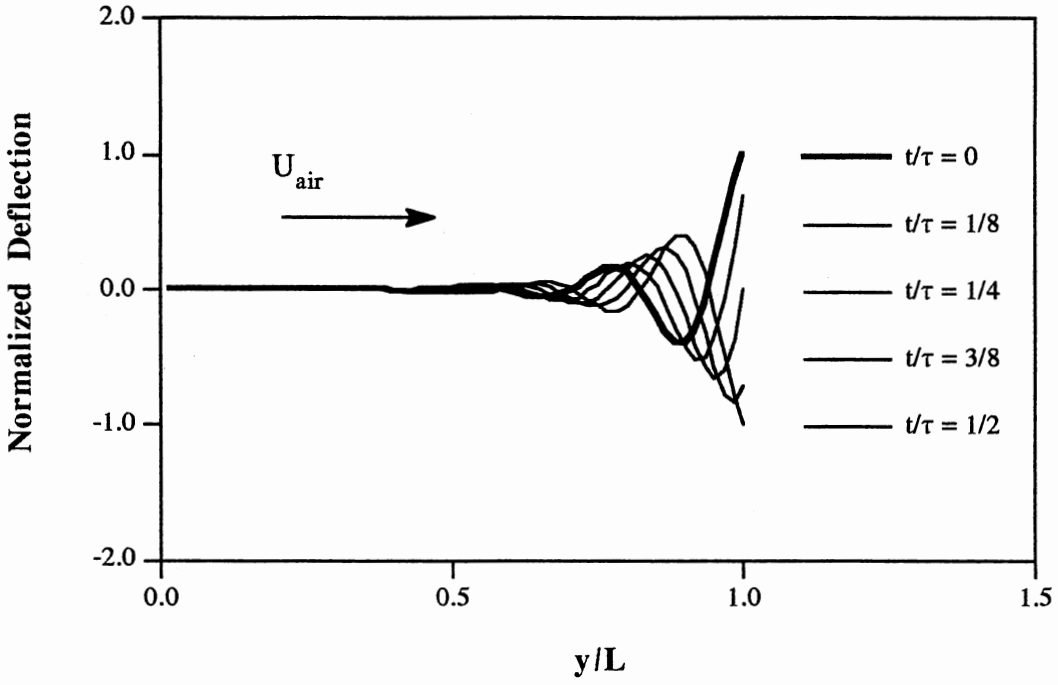

Figure 24(a) Pattern of Edge Flutter (First Half Cycle)

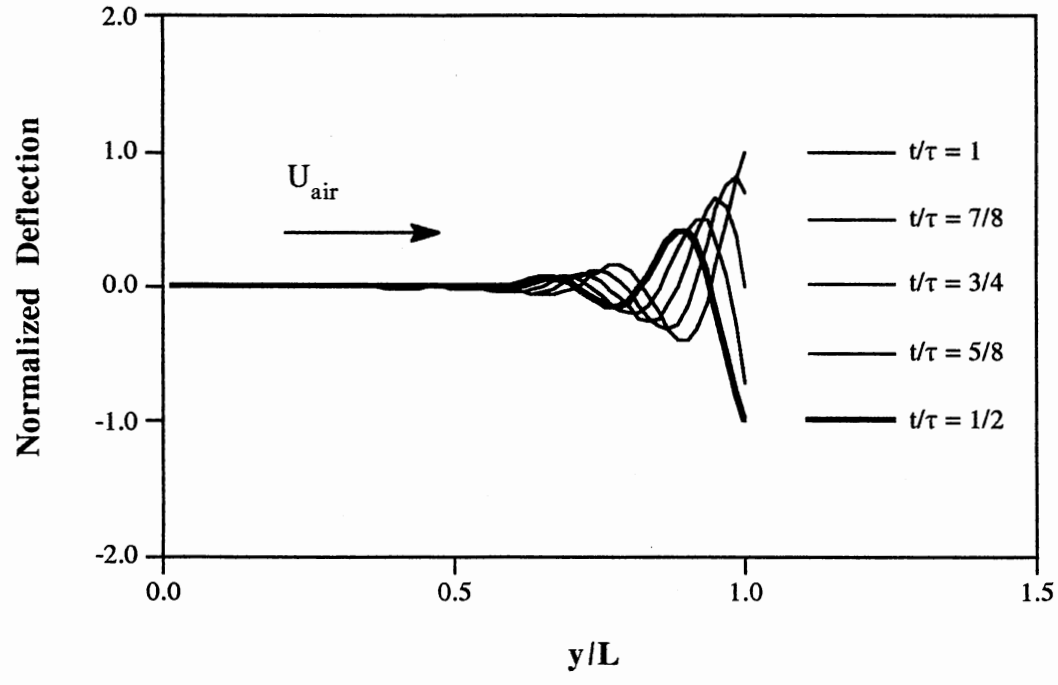

Figure 24(b) Pattern of Edge Flutter (Last Half Cycle)

Unlike the wave traveling in the flow direction, a cross-flow directional wave has normal modes (standing waves) as shown in Figure 25. In most cases, zero-node deflection was observed along the cross-flow direction; in some cases, higher modes could be observed at high flow speeds.

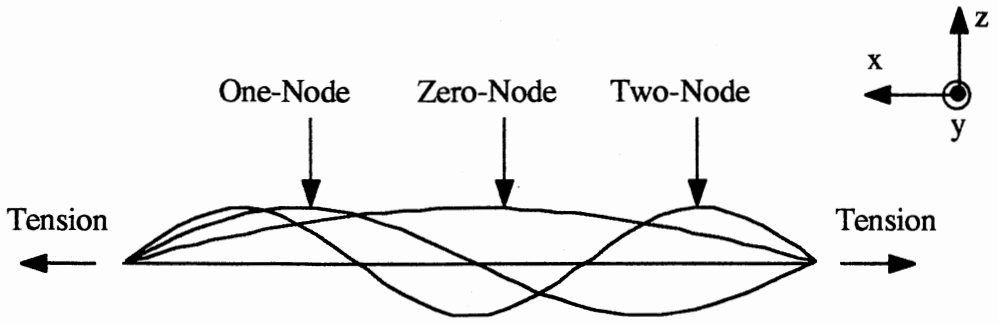

Figure 25 Modes of Web Deflection along the Cross-Flow Direction
(Upstream View of Free Edge)

Based on the observations, the flutter pattern could be expressed in the form

$$\eta = A\, e^{i(\omega t - \sigma y)} \cos\left(\frac{n\pi x}{d}\right) \tag{4.2.1}$$

or

$$\eta = A\, e^{\sigma_i y} \sin(\omega t - \sigma_r y) \cos\left(\frac{n\pi x}{d}\right) \tag{4.2.2}$$

where n is an integer; n = 1 for zero-node deflection along the cross-flow direction.

Effects of Web Tension. As web tension is increased, the onset of edge flutter is delayed as shown in Figure 26. Similar trends were observed in most other cases.

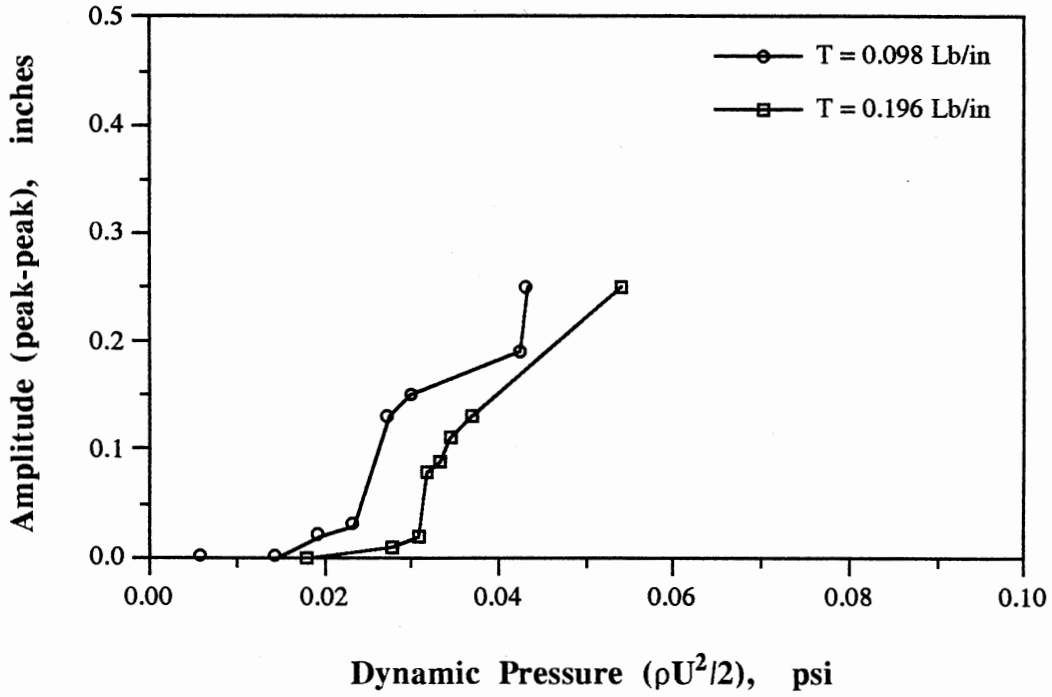

Figure 26 Effect of Tension on the Amplitude Response of a Paper Web (Setup 1, 9"x15")

Critical conditions for instability of paper webs having dimensions of 9"x18" are plotted in Figure 27. The effect of tension for each setup is clear but the results show much scattering. It is believed that the scattering is due to poor adjustment of tension distribution. Whenever a new paper web is mounted, tension distribution is changed and it was very difficult to obtain uniform tension on paper webs.

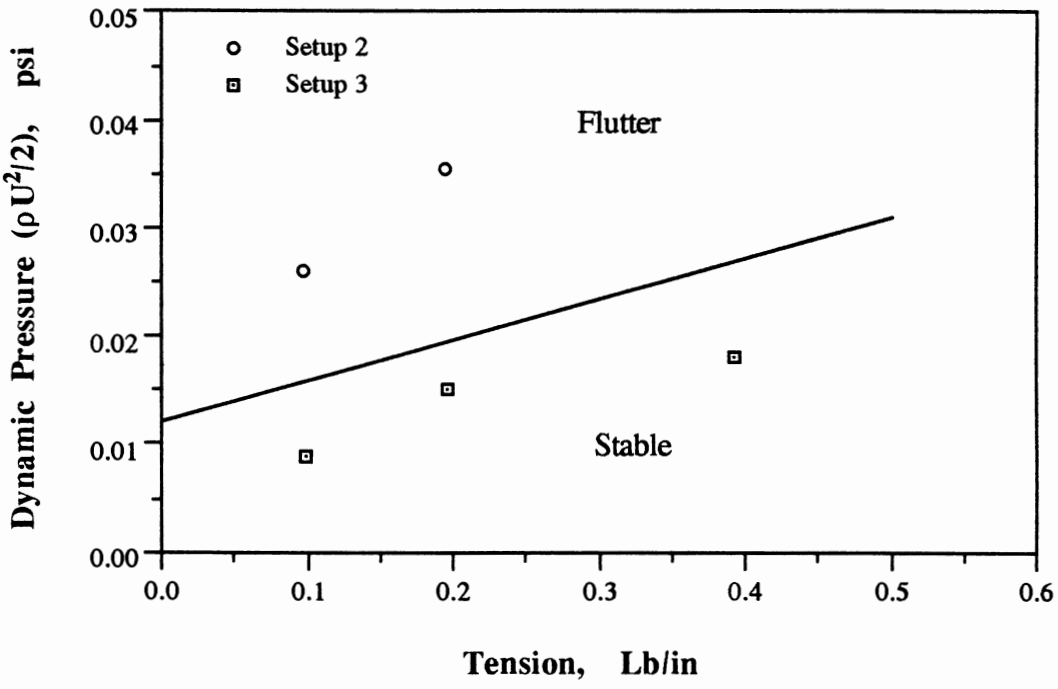

Figure 27 Effect of Tension on the Stability of Paper Webs (9"x18")

Stability boundaries for plastic webs having areal densities of 3.3×10^{-5}, 1.7×10^{-4}, and 3.4×10^{-4} Lb/in^2 are shown in Figure 28, Figure 29, and Figure 30 respectively. All of them have the same size, 9"x18". By comparing Figure 27 with Figure 29, it is seen that the data scattering for plastic webs is much less than for paper webs.

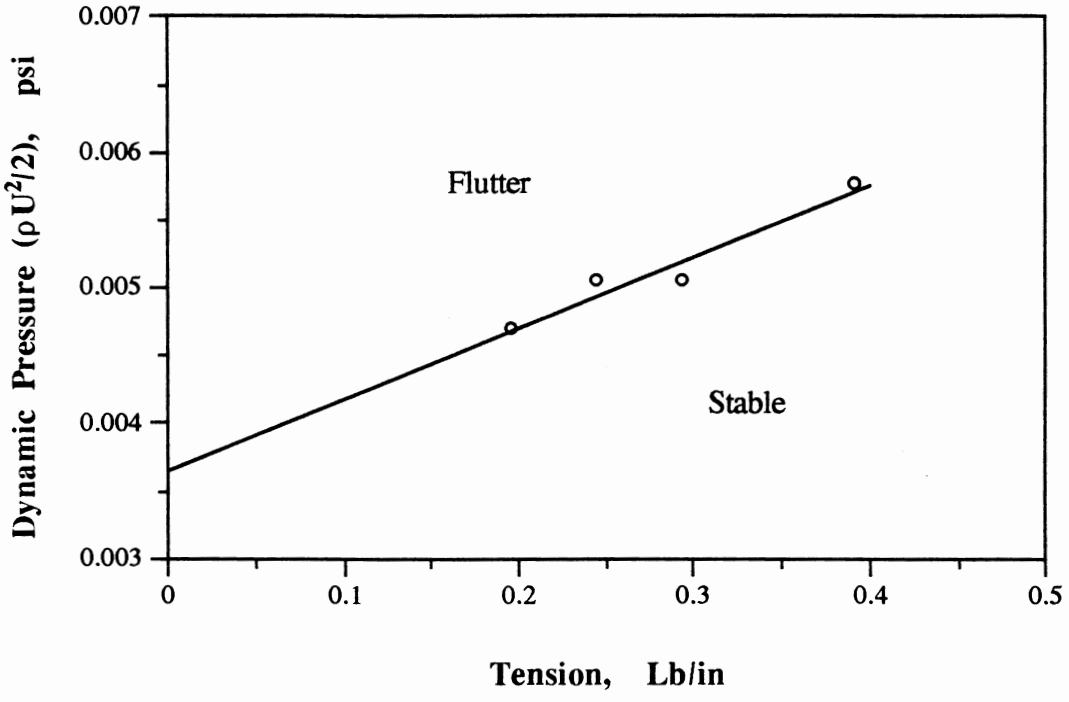

Figure 28 Effect of Tension on the Stability of a Plastic Web ($3.3x10^{-5}$Lb/in^2)

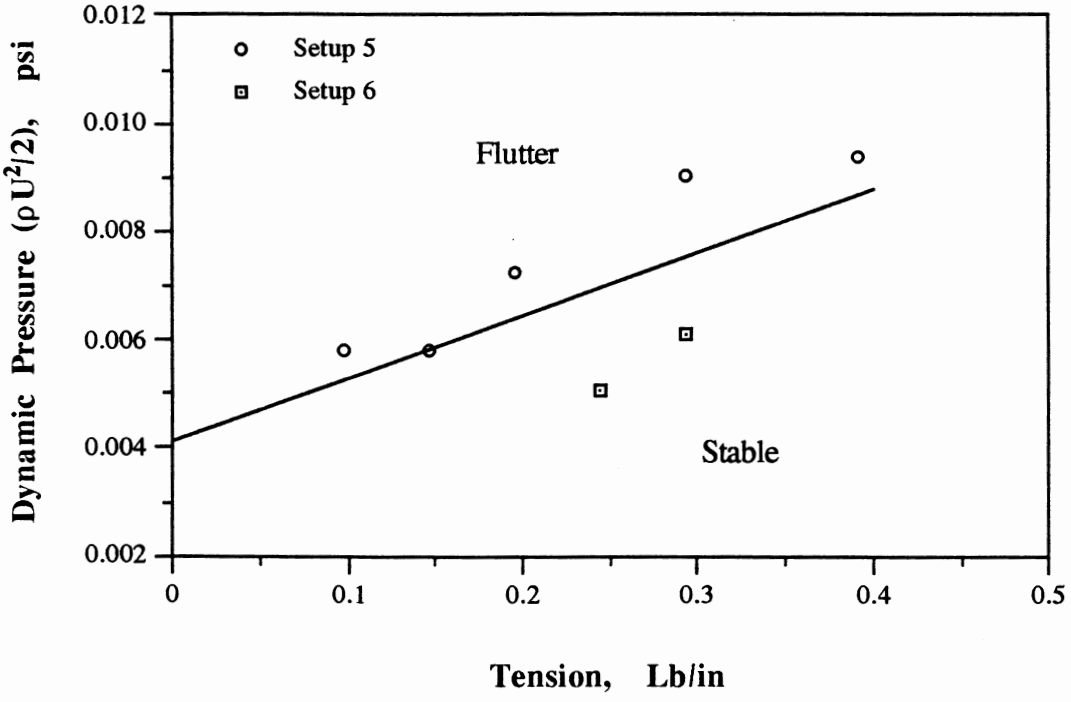

Figure 29 Effect of Tension on the Stability of a Plastic Web ($1.7x10^{-4}$ Lb/in^2)

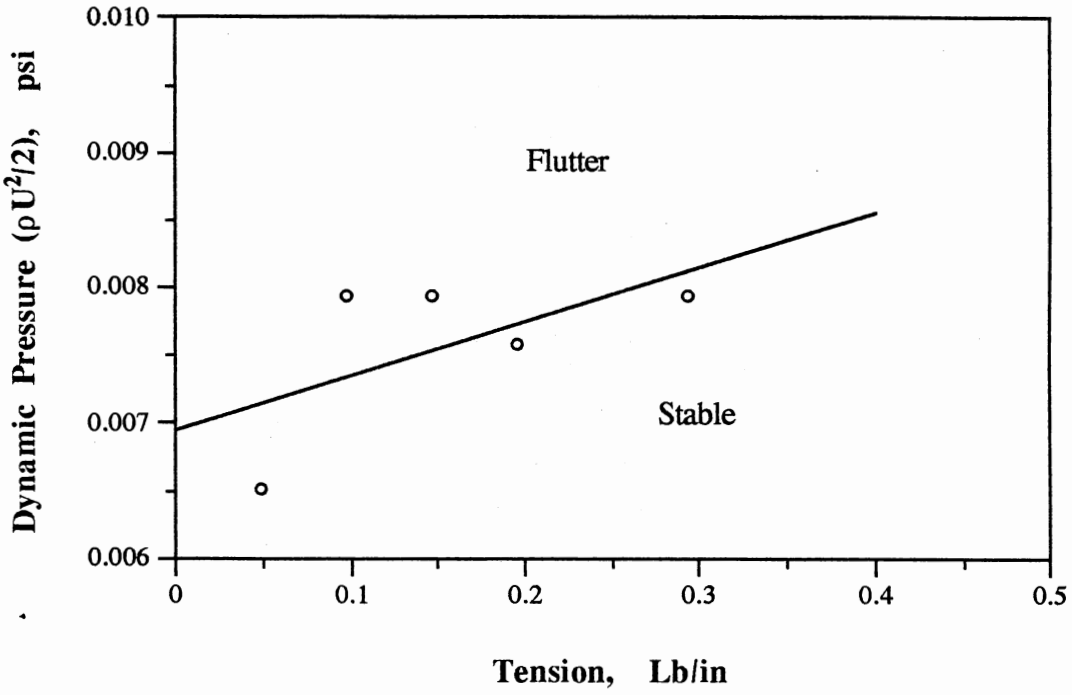

Figure 30 Effect of Tension on the Stability of a Plastic Web (3.4×10^{-4} Lb/in^2)

Flutter frequency also is very sensitive to web tension as shown in Figure 31. The higher the web tension is, the higher its frequency is. It should be noted that the flutter frequency depends on flow speed and the web does not have its own natural frequencies. No appreciable change of wave length was found during the tests; the frequency change means the change of wave speed.

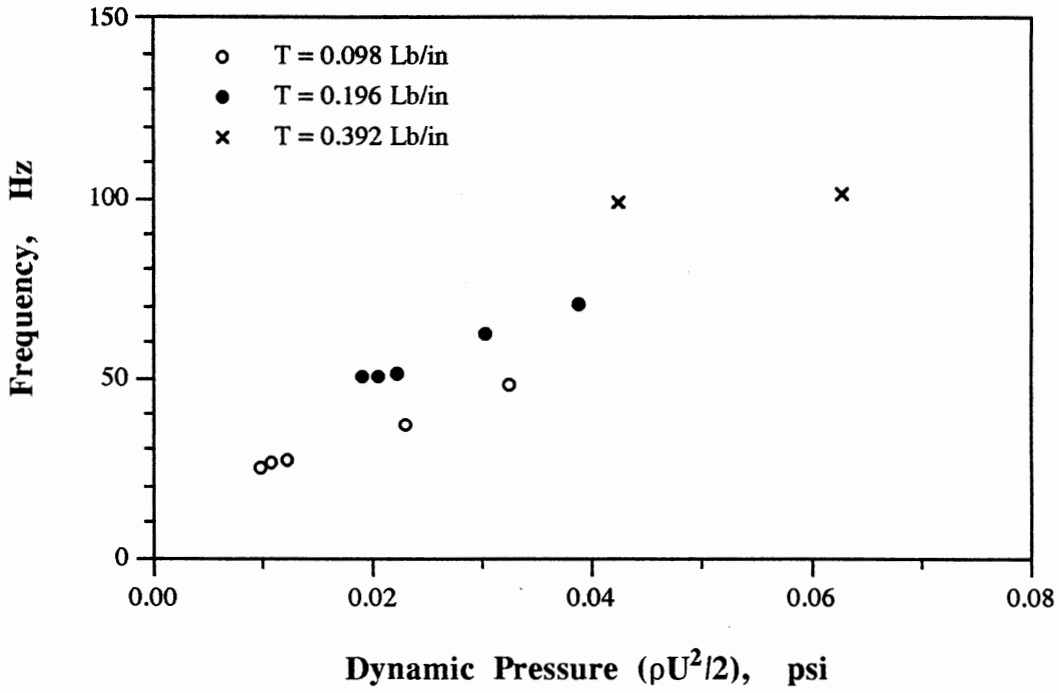

Figure 31 Effect of Tension on the Frequency of a Paper Web (Setup 3, 9"x18")

Effects of Web Sizes. In Figure 32 and Figure 33, stability boundaries of paper webs are shown as functions of web length. Though it is difficult to draw any conclusions because the data scatter so much and the trend is not clear, it seems that the longer webs tend to be more unstable than shorter ones. Flutter frequency is sensitive not only to web tension but also to web length as shown in Figure 34. Longer web has lower frequency.

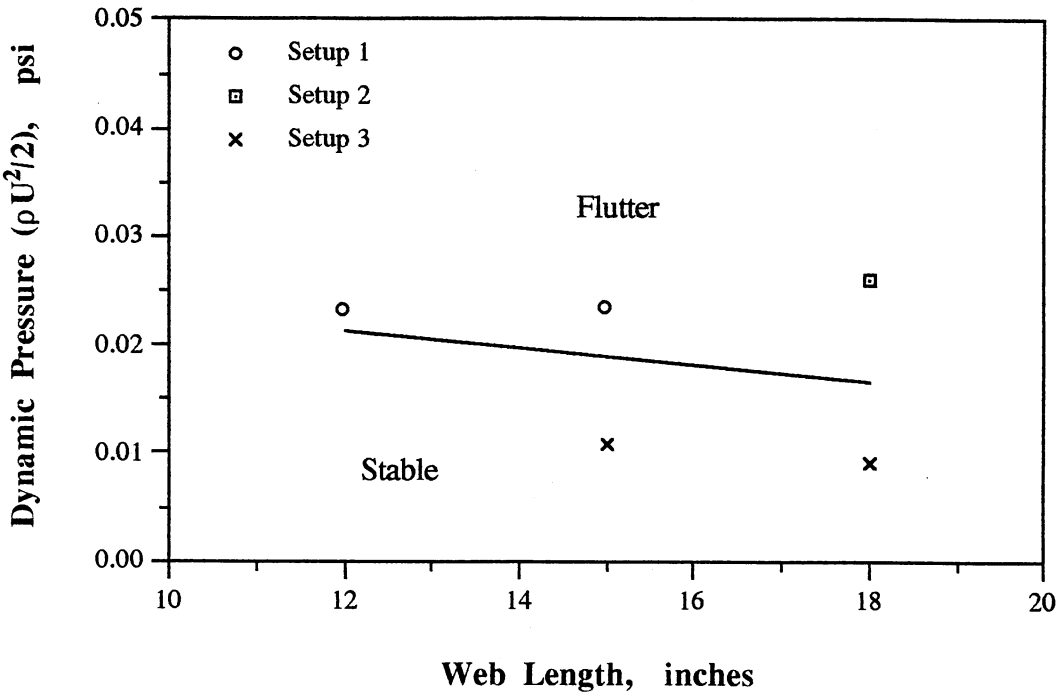

Figure 32 Effect of Web Length on the Stability of Paper Webs (T=0.098 Lb/in)

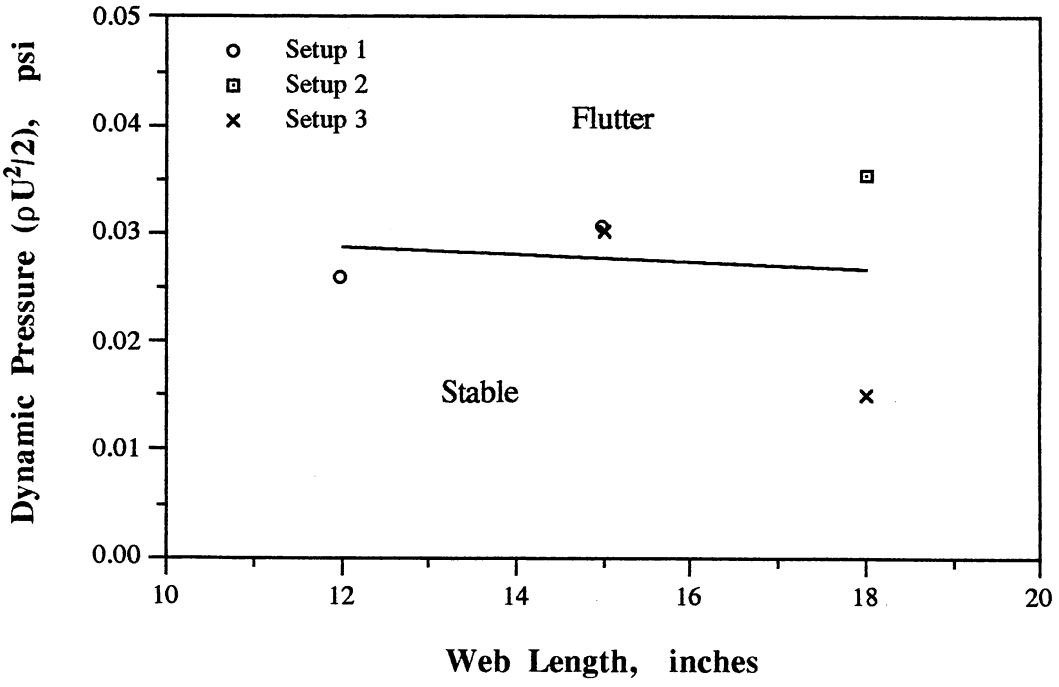

Figure 33 Effect of Web Length on the Stability of Paper Webs (T=0.196 Lb/in)

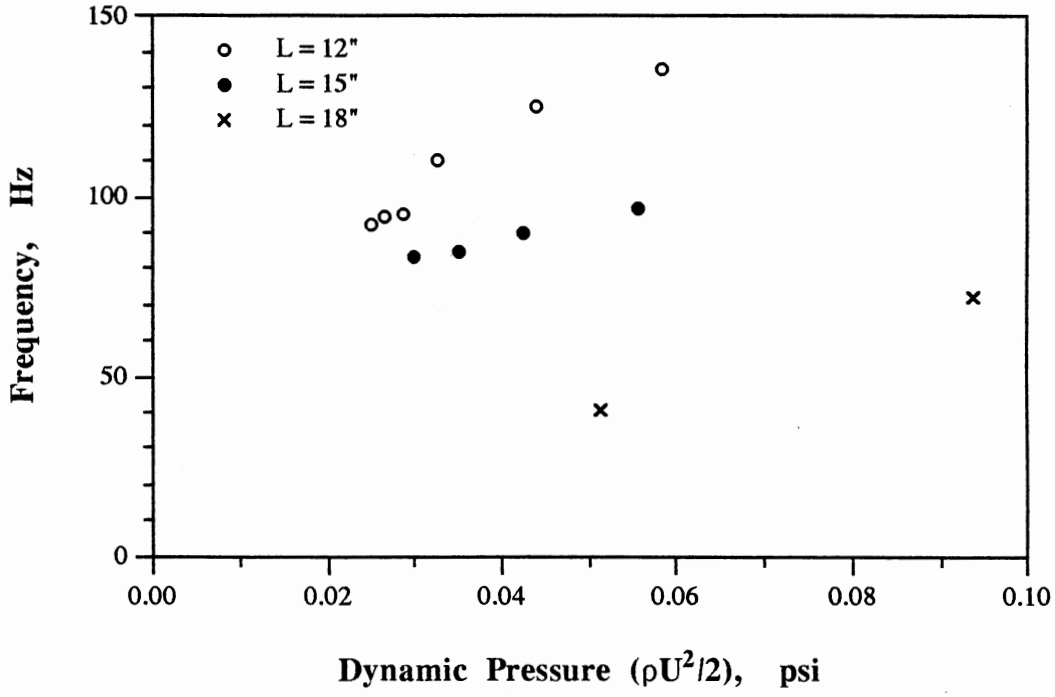

Figure 34 Effect of Web Length on the Frequency of Paper Webs (Setup 1, T = 0.098 Lb/in)

Stability Criteria

In order to obtain a generalized expression of stability criterion, one needs to find the functional relationship among nondimensional parameters that play important roles in edge flutter. Nondimensional parameters are obtained either by Buckingham Pi Theorem or by nondimensionalizing the governing equation of the problem if the equation is known [H1, 2]. The following are the physical variables that are considered important in the present problem and the nondimensional parameters derived from them:

Dependent Variables		Dimension
U	Critical flow speed	LT^{-1}
ω	Flutter frequency	T^{-1}

Independent Variables		Dimension
ρ	Air density	ML^{-3}
ν	Kinematic viscosity	L^2T^{-1}
a	Sound speed in air	LT^{-1}
d	Web width	L
L	Web length	L
m	Basis weight (areal density) of web	ML^{-2}
D	Bending stiffness of web (per unit width)	ML^2T^{-2}
T	Web tension in cross-flow direction (per unit width)	MT^{-2}

Nondimensional Parameters

$\frac{U}{\omega d}$	Reduced velocity
$\frac{Ud}{\nu}$	Reynolds number
$\frac{U}{a}$	Mach number
$\frac{L}{d}$	Slenderness ratio
$\frac{m}{\rho d}$	Mass ratio
$\frac{D}{Td^2}$	Stiffness parameter
$\frac{T}{md^2\omega^2}$	Tension parameter

The meaning and importance of these parameters are as follow:

(1) The first parameter, reduced velocity, is one of the most important parameters for a variety of flow-induced vibration problems. It represents the ratio of flow speed to the speed of structural motion. For convenience, a variation of reduced velocity is defined as

$$\frac{q}{\rho d^2 \omega^2}$$

This new parameter, named pressure parameter, will be used instead of reduced velocity in analyzing the experimental data. This parameter, as well as the reduced velocity, contains ω. For most flow-induced vibration problems, vibration frequency can be predicted; that is not the case for edge flutter. This fact may limit the application of a stability criterion that contains ω.

(2) The second one, Reynolds number, is the ratio of fluid inertia to viscous force, and it gives a measure of boundary layer thickness and transition from laminar to turbulent flow [H5]. Reynolds number is a crucial parameter in general fluid dynamics problems, but in studying flow-induced vibrations, the effects of Reynolds number are usually neglected [H3, 6] and sometimes the requirement of Reynolds number cannot be met because of its incompatibility with the reduced velocity [H4]. The effect of Reynolds number is not considered in this study.

(3) Mach number is the ratio of flow speed to the sound speed; it is a measure of fluid compressibility and is important only when its value is high enough, say greater than 0.3. For the present study, Mach number is low enough that its effect is neglected.

(4) Slenderness ratio determines the severity of three-dimensional behavior of web motion and air flow. If it is very large or very small then the phenomenon is considered two-dimensional. For the present test models, $1.3 < L/d < 2.0$.

(5) Mass ratio is very important in flow-induced vibration problems; it is believed to be crucial in edge flutter phenomenon.

(6) The forms of the last two parameters are derived from the equation of motion,

$$m\frac{\partial^2\eta}{\partial t^2} - T\frac{\partial^2\eta}{\partial x^2} + D\left(\frac{\partial^2}{\partial x^2} + \frac{\partial^2}{\partial y^2}\right)^2 \eta = f(x,y,t) \tag{4.2.3}$$

where f(x,y,t) represents aerodynamic forces. The stiffness parameter defines the relative importance of bending rigidity and tension.

(7) The last parameter, named tension parameter, contains a dependent variable, flutter frequency. The information of critical flow speed is more important than flutter frequency for practical purposes. Therefore, by combining it with other parameters, the tension parameter can be changed to be

$$\frac{qd}{T}$$

The ranges of these parameters are shown in Table III. The stability criterion might be expressed as a functional relationship of

$$f_1\left(\frac{q}{\rho d^2\omega^2}, \frac{qd}{T}\right) = f_2\left(\frac{m}{\rho d}, \frac{D}{Td^2}, \frac{L}{d}\right) \tag{4.2.4}$$

As already described, the effect of slenderness ratio is not certain, so that its effect is not considered. Therefore, the stability criterion will be determined in two different forms:

$$\frac{q}{\rho d^2 \omega^2} = f\left(\frac{m}{\rho d}, \frac{D}{Td^2}\right) \tag{4.2.5}$$

and

$$\frac{qd}{T} = f\left(\frac{m}{\rho d}, \frac{D}{Td^2}\right) \tag{4.2.6}$$

TABLE III

RANGES OF NONDIMENSIONAL PARAMETERS

	Paper	Plastic 1	Plastic 2	Plastic 3
$\frac{q}{\rho d^2 \omega^2}$	0.0033-0.040	0.0012-0.0013	0.0062-0.011	0.014-0.035
$\frac{qd}{T}$	0.42-2.2	0.13-0.22	0.22-0.53	0.24-0.73
$\frac{m}{\rho d}$	0.21	0.085	0.44	0.87
$\frac{L}{d}$	1.3-2	2	2	2

Stability Criterion (Type 1). As a first step, the relationship between pressure parameter and stiffness parameter is checked. Figure 35 shows that relationship for paper webs having various dimensions; the relationship is not clear.

For plastic webs, those two parameters are closely related as shown in Figure 36. It should be noted that (1) T is the only working variable in the parameter (D/Td^2) in Figure 35, while in Figure 36, both D and T are changing, (2) including mass term does not affect Figure 35 because the mass ratio is constant for paper webs, while Figure 36 will be affected.

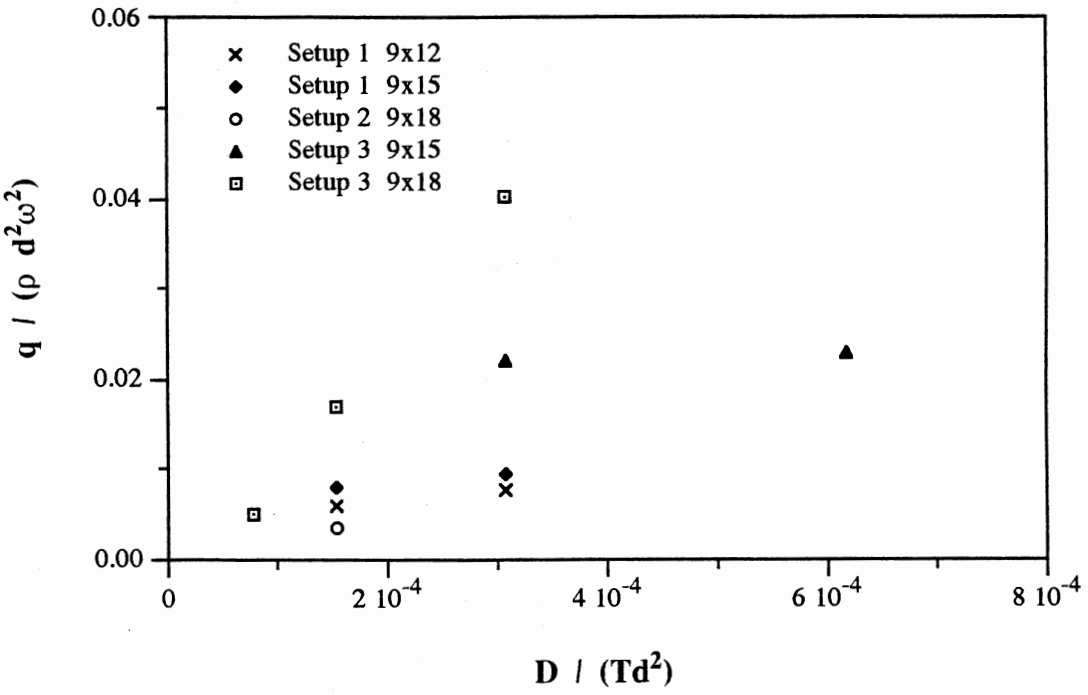

Figure 35 Pressure Parameter vs. Stiffness Parameter for Paper Webs

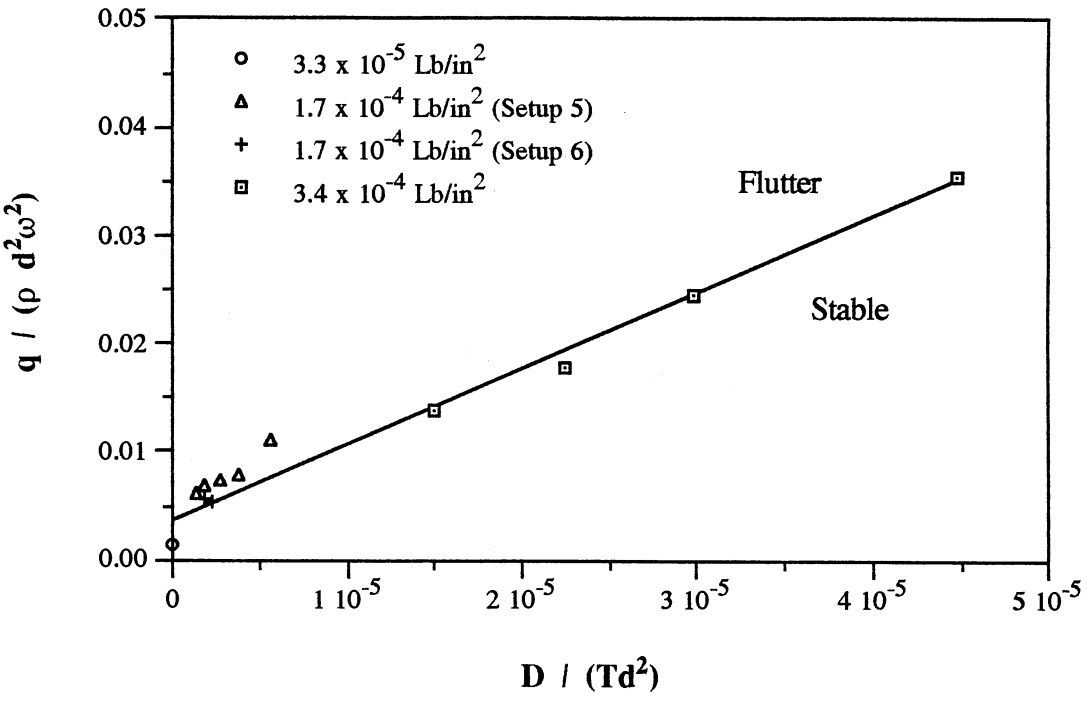

Figure 36 Pressure Parameter vs. Stiffness Parameter for Plastic Webs

As a second step, correlation among all three parameters is determined. The trial form is

$$\left(\frac{q}{\rho d^2 \omega^2}\right) = A\left(\frac{m}{\rho d}\right)^a \left(\frac{D}{Td^2}\right)^b + B \qquad (4.2.7)$$

where A, B, a, and b are unknown constants. The procedure for determining those four constants is:

(1) Set values of the powers, a and b.

(2) Obtain an x-y chart of the the two groups of experimental data, one group for paper webs and the other for plastics, where

$$x = \left(\frac{m}{\rho d}\right)^a \left(\frac{D}{Td^2}\right)^b \quad \text{and} \quad y = \frac{q}{\rho d^2 \omega^2}$$

(3) Determine the best-fit linear curve for each group of data.

(4) Change the values of a and b to find ranges of them that make the two curves overlap or come close.

(5) Change a and b within these ranges and find the best-fit linear curve and the corresponding correlation coefficient for the whole data set. Repeat it until the largest value of correlation coefficient is found.

After many trials, Figure 37 was obtained with a correlation equation of

$$\frac{q}{\rho d^2 \omega^2} = 4.78 \left(\frac{m}{\rho d}\right)^{1.2} \left(\frac{D}{Td^2}\right)^{0.5} + 0.00185 \qquad (4.2.8)$$

The corresponding correlation coefficient is r = 0.88. In deriving the above equation, one data point for paper web, the highest point in Figure 35, was omitted because it deviates so much when plotted into Figure 37.

Stability Criterion (Type 2). The relationship between two parameters (qd / T) and (D/Td^2) was checked; no direct correlation was found as implied by Figure 38 and Figure 39. The stability criterion, determined by the same method as for the first one, is

$$\frac{qd}{T} = 779 \left(\frac{m}{\rho d}\right)^{0.5} \left(\frac{D}{Td^2}\right)^{0.7} + 0.200 \qquad (4.2.9)$$

with a correlation coefficient of r = 0.85.

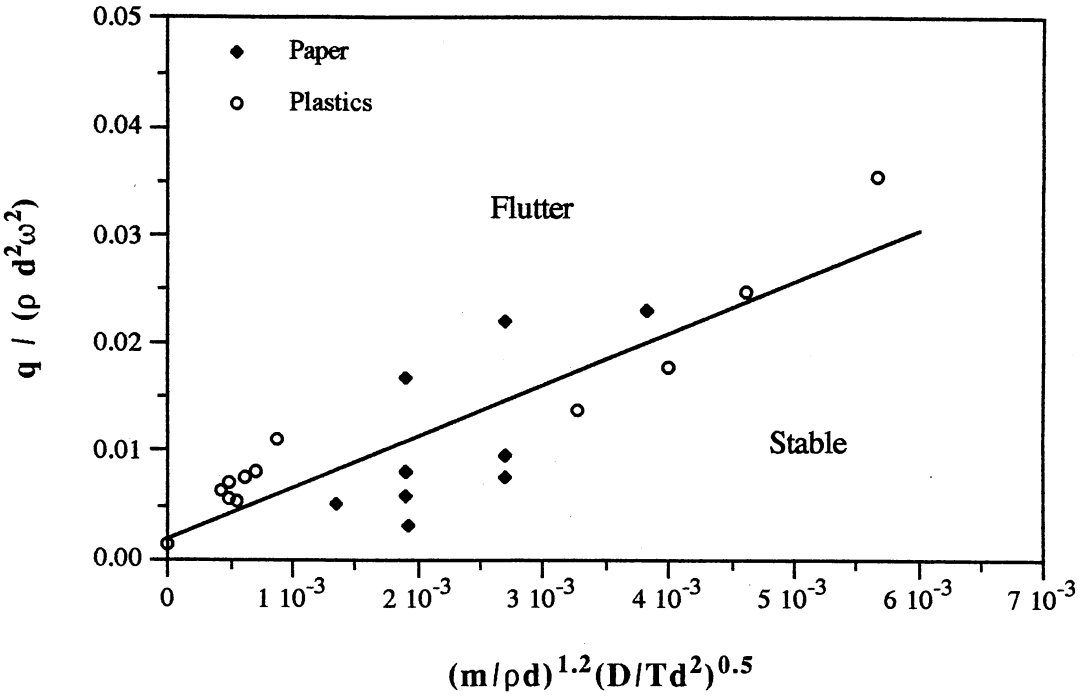

Firgure 37 A Tentative Stability Criterion (Type 1)

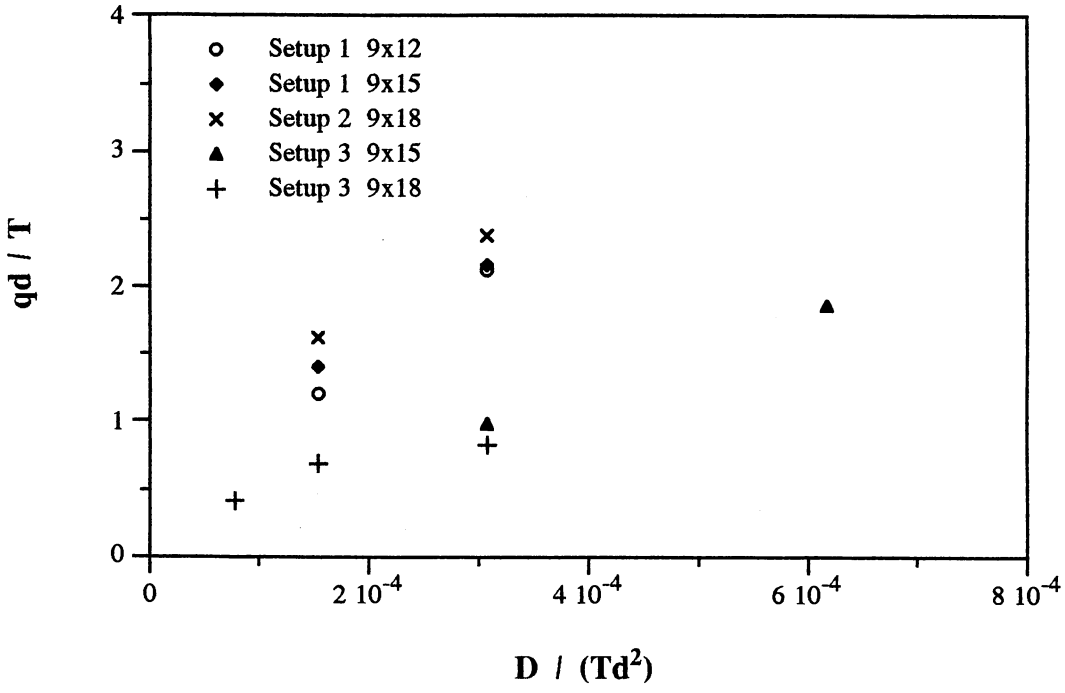

Figure 38 Pressure-Tension Parameter vs. Stiffness Parameter for Paper Webs

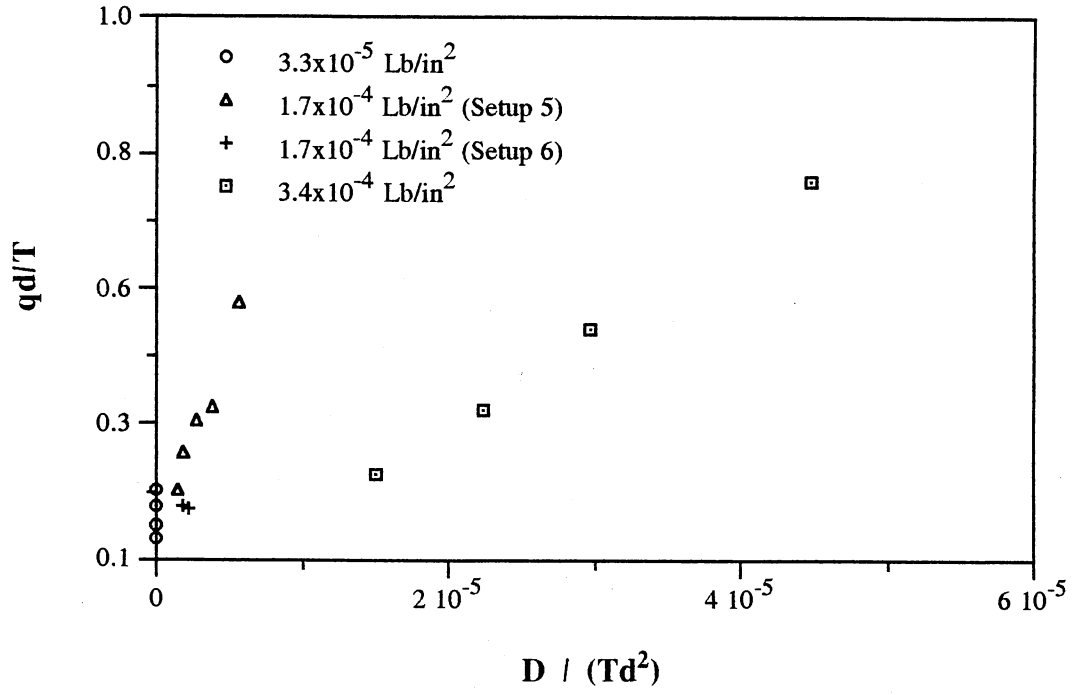

Figure 39 Pressure-Tension Parameter vs. Stiffness Parameter for Plastic Webs

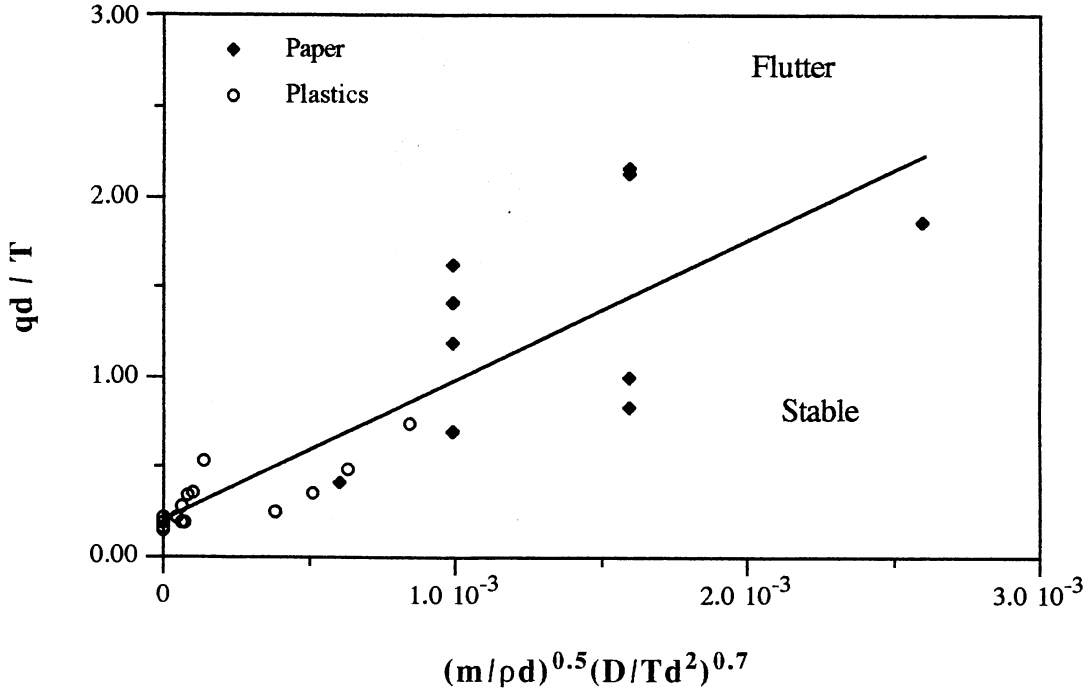

Firgure 40 A Tentative Stability Criterion (Type 2)

CHAPTER V

SUMMARY AND CONCLUSIONS

Web flutter was studied experimentally and analytically. Two different modes of web flutter were considered separately: string-mode instability and edge flutter. In string-mode instability, the web is assumed to behave like a threadline traveling between two rollers so that all the points across the direction of running motion have the same deflection. In edge flutter, the web behavior near the free edges was considered. For both cases, the current study is focused on the effects of air flows.

5.1 String-Mode Instability

At the first phase of study, the dynamics of a traveling threadline was considered. Then the threadline model was generalized to include the aerodynamic effects. The aerodynamic terms, like the inertia terms appearing in a traveling threadline, consist of three components: transverse inertia, Coriolis inertia, and centripetal inertia. Closed form solutions of natural frequencies and stability criteria were obtained for arbitrary values of the aerodynamic terms.

The successful application of the traveling threadline model of a running web depends on the correct application of the three aerodynamic terms. Expressions for evaluating the aerodynamic terms were obtained for a number of cases. The finite-difference scheme was used to calculate the transverse inertia term for a web in an enclosure.

Wind tunnel tests were performed to verify the analytical expression of the aerodynamic forcing terms for a slender (narrow and long) web. The tests were limited to

stationary (non-traveling) rectangular webs. The test results were compared with theory. Both steady deflection and flutter were observed as expected by the theory. The experimental results show the same trends as the slender-body theory, but the experimental critical flow speeds for static divergence are higher than the theoretical values, while for the flutter case the experimental values fall below the theoretical prediction curve. Except for these small discrepancies, the slender-body model appears to represent the physics of the instability of a slender web correctly. Therefore this approach seems to be well suited to long-span web motions, such as occur in drying ovens etc.

The importance of the effects of air flow was proved. The surrounding air appreciably affect the dynamic characteristics of the traveling web and cause instability.

5.2 Edge Flutter

Wind runnel tests were performed on edge flutter model. It was found that edge flutter, like fluid-elastic instability of tube arrays in a cross flow, onsets at a critical flow speed and its amplitude grows drastically with flow speed. The actual environments of paper webs in a paper machine are much different from our simplified test model. It seems safe, however, to conclude that the air flow, without any other suspected causes, can induce detrimental edge flutter.

Only a small portion near the free edge experiences high-amplitude flutter. It seems that the mechanism of edge flutter is involved with local interaction between the free edge and air flow. The pattern might become different when tension distribution is not uniform; slack areas are more vulnerable to flutter than tight areas.

Unlike common structural vibrations, edge flutter is a traveling-wave type vibration which does not have normal modes or natural frequencies. Flutter frequency depends on flow speed. This limits the analysis; any analytical method that assumes normal modes is not applicable.

Without a proper theoretical model, a dimensional analysis was performed to find out important nondimensional parameters for edge flutter. The experimental results were analyzed based on those nondimensional parameters and empirical stability criteria were developed. The stability criteria, though they are approximate and tentative, show how each variable contributes in edge flutter and give a direction for preventing or solving edge flutter problems. The first type criterion, Eq. (4.2.8) contains frequency term. If the frequency is not known the criterion cannot be used directly. The second criterion, Eq. (4.2.9), implies that the edge flutter can be prevented by increasing web tension, bending rigidity, and basis weight.

The application of the stability criteria are limited within the ranges of nondimensional parameters covered in this study; they may not be extrapolated.

REFERENCES

A. Field Study of Web Flutter

A1. DeCrosta, E.F. and Vennos, S.L.N., "Air Movement and Dryer Fabrics," *Southern Pulp and Paper Manufacturer*, Jan. 10, 1967, pp.72, 74-75.

A2. Vennos, S.L.N. and DeCrosta, E.F., "What Happens in a Dryer Pocket, Part I. Preliminary Velocity Measurements in Three Dimensions," *Pulp & Paper Magazine of Canada*, Vol.68, No.8, Aug. 1967, pp.T354-T358.

A3. Swanberg, O. and Svensson, K., "How Open Mesh Dryer Fabrics Affect Pocket Ventilation," *Paper Trade J.*, Vol.151, No.38, Sep. 18, 1967, pp.60-64.

A4. Race, E., Wheeldon, J.B., and Fraser-Clark, D., "Air Movement Induced by Felts and Fabrics and its Ventilation Effect on Dryer Pockets," *TAPPI*, Vol.51, No.7, July 1968, pp.51A-56A.

A5. Vennos, S.L.N. and DeCrosta, E.F., "What Happens in a Dryer Pocket, Part II. Air Flow Induced by the Dryer Fabric," *TAPPI*, Vol.51, No.7, July 1968, pp.289-298.

A6. Kottick, G.J., "Synthetic Dryer Clothing Combined with a Moisture Profiling Air System on High-Speed News Print Machines," *Pulp and Paper Magazine of Canada*, Vol.70, Feb. 21, 1969, pp.55-65.

A7. Soininen, M., "Pocket Ventilation at Different Geometries of a Multi-Cylinder Dryer Section with Mesh Screens," *Paper and Timber (Papper och Tra, Paperi ja Puu)*, Vol.52, No.11, 1970, pp.735-745.

A8. Soininen, M., "Air Flow Phenomena in a Multicylinder Dryer with Drying Screens," *Paper and Timber (Papper och Tra, Paperi ja Puu)*, Vol.52, Specialnummer 4a, 1970, pp.187-196.

A9. Cedercreutz, A.V., "Combatting the Edge Flutter Problem in a Paper Machine," *Paper Trade J.*, Vol.155, No.51, Dec. 20, 1971, pp.35.

A10. Race, E., "Function of Felt on Felt-Covered Cylinders," *Drying of Paper and Paperboard*, Edited by Gavelin, G., Lockwood Pub., N.Y., 1972, pp.66-83.

A11. Osterberg, L. and Norinder, S.O., "Dryer Fabrics Versus Conventional Felts," *Drying of Paper and Paperboard*, Edited by Gavelin, G., Lockwood Pub., N.Y., 1972, pp.84-96.

A12. Kottick, G., "Paper Machine Pocket Ventilation," *Drying of Paper and Paperboard*, Edited by Gavelin, G., Lockwood Pub., N.Y., 1972, pp.109-113.

A13. Soininen, M., "Air Flow and Pocket Ventilation," *Drying of Paper and Paperboard*, Edited by Gavelin, G., Lockwood Pub., N.Y., 1972, pp.114-123.

A14. Smook, G.A., "Use of Survey Methods in the Study of Drying," *Drying of Paper and Paperboard*, Edited by Gavelin, G., Lockwood Pub., N.Y., 1972, pp.188-211.

A15. Larsson, K.O., "Modernization of Paper Machines for Improved Quality and Production," *APPITA*, Vol.26, No.6, May 1973, pp.449-453.

A16. Mujumdar, A.S., "Sheet Flutter in High Speed Paper Dryers," *IPPTA (Indian Pulp and Paper Technical Association)*, Vol.11, No.2, April, May & June, 1974, pp.93-102.

A17. Mardon, J., et al., "Basis Weight Variation on a High Speed Newsprint Machine - Some Causes and Effects," *APPITA*, Vol.28, No.2, Sep. 1974, pp.104-111.

A18. Edgar, C.B., Jr., "New Dryer Felt Seam Reduces Sheet Flutter at High Speeds," *Pulp & Paper*, Vol.48, No.13, Dec. 1974, pp.80-82.

A19. Cutshall, K.A. and Mardon, J., "Causes of Instability in Paper Machine Wet Ends," *APPITA*, Vol.28, No.4, Jan. 1975, pp.252-260.

A20. Smook, G.A., "A Consolidated View of the Dryer Edge Wrinkling Problem on High Speed Machines," *CPPA, Trans. of the Technical Section*, Vol.2, No.1, March 1976, pp.14-20.

A21. Edgar, C.B., Jr., "Sheet Flutter Can Be Reduced Through Use of Single Felting, Mill Trials Indicate," *Paper Trade J.*, Vol.161, No.2, Jan. 15, 1977, pp.33-35.

A22. Sahay, A., "Single Fabric in First Dryer Section Ends Sheet Flutter, Lower Breaks," *Canadian Pulp and Paper Industry*, March 5, 1977, pp.36-37.

A23. Epton, J.B.A., "Pulsation and Vibration Studies at the Wet End of a Paper Machine," *Paper Technology and Industry*, Vol.18, No.4, April 1977, pp.114-117.

A24. Palazzolo, S., "Positive & Negative Aspects of Serpentine Felt Drying - Benefits Outweigh Detriments," *Paper Trade J.*, Vol.162, No.10, May 16-31, 1978, pp.33-35.

A25. Edgar, C.B.Jr., "The Uno Run Felt Concept," *Paper Age*, June 1978, pp.16, 22-25.

A26. Bringman, D.J. and Jamil, Q.H., "Engineering Considerations for Lightweight Paper Drying in High Speed Machines," *Paper Technology and Industry*, Vol.19, No.6, July - Aug. 1978, pp.194-197, 200.

A27. Cutshall, K.A., Ilott, G.E., and Brooks, B.W., "Causes of MD Basis Weight Variation," *Pulp and Paper Magazine of Canada*, Vol.80, No.6, June 1979, pp.148-152.

A28. Sahay, A. and Edgar, C.D., Jr., "Practical Aspects of Single Dryer Felting," *Pulp and Paper Magazine of Canada*, Vol.81, No.1, Jan. 1980, pp.65-66, 69-70.

A29. Meinander, S. and Lindqvist, U., "Runnability and Color Register Versus Paper Web Behavior in Offset," 1982 Printing and Graphics Arts Conference, pp.31-35.

A30. Eriksson, L., "What Happens to a Paper Roll in the Printing Plant," *Advances and Trends in Winding Technology*, pp.195-212.

A31. Hill, K.C., "Dryer Sheet Stability for Older Paper Machines," *TAPPI*, Aug. 1988, pp.55-59.

A32. Wedel, G.L., "No-Draw Drying Restraint," *TAPPI*, April 1989, pp.93-97.

B. Traveling String

B1. Skutsch, R., "Ueber die Bewegung eines gespannten Fadens, welcher gezwungen ist, durch zwei feste Punkte mit einer constanten Geschwindigkeit zu gehen, und zwischen denselben in Transversalschwingungen von geringer Amplitude versetzt wird," *Annalen der Physik und Chemie*, Vol.61, 1897, pp.190-195.

B2 Stamets, W.K., Jr., "Dynamic Loading of Chain Drives," *Trans. ASME*, Vol.73, July 1951, pp.655-665.

B3. Sack, R.A., "Transverse Oscillations in Travelling Strings," *British J. of Applied Physics*, Vol.5, June 1954, pp.224-226.

B4. Mahalingam, S., "Transverse Vibrations of Power Transmission Chains," *British J. of Applied Physics*, Vol.8, April 1957, pp.145-148.

B5. Archibald, F.R. and Emslie, A.G., "The Vibration of a String Having a Uniform Motion Along its Length," *Trans. ASME, J. of Applied Mechanics*, Vol.80, 1958, pp.347-348.

B6. Miranker, W.L., "The Wave Equation in a Medium of Motion," *IBM J.*, Jan. 1960, pp.36-42.

B7. Swope, R.D. and Ames, W.F., "Vibrations of a Moving Threadline," *J. of Franklin Institute*, Vol.275, No.1, Jan. 1963, pp.36-55.

B8. Zaiser, J.N., "Nonlinear Vibrations of a Moving Threadline," Ph.D. Dissertation, University of Delaware, Newark, Delaware, 1964.

B9. Mote, C.D., Jr., "On the Nonlinear Oscillation of an Axially Moving String," *Trans. ASME, J. of Applied Mechanics*, Vol.88, June 1966, pp.463-464.

B10. Bapat, V.A. and Srinivasan, P., "Nonlinear Transverse Oscillations in Traveling Strings by the Method of Harmonic Balance," *Trans. ASME, J. of Applied Mechanics*, Sep. 1967, pp.775-777.

B11. Ames, W.F., Lee, S.Y., and Zaiser, J.N., "Nonlinear Vibration of a Traveling Threadline," *Int. J. of Nonlinear Mechanics*, Vol.3, 1968, pp.449-469.

B12. Naguleswaran, S. and Williams, C.J.H., "Lateral Vibration of Bandsaw Blades, Pulley Belts and the Like," *Int. J. of Mechanical Science*, Vol.10, 1968, pp.239-250.

B13. Lee, S.Y., "On the Equation of Motion of a Moving Threadline," *Developments in Mechanics*, Vol.5, 1969, pp.543-554.

B14. Ames, W.F. and Vicario, A.A., Jr., "On the Longitudinal Wave Propagation on a Traveling Threadline," *Developments in Mechanics*, Vol.5, 1969, pp.733-746.

B15. Ames, W.F., Lee, S.Y., and Vicario, A.A., Jr., "Longitudinal Wave Propagation on a Traveling Threadline - II," *Int. J. of Nonlinear Mechanics*, Vol.5, 1970, pp.413-426.

B16. Rhodes, J.E., Jr., "Parametric Self-Excitation of a Belt Into a Transverse Vibration," *Trans. ASME, J. of Applied Mechanics*, Dec. 1970, pp.1055-1060.

B17. Shih, L.Y., "Three-Dimensional Nonlinear Vibration of a Traveling String," *Int. J. of Nonlinear Mechanics*, Vol.6, 1971. pp.427-434.

B18. Kim, Y.I. and Tabarrok, B., "On the Nonlinear Vibration of Travelling Strings," *J. of Franklin Institute*, Vol.293, No.6, June 1972, pp.381-399.

B19. Bhat, R.B., Xistris, G.D., and Sankar, T.S., "Dynamic Behavior of a Moving Belt Supported on Elastic Foundation," *Trans. ASME, J. of Mechanical Design*, Vol.104, Jan. 1982, pp.143-147.

B20. Wickert, J.A. and Mote, C.D., Jr., "On the Energetics of Axially Moving Continua," *JASA*, Vol.85, No.3, March 1989, pp.1365-1368.

B21. Perkins, N.C., "Linear Dynamics of a Translating String on an Elastic Foundation," *Trans. ASME, J. of Vibration and Acoustics*, Vol.112, Jan. 1990, pp.2-7.

C. Traveling Web

C1. Mujumdar, A.S. and Douglas, W.J.M., "Analytical Modeling of Sheet Flutter," *Svensk Papperstidning*, Vol.79, No.6, 1976, pp.187-192.

C2. Soininen, M., "The Physics of Paper Machine Sheet Flutter," 1982 Int. Water Removal Symposium, Vancouver, BC, Oct. 26-28, 1982, pp.85-86.

C3. Soininen, M., "The Physics of Sheet Flutter in a Paper Drying Machine," *Pulp & Paper Canada*, Vol.85, No.5, May 1985, pp.61-63.

C4. Pramila, A., "Sheet Flutter - An Analytical and Experimental Study," Tampere University, Laboratory of Applied Mechanics, Report No.30, Tampere, Finland, 1985.

C5. Pramila, A., "Sheet Flutter and the Interaction Between Sheet and Air," *TAPPI*, July 1986, pp.70-74.

C6. Pramila, A., "Natural Frequencies of a Submerged Axially Moving Band," *J. of Sound and Vibration*, Vol.113, No.1, 1987, pp.198-203.

C7. Niemi, J. and Pramila, A., "FEM-Analysis of Transverse Vibrations of an Axially Moving Membrane Immersed in Ideal Fluid," *Int. J. Numerical Methods Eng.*, Vol.24, No.12, Dec. 1987, pp.2301-2313.

D. Plate Flutter

D1. Miles, J.W., "On Non-Steady Motion of Slender Bodies," *Aeronautical Quarterly*, Vol.2, Nov. 1950, pp.183-194.

D2. Jordan, P.F., "The Physical Nature of Panel Flutter," *Aero Digest*, Feb. 1956, pp.34-36, 38.

D3. Greenspon, J.E., Goldman, R.L., and Jordan, P.F., "Flutter of Thin Panels at Subsonic and Supersonic Speeds," AFOSR TR 57-65, Martin Co., July 1957.

D4. Lighthill, M.J., "Mathematics and Aeronautics," The 48th Wilbur Wright Memorial Lecture, *J. of the Royal Aeronautical Society*, Vol.64, No.595, July 1960, pp.375-394.

D5. Fung, Y.C.B., "A Summary of the Theories and Experiments on Panel Flutter," NATO AGARD Manual on Aeroelasticity, Part III, Chapter 7, Ed. Jones, W.P., Feb. 1961.

D6. Johns, D.J., "Some Panel Aeroelastic Instabilities," NATO AGARD Report No.474, Sep. 1963.

D7. Voss, H.M. and Dowell, E.H., "Effect of Aerodynamic Damping on Flutter of Thin Panels," *AIAA J.*, Vol.2, No.1, Jan. 1964, pp.119-120.

D8. Johns, D.J., "The present Status of Panel Flutter," NATO AGARD Report No.484, Oct. 1964.

D9. Ishii, T., "Aeroelastic Instabilities of Simply Supported Panels in Subsonic Flow," AIAA Meeting, Nov. 15-18, 1965, LA, CA, Paper No.65-772.

D10. Dzygadlo, Z. and Kaliski, S., "Parametric Self-Excited Vibrations of Elastic and Aeroelastic Systems with Traveling Waves," *Bulletin De L'Academie Polonaise Des Sciences*, Vol.14, No.1, 1966, pp.1-10.

D11. Dzygadlo, Z. and Kaliski, S., "Instability Limits of Parametric Self-Excited Vibrations of Elastic and Aeroelastic Systems with Traveling Waves," *Archiwum Mechanik Stosowanej*, Vol.20, No.4, 1968, pp.461-471.

D12. Kornecki, A., "Influence of Damping on the Aeroelastic Stability of an Unbounded Plate in a Potential Flow," *Israel J. of Technology*, Vol.7, No.4, 1969, pp.335-349.

D13. Dowell, E.H., "Nonlinear Flutter of Curved Plates," *AIAA J.*, Vol.7, No.3, March 1969, pp.424-431.

D14. Dowell, E.H., "Nonlinear Flutter of Curved Plates - II," *AIAA J.*, Vol.8, No.2, Feb. 1970, pp.259-261.

D15. Kornecki, A., "Traveling-Wave-Type Flutter of Infinite Elastic Plates," *AIAA J.*, Vol.8, No.7, July 1970, pp.1342-1344.

D16. Weaver, D.S. and Unny, T., "The Hydroelastic Stability of a Flat Plate," *Trans. ASME, J. of Applied Mechanics*, Vol.37, Sep. 1970, pp.823-827.

D17. Gislason, T., Jr., "Experimental Investigation of Panel Divergence at Subsonic Speeds," *AIAA J.*, Vol.9, No.11, Nov. 1971, pp.2252-2258.

D18. Kornecki, A., "Travelling Wave Type Flutter of Flat Panels in Inviscid Flow : Part I: Infinite Panels," Publ. No.132, Agricultural Eng.Faculty, Technion-Israel Institute of Technology, Haifa, Israel, Sep. 1971.

D19. Kornecki, A., "Travelling Wave Type Flutter of Flat Panels in Inviscid Flow : Part II : Panels of Finite Length," Publ. No.133, Agricultural Eng. Faculty, Technion-Israel Institute of Technology, Haifa, Israel, Oct. 1971.

D20. Vaicaitis, R., Jan, C.M., and Shinozuka, M., "Nonlinear Panel Response From a Turbulent Boundary Layer," *AIAA J.*, Vol.10, No.7, July 1972, pp.895-899.

D21. Kuo, C-C. and Morino, L., "Perturbation and Harmonic Balance Methods for Nonlinear Panel Flutter," *AIAA J.*, Vol.10, No.11, Nov. 1972, pp.1479-1484.

D22. Vaicaitis, R., Dowell, E.H., and Ventres, C.S., "Nonlinear Panel Response by Monte Carlo Approach," *AIAA J.*, Vol.12, No.5, May 1974, pp.685-691.

D23. Dowell, E.H., "*Aeroelasticity of Plates and Shells*," Noordhoff International Pub., 1974.

E. Membrane Flutter

E1. Squire, H.B., "Investigation of the Instability of a Moving Liquid Film," *British J. of Applied Physics*, Vol.4, June 1953, pp.167-169.

E2. Stearman, R.O., "Small Aspect Ratio Membrane Flutter," AFOSR TR 59-45, Guggenheim Aeronautical Lab., California Inst. Tech., Jan. 1959.

E3. Thomas, M., "Some Investigations into Panel and Membrane Aeroelastic Instabilities," Thesis (unpublished) Submitted to College of Aeronautics, Cranfield, U.K., June 1961.

E4. Ellen, C.H., "Approximate Solutions of the Membrane Flutter Problem," *AIAA J.*, Vol.3, No.6, June 1965, pp.1186-1187.

E5. Kelly, R.E., "The Stability of an Unsteady Kelvin-Helmholtz Flow," *J. of Fluid Mechanics*, Vol.22, Part 3, 1965, pp.547-560.

E6. Sundararajan, V., "Stability of Flexible Nozzle Structures," Ph.D. Dissertation, University of Kansas, Lawrence, 1966.

E7. Roth, W., "Eine Theorie zur Berechnung von Flatterschwingungen bei Unterschallstromungen (A Theory of Flutter Vibrations in Subsonic Flow)," *Acta Mechanica*, Vol.6, 1968, pp.22-41. (An Abbreviated English Translation by Peter Moretti, Oklahoma State University)

E8. Spriggs, J.H., et al., "Membrane Flutter Paradox - An Explanation by Singular-Perturbation Methods," *AIAA J.*, Vol.7, No.9, Sep. 1969, pp.1704-1709.

E9. Binnie, A.M., "Air-Generated Waves on a Moving Membrane," *J. of Mechanical Engineering Science*, Vol.12, No.3, 1970, pp.230-231.

E10. Kornecki, A., "Travelling Wave Type Flutter of Flat Panels in Inviscid Flow : Part I: Infinite Panels," Publ. No.132, Agricultural Eng.Faculty, Technion-Israel Institute of Technology, Haifa, Israel, Sep. 1971.

E11. Kornecki, A., "Travelling Wave Type Flutter of Flat Panels in Inviscid Flow: Part II: Panels of Finite Length," Publ. No.133, Agricultural Eng. Faculty, Technion-Israel Institute of Technology, Haifa, Israel, Oct. 1971.

F. Flag Flutter

F1. Fairthorne, R.A., "Drag of Flags," ARC Reports and Memoranda No.1345, May 1930.

F2. Thoma, D., "Warum Flattert die Fahne (Why Does the Flag Flutter?)," *Mitteilungen des Hydraulishen Instituts der Technischen Hochschule*, Muenchen, No.9, 1939, pp.30-34. (An Abbreviated English Translation by Peter Moretti, Oklahoma State University)

F3. Thoma, D., "Das Schlenkernde Seil (The Oscillating Rope)," *ZAMM*, Vol.19, No.5, Oct. 1939, pp.320-321. (An Abbreviated English Translation by Peter Moretti, Oklahoma State University)

F4. Hoerner, S.F., "*Fluid-Dynamic Drag*," Published by the Author, N.J., 1958, pp.3:25.

F5. Sparenberg, J.A., "On the Waving Motion of a Flag," *Proceedings of Nederland Academy of Sciences*, Ser.B, Vol.65, 1962, pp.378-392.

F6. Uno, M., "Fluttering of Flexible Bodies," *J. of the Textile Machinery Society of Japan*, Vol.19, No.4-5, Aug.-Oct. 1973, pp.103-109.

F7. Datta, S.K. and Gottenberg, W.G., "Instability of an Elastic Strip Hanging in an Airstream," *Trans. ASME, J. of Applied Mechanics*, March 1975, pp.195-198.

G. Radiation Impedance and Air Loading

G1. Pabst, W., "Theorie des Landestosses von Seeflugzeugen," *Zeitschrift fur Flugtechnik und Motorluftschiffahrt*, Vol.21, 1930, pp.217-226.

G2. Lamb, H., "*Hydrodynamics*," Dover Publications, Inc., N.Y., 1945, (Reprint of the Sixth Edition, 1932), Chapter IV.

G3. Yu, Y.T., "Virtual Masses of Rectangular Plates and Parallelepipeds in Water," *J. of Applied Physics*, Vol.16, Nov. 1945, pp.724-729.

G4. Keulegan, G.H. and Carpenter, L.H., "Forces on Cylinders and Plates in an Oscillating Fluid," *J. of Research of the National Bureau of Standards*, Vol.60, No.5, May 1958, pp.423-440.

G5. Lighthill, M.J., "Note on the Swimming of Slender Fish," *J. of Fluid Mechanics*, Vol.9, 1960, pp.305-317.

G6. Hanish, S., "The Mechanical Self Resistance and the Mechanical Mutual Resistance of an Unbaffled Rigid Disk Radiating Sound from a Single Face into an Acoustic Medium," Naval Research Lab. Report No. 5538, U.S. Naval Research Lab., Washington, D.C., 1960.

G7. Greenspon, J.E., "Vibrations of Cross-Stiffened and Sandwich Plates with Application to Underwater Sound Radiators," *JASA*, Vol.33, No.11, Nov., 1961, pp.1485-1479.

G8. Blagoveshchensky, S.N., "*Theory of Ship Motion*," Dover Publications, Inc., N.Y., 1962, (Translated from Russian, Originally Published in Leningrad in 1932), p.63.

G9. Morse, P.M. and Ingard, K.U., "*Theoretical Acoustics*," McGraw-Hill Book Co., N.Y., 1968.

G10. Mayerhoff, W.K., "Added Masses of Thin Rectangular Plates Calculated from Potential Theory," *J. of Ship Research*, Vol.14, June 1970, pp.100-111.

G11. Chang, Y.M., "The Mean Flow Effect on the Acoustic Impedance of a Rectangular Panel," Report No. 82464-1, Acoustics and Vibration Laboratory, MIT, Massachusetts, Feb. 1977.

G12. Kinsler, L.E., et al., "*Fundamentals of Acoustics*," Third Edition, John Wiley & Sons, N.Y., 1982.

G13. Chow, C.Y., "*An Introduction to Computational Fluid Mechanics*," John Wiley & Sons, 1979.

H. Dimensional Analysis

H1. Langhaar, H.L., "*Dimensional Analysis and Theory of Models*," Wiley, N.Y., 1951.

H2. Lecher, W.A., "Considerations of Similarity for Hydroelastic Vibration," *Proc. Instn. Mech. Engrs.*, 1966-1967, Vol.181, Pt. 3A, pp.25-31.

H3. Baker, W.E., Westine, P.S., and Dodge, F.T., "*Similarity Methods in Engineering Dynamics: Theory and Practice of Scale Modeling*," Hayden Book Co., N.J., 1973.

H4. Dubourg, M., et al., "Model Experimentation and Analysis of Flow-Induced Vibrations of PWR Internals," *Nuclear Engineering and Design*, Vol.27, 1974, pp.315-333.

H5. Blevins, R.D., "*Flow-Induced Vibration*," Van Nostrand Reinhold Co., N.Y., 1977.

H6. Lee, Hae, "Fluid-Elastic Parameters for Reactor Internals Model Testing," *J. of Korean Nuclear Society*, Vol.12, No.4, Dec. 1980, pp.286-292.

APPENDIX

MEASUREMENT OF YOUNG'S MODULUS OF A PAPAER WEB

A.1 Method

Vibration testing was done to measure the dynamic Young's modulus of a paper web. The paper strip was hung on a heavy steel structure and stretched by a weight as shown in Figure 41. The whole system is considered as a spring-mass system. The natural frequency of up-and-down motion of the weight is a measure of axial stiffness (EA) of the paper. Natural frequency of the system is

$$f_n = \frac{1}{2\pi}\sqrt{\frac{K\,g}{W}} \tag{A.1}$$

where

$$K = \frac{EA}{L} \tag{A.2}$$

Therefore, the Young's modulus can be expressed as

$$E = (2\pi f_n)^2 \frac{LW}{A\,g}$$

$$= \frac{(2\pi)^2 \text{x } 95}{0.004 \text{ x} 1.25 \text{ x} 386} W f_n^2$$

$$= 1940\ W\ f_n^2 \qquad (psi) \tag{A.3}$$

Four different weights were used. For each weight, tests were repeated at least ten times to obtain reliable results.

A.2 Test Setup and Instrumentation

The test setup is shown in Figure 41. A Proximiter (Bently 3115/2800) was used to measure the motion of the weight. The signal was observed and analyzed using a Digitizing Oscilloscope. The image on the oscilloscope was hard-copied by a ThinkJet Printer.

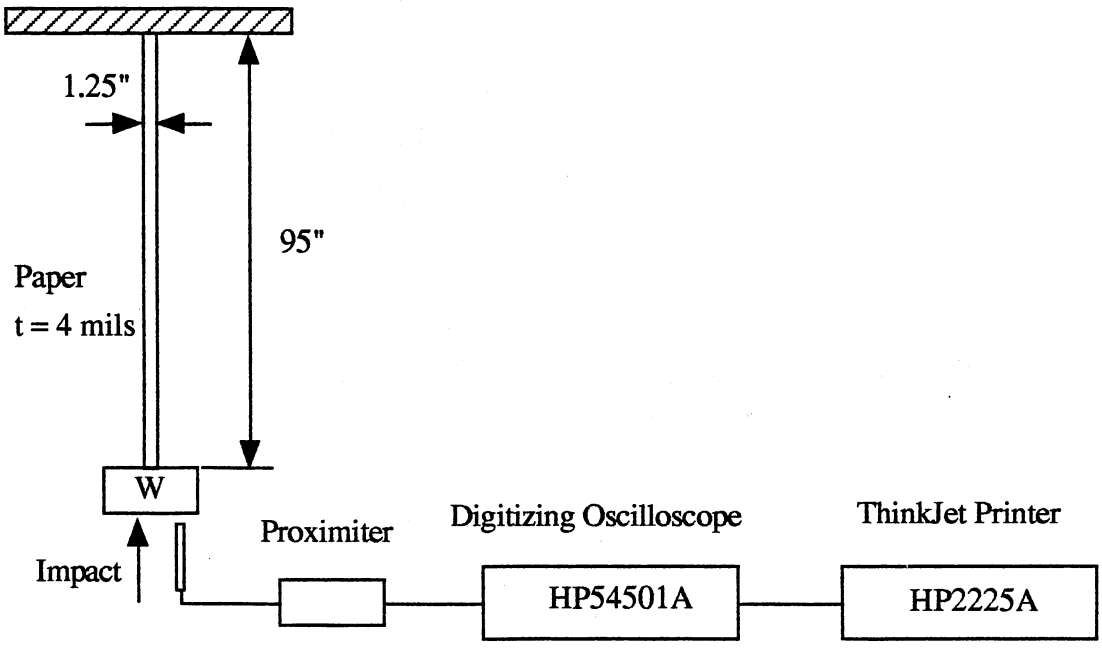

Figure 41 Test Setup for EA Measurement of a Paper Web

A.3 Results

Typical records of oscillation are shown in Figure 42. The curves show exponentially decaying sinusoidal motions. The results are very consistent and not dependent on the magnitude of impact. The natural frequency and corresponding Young's modulus for each condition are shown in Table IV.

When W = 1.45 Lb, the maximum acceleration of the weight for the amplitude of 1.0 mm is greater than the gravitational acceleration. This will affect the results. Therefore, the result for W = 1.45 Lb is uncertain. The dynamic Young's moduli of the paper strip are averaged, excluding the data for W = 1.45 Lb.

$$E = 9.9 \times 10^5 \text{ psi } (6.8 \times 10^9 \text{ Pa}) \tag{A.4}$$

TABLE IV

EA MEASUREMENT DATA

W (Lb)	T (Lb/in)	f_n (Hz)	E (psi)
1.45	1.16	18.3	9.4×10^5
2.45	1.96	14.4	9.9×10^5
3.45	2.76	12.1	9.8×10^5
6.45	5.16	9.0	10×10^5

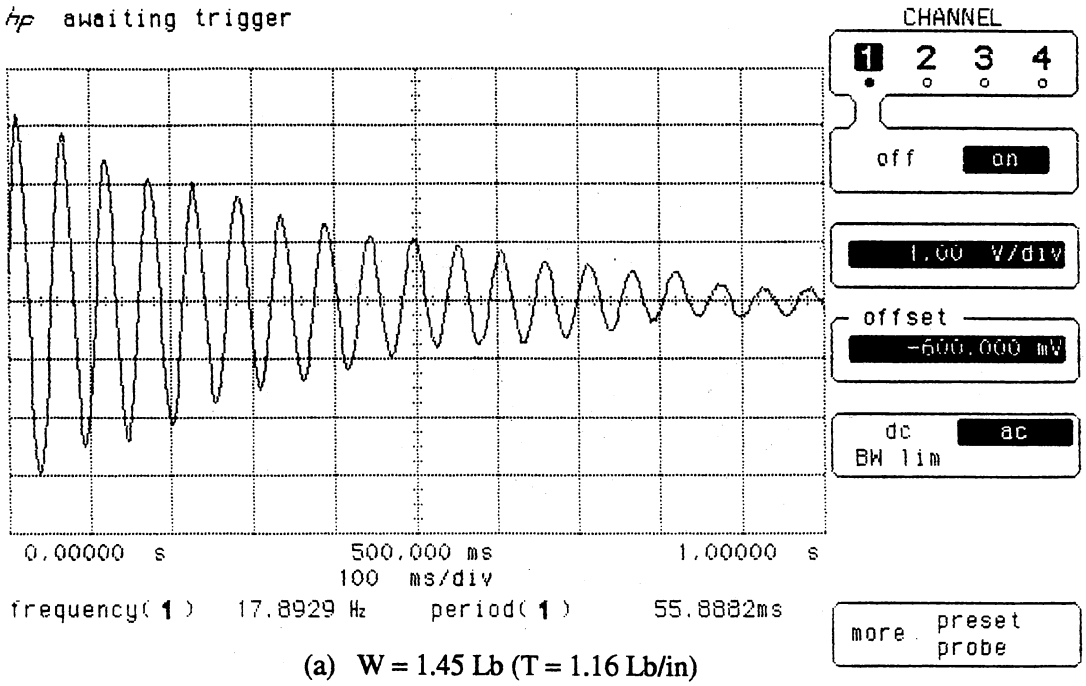

(a) W = 1.45 Lb (T = 1.16 Lb/in)

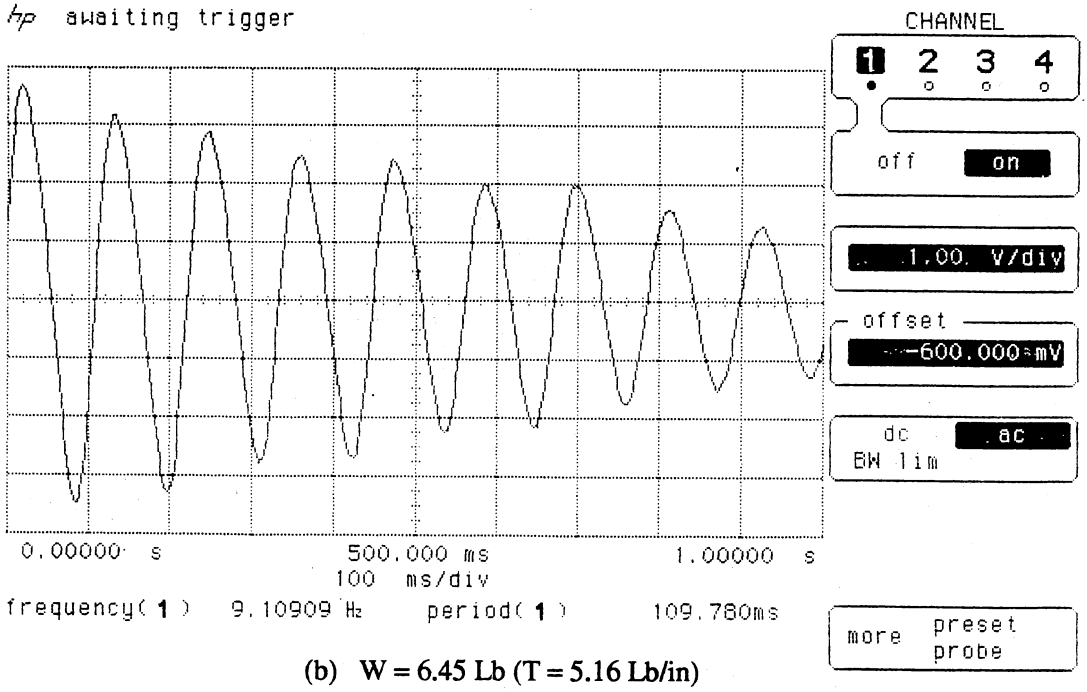

(b) W = 6.45 Lb (T = 5.16 Lb/in)

Figure 42 Typical Time History of the Axial Vibration of a Paper Web

VITA

Young Bae Chang

Candidate for the Degree of

Doctor of Philosophy

Thesis: AN EXPERIMENTAL AND ANALYTICAL STUDY OF WEB FLUTTER

Major Field: Mechanical Engineering

Biographical:

Personal Data: Born in Kyung-Ki-Do, Korea, May 24, 1955, the son of Mr. and Mrs. Seok Chang.

Education: Received the Bachelor of Science degree in Aeronautical Engineering from Hankuk Aviation College in February, 1979; received the Master of Science degree in Production Engineering from Korea Advanced Institute of Science and Technology in February, 1981; completed the requirements for the Doctor of Philosophy degree at Oklahoma State University in December, 1990.

Professional Experience: Research Scientist, Korea Advanced Energy Research Institute, 1981-1984; Senior Research Scientist, Korea Institute of Machinery & Metals, 1984-1986; Graduate Research Assistant, School of Mechanical and Aerospace Engineering, Oklahoma State University, 1987-1990.